An approach to the design of surface stress-based PDMS micro-membrane biosensors —

Concept, Numerical simulations and Prototypes

(PDMS-Mikro-Membran-Biosensoren auf Basis der Analyse von Oberflächenspannungen — Konzept, numerische Simulation und Prototypenbau)

Dissertation

zur Erlangung des akademischen Grades
Doktoringenieur (Dr.-Ing.)

vorgelegt der Fakultät für Maschinenbau
der Technischen Universität Ilmenau

von

M.-Eng. Shengbo Sang
geboren am 24. April 1979 in Shandong, P.R. China

urn:nbn:de:gbv:ilm1-2010000423

Tag der Einreichung: 15. Juni 2010
Tag der Verteidigung: 12. November 2010

1. Gutachter: Univ.-Prof. Dipl.-Ing. Dr. med. (habil.) Hartmut Witte
(Technische Universität Ilmenau)

2. Gutachter: Prof. Dr.-Ing. Klaus Liefeith
(Institut für Bioprozess- und Analysenmesstechnik e.V.)

3. Gutachter: Professor Dr.-Ing. Theodor Doll
(Johannes-Gutenberg-Universität Mainz)

Acknowledgments

Taking the chance, I would like to acknowledge a number of people who have contributed to the development of this thesis and to my overall experience as a PhD student at Ilmenau University of Technology. First and foremost, I would like to thank my supervisor Professor Hartmut Witte for having given me the opportunity to conduct research in the exciting field of BioMEMS. I am also deeply indebted to him for his support, encouragement and guidance as well as the freedom he gave me to work on areas of my interest during my graduate study. The professional interaction with my colleagues in biomechatronic group has had a significant influence on my research work, especial Dipl.-Ing. Ulrike Fröber, Dipl.-Ing. Mike Stubenrauch.

I would also like to thank Dr. Arne Albrecht, Dipl.-Ing. Lars Dittrich and other colleagues in the Center for Micro- and Nanotechnologies (ZMN) for their help and support to the fabrication. Thanks to Prof. Michael Köhler, Dipl.-Ing. Jialan Cao, M.Sc. Shuning Li and Dipl.-Ing. Steffen Schneider in the Department of Physical Chemistry and Microreaction Technology. They not only provided me free the functional chemical material and the media with *E.coli*, but technological advices and supports. Thank also to Dipl.-Ing. Daniel Kapusi and Dipl.-Ing. Torsten Machleidt in Department of Computer Sciences and Automation for the free use of smart white light interferometer system and technological support.

I would also like to acknowledge the help and support from other colleagues and friends, both past and present, namely (in no particular order) Dr. Cornelius Schilling, Dr. Emanuel Andrada, Dipl.-Inf. Silvia Lehmann, Kerstin Schmidt, Wolfgang Kempf.

I would also give thank to my family for their encouragement, support and motivation throughout my entire life. The uncompromising attitude of my family towards my education through difficult times is greatly responsible for what I have achieved today and the gratitude that I have for them cannot be expressed in simple words.

Finally, I would like to dedicate my dissertation to my passed away father. I miss and love him very much all the time.

Abstract

BioMEMS (Biological Micro-Electro-Mechanical Systems) technology, especially for biosensors, plays a critical role in the process of information gathering with the technologically advanced development of our civilization. “Surface stress-based biosensors” are a relatively new class of biosensors, which make use of the free energy change, the underlying concept in any binding reaction, and hence offer a universal platform for biological or chemical sensing. In the dissertation, a new surface stress-based polydimethylsiloxane (PDMS) micro membrane biosensor is proposed, designed, fabricated and tested. The biosensor is made of two main conponents: microfluidics and sensor. Each sensor consists of two micro membranes, one acts as active membrane and the other as reference. This design has sensitive surface stress measurements associated with specific analytes interactions on the active membrane’s surface.

The biosensors were fabricated successfully conquering many challenges in design and fabrication, like integration of PDMS processing with conventional microfabrication processes, fabrication of “perfect” PDMS thin films and release of PDMS membranes. Furthermore, the bonding technology, uncured PDMS as the intermediate layer method for the bond between biosensors and microfluidic devices or components, was studied and tested and the bond strength is close to the bulk PDMS.

Two biosensor test systems were built for testing the biosensor and its application. One is with a smart white light interferometer (smartWLI), and another is with a fiber optic interferometer (FOI). The smartWLI-based biosensor test system has a better spatial resolution (1 nm), and the FOI-based biosensor test system has a higher time resolution (< 0.5 sec.). Three alkanethiol molecules with different functional end groups were tested as the membrane coating layer for *E. coli* detection. The results of the experiments showed that the MUA is a better functional material to functionalize the biosensor membranes than MUO and DOT. The status of *E. coli* can be measured based on the surface analysis. Furthermore, the properties can be analyzed according to the change of membrane deflection.

Zusammenfassung

Die BioMEMS(Biological Micro-Electro-Mechanical Systems)-Technologie spielt vor allem für Biosensoren eine entscheidende Rolle im Prozess der Informationsbeschaffung für die technologisch fortschreitende Entwicklung unserer Zivilisation. „Oberflächenspannungsbasierte Biosensoren“ sind eine relativ neue Klasse von Biosensoren, welche die Änderung der freien Energie nutzen (das zugrunde liegende Prinzip jeder Bindungsreaktion), und bieten somit eine universelle Plattform für biologische oder chemische Sensorik. In der Dissertationsschrift wird ein neuer oberflächenspannungsbasierter Polydimethylsiloxan (PDMS)-Mikro-Membran-Biosensor vorgeschlagen, konstruiert, gefertigt und getestet. Der Biosensor besteht aus zwei Haupt-Funktionskomponenten: Mikrofluidik und Sensorik. Jeder Sensor besteht aus zwei Mikro-Membranen, einer aktiven Membran und einer Referenzmembran.

Die Biosensoren wurden erfolgreich unter Bewältigung vieler Herausforderungen aufgebaut. Diese lagen insbesondere in den Bereichen Design und Herstellung, wie zum Beispiel der Integration der PDMS-Mikroverarbeitung mit herkömmlichen Verfahren, der Herstellung von „perfekten“ PDMS-Dünnschichten und der Gewinnung der PDMS-Membran. Darüber hinaus wurde eine Klebetechnik, welche unausgehärtes PDMS als Zwischenschicht für die Bindung zwischen Biosensor und Mikrofluidikkomponenten oder -bauteilen nutzt, untersucht und getestet.

Für die Prüfung und Anwendung der Biosensoren wurden zwei Biosensor-Testsysteme eingerichtet. Eines mit einem „smart Weißlichtinterferometer“ (smartWLI) und ein anderes mit einem „Fiberoptic Interferometer“ (FOI). Drei Alkanthiol-Moleküle mit verschiedenen funktionellen Endgruppen wurden als Biosensor-Überzugsschichten für die Anwendung getestet. MUA ist das derzeit beste „funktionelle“ Material, um die Membran für den Nachweis von *E. coli* zu funktionalisieren. Der PDMS-Mikro-Membran-Biosensor auf Basis der Analyse von Oberflächenspannungen besitzt gute Empfindlichkeit, Reproduzierbarkeit und Biokompatibilität. Der Zustand von *E. coli-Bakterien* kann auf der Grundlage der Analyse der Oberflächenspannungen gemessen werden.

Table of contents

Index of figures

Index of Tables

Nomenclature

Terms

α_g :	Coefficient of thermal expansion
c:	Specific Heat
δ:	Loss tangent
$\Delta\zeta_1$:	Surface stress acting on the front side of cantilever
$\Delta\zeta_2$:	Surface stress acting on the back side of cantilever
T:	Temperature load
Δ*z*:	Tip deflection of cantilver
E_g :	Young's modulus
F:	Force
G:	Shear modulus
$H_{solvent}$:	Heat of vaporization of solvent
l:	Half length of square membrane
I:	Moment of inertia of cantilever/beam
I_1:	Reference signal
I_2:	Sensing signal
l_m:	Membrane length
L:	Length of cantilever/beam
κ:	Electric conductivity
n:	Index of refraction
p:	Pressure
ρ:	Distribution load
P_{gold} :	The size of gold
$P_{submaterial}$:	The size of PDMS
ρ:	Density
r:	Radius of round membrane
R:	*R*adius of curvature of cantilever
R_1:	Reflection at the fiber/air interface
R_2:	Reflection at the air/membrane interface
$R_{solvent}$:	Evaporation rate of solvent

R_{water} : Evaporation rate of water

ζ_s : Surface stress load

t: Thickness of cantilever/beam/membrane

T_g : Thickness of gold coating

T_G: Glass transition temperature

u: Poisson ratio,

w: The width of cantilever/beam

X: The air gap between the fiber and membrane

Abbreviations:

AFM: Atomic force microscope

AlN: Aluminium Nitride

ATP: Adenosine Tri-Phosphate

BioMEMS: Biological micro-electro-mechanical systems

BSA: Bovine serum albumin

CL: Chemiluminescence

CMOS: Complementary metal oxide semiconductor

CMP: Chemical-mechanical planarization

CVD: Chemical vapor deposition

DC: Direct current

DNA**:** Deoxyribonucleic acid

DOT: Dodecane thiol (SH-$(CH_2)_{11}$-CH3)

DRIE: Deep reactive-ion etching

E. coli: Escherichia coli

ELISA: Enzyme-linked immunosorbent assay

ER: Endoplasmic reticulum

FE: Finite element

FOI: Fiber optic interferometer

HEPES: N-2-hydroxyethylpiperazine-N'-2-ethanesulfonic

IDDM: Diabetes mellitus type 1

IGg: Immunoglobulin G

IPA: Isopropyl alcohol

LDL**:** Low-density lipoprotein

LPCVD: Low Pressure CVD

LPS:	Lipopolysaccharide
µTAS:	Micro total analysis systems
MEMS:	Micro-electro-mechanical systems
MUA:	11 Mercapto 1 undecanoicacid (SH-$(CH_2)_{10}$-COOH)
MUC5AC:	Oligomeric mucus/gel-forming
MUO:	11 Mercapto 1 undecanol (SH- $(CH_2)_{11}$-OH)
oxLDL:	Oxidated low-density lipoproteins
PAHs:	Polycyclic aromatic hydrocarbons
PCBs:	Polychlorinated biphenyls
PCD:	Programmed cell death
PCR:	Polymerase chain reaction
PDMS:	Polydimethylsiloxane
PECVD:	Plasma Enhanced CVD
PEG-silane:	2-[Methoxy(polyethylenoxy)propyl]trimethoxysilane
PMA:	Phorbol-12-myristate-13-acetate
PMMA:	polymethylmethacrylate
PrP^{c}:	The normal (cellular) form of prion protein
PrP^{TSE}:	Disease-associated form of prion protein
PSA:	Prostate-specific antigen
PVD:	Physical vapor deposition
RA:	Rheumatoid arthritis
RER:	Rough endoplasmic reticulum
RIE:	Reactive-ion etching
SAM:	Self-assembled monolayer
SER:	Smooth endoplasmic reticulum
SiN:	Silicon Nitride
SLE:	Systemic lupus erythematosus
smartWLI:	Smart white light interferometer
SNR:	Signal-to-noise ratio
SPR:	Surface plasmon resonance
STM:	Scanning tunneling microscope
UV:	Ultraviolet
VOC:	Volatile organic compounds

Chapter 1 Introduction

1.1 Overview on BioMEMS

“Microelectromechanical systems” (MEMS) and relevant microfabrication technologies have shown an exciting development since the birth of first transistor at Bell Telephone Laboratories in 1947. There have been many commercial applications, such as the commercially most successful MEMS devices and systems: accelerometers and pressure sensors. In recent years, technologies have taken a rapid expansion into different fields of physical sciences, engineering, and biomedicine. MEMS technologies are also assisting in bridging the gap between computers with our analog world. For example, various sensors and actuators produced using MEMS technologies can be used as interfaces between computers and the physical environment for purposes of information processing and intelligent control [1].

“Biological microelectromechanical systems” (BioMEMS) is a special class of MEMS where biological matter is manipulated for analyses and measures of its activity, characterisations under any class of scientific study. The BioMEMS-based devices are an attractive area of development based on microtechnology. The techonolgy has more exciting developments in the application of MEMS technology in recent decades. For scientific analysis and measurement, various novel sensor and detection platforms in the BioMEMS and microfluidic fields are required and have been reported, in addition to basic components, such as microchannels, micropumps, microvalves, micromixers and microreactors for flow management at microscopic volumes [1]. Any of the most important applications based on BioMEMS are: biomedical and biological analysis and measurements, micro total analysis systems (μTAS) and lab-on-a-chip systems [2-5], which will give new applications in biomedicine and biology, especially the ability to perform point-of-care measurements. The advantages of such systems are that they can deliver and process the biological or biomedical samples in microvolumes for testing and analysis in an integrated way therefore dramatically reducing the requirement to the manipulation steps and the samples, and improving data quality and quantitative

capabilities. The BioMEMS technology also helps to reduce overall cost and time for the measurement. At the same time it improves the sensitivity and specificity of the analysis [1].

Sensing, therapeutic intervention (e.g. drug delivery), fluid handling, bio-reactors and so on are areas of opportunity in the BioMEMS market. Following closely the BioMEMS market has profound significance like Charles Cooney said “this very broad interface between biology, electronic systems, mechanical systems, IT ... and bringing that interface to some market opportunity” (web.mit.edu). The BioMEMS worldwide market was around $10 billion in 2002 based on the investigation by the European Nexus organization (www.nexus.org). The BioMEMS drug-delivery market in the U.S. alone has been increased from $14.4 billion in 2002 to about $28.8 billion in 2005 based on the research firm UBS Warburg LLC (www.ubswarburg.com). According to Michael Reed who is a researcher at the University of Virginia (www.uva.edu), the market for treating coronary restenosis (scar-tissue blockages) increased from $2 billion in 2001 to about $5 billion in 2005 in the world. As well, the revenues for the cancer/drug therapy market have increased from 1999’s $20 billion to $31 billion by 2004 in the world, says President John T. Santini of Microchips Inc (www.mchips.com). Technology consulting company Yole Development (www.yole.fr) predicts that the worldwide market will grow from 30 % to 50 % annually in the field of DNA microarrays. The global medical equipment industry business volume was at $2.17 billion in 2006, growing at 15 % per year to reach $4.97 billion by 2012 based on an analysis by Ernst & Young pegs. Yole’s BioMEMS 2008 report gave the tendency of MEMS components for life sciences market from 2005 to 2012, Figure 1-1(www.yole.fr).

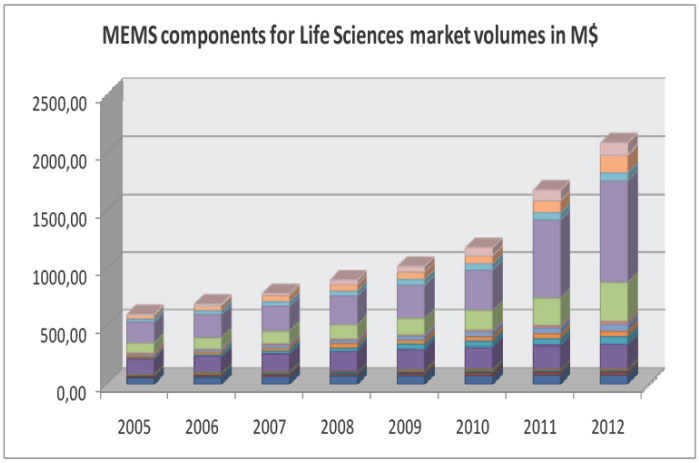

Figure 1-1: MEMS components for life sciences market from 2005 to 2012(www.yole.fr)

1.2 Biosensors

To the BioMEMS technology and application, biosensors play a critical role in the process of information gathering with the technologically advanced development of our civilization, demand for information. With new applications in the areas – genetics, diagnostics, drug discovery, environment and industrial monitoring, quality control as well as security and threat evaluation [6], the need for high throughput label-free multiplexed sensors for biological sensing has increased in the last decade.

A biosensor is a device for the detection of an analyte that combines a biological component with a physicochemical detector component [7]. In general, one concept of biological sensors encompasses two main features in addition to the associated signal processors used for the display of the results in a user-friendly way: the sensitive biological element which is a chemically receptive or selective layer, and the transducer or the detector element (it can work in a physico-chemical way, optical, piezoelectric, electro-chemical, etc.) that transforms the signal induced by the interaction between the analytes and the biological element into another more easily measured and quantified signal, Figure 1-2. The chemical layer provides specific binding sites for the target analyte of interest, such as molecules, proteins and cells. To most biological and chemical sensors, sensitivity has been increased tremendously in recent years, but it still has some deficiency and needs more improvement. The selectivity of the receptive layer can be designed employing principles of molecular and biomolecular recognition; for example antigen-antibody binding (i.e. any chemicals, bacteria, viruses, or pollen binding to a specific protein) [8]. Other surface functionalizations such as self-assembled monolayer [9, 10] and polymer coatings are also employed. The selectivity is then achieved by a specific chemical reaction on the functionalized sensor's surface. However, absolute selectivity remains a major challenge. In fact, most sensing technologies are faced with the issue of non-specific interactions which can complicate the sensor response, produce false positives, and affect the reproducibility and the suitability of the sensor system for a particular application. Therefore, the chemical layer must be designed to maximize the sensor's sensitivity to the specific response.

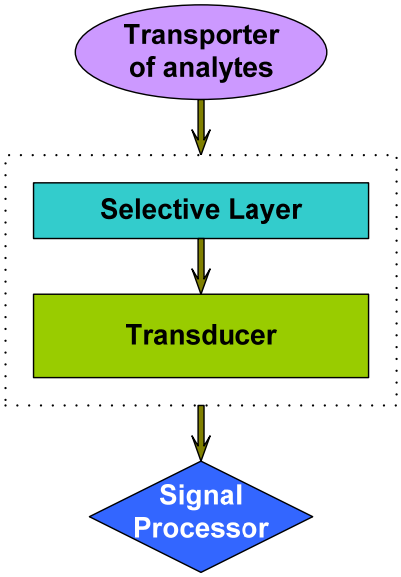

Figure 1-2: Generalized schematic representation of a biological sensor

Once the analyte is recognized by the chemical layer, the transducer converts the chemical stimulus into a measurable output signal, as shown in Figure 1-2. Both the chemical layer and the physical transducer impose limitations on the performance of a certain class of sensors. Nevertheless it is often the physical transducer which determines the limits of detection attainable. The search for new transduction principles is therefore constantly stimulated [8]. In fact, each step depicted in Figure 1-2 has an influence on the sensor's performance. From the mechanism that drives the analyte to the sensor (e.g. microfluidic, activated diffusion, etc.), to the instrument reading the output signal of the transducer; all stages are the subject of extensive research efforts.

Cantilevers are the most commonly used sensitive elements of sensors and since their advent as a transducer in an AFM, their application space has expanded tremendously in the areas of physical, chemical and biological sensing [8, 9, 11, 12]. Several groups have researched and reported the application of cantilever sensors through the measurement of physical properties either by bending or resonant frequency change. The physical properties include temperature [13-28], power [22-25], pressure [19], Young's and shear modulus [26], viscosity and density [29-35], current [36], piezoelectric charge constant [37-43], frequency [43-53]. Many different cantilever platforms have also been developed and utilized in the measurements of several chemicals and chemical properties such as gases [54-72] (which includes vapor concentration [54, 55], gas concentration [66-70], nerve agent [71], and

explosive [72]), pH [73], pesticide concentration [74], ethanol/water concentration [75], and ion concentration [76-79]. Other researchers have demonstrated the capability of surface stress based cantilever sensors in detecting a variety of reactions, which include alkanethiol immobilization [80], water vapour adsorption [11], DNA hybridization [81-84], antigen-antibody binding [85], and explosive vapor detection [86]. A summary to some of the biochemical measurements using cantilevers has been done in Table 1-1.

Table 1-1: The examples of biochemical measurements using cantilevers

Analyte	Sensitivity/Range	Cantilever type	Detection method
DNA	6×10^{12} chains/cm^2 [87] 5 nN [88] 1 μM [89] 3 μM - 8 μM [90]	Flexoelectric [87] Optical [88, 90] Piezoresistor [89]	Bending mode [87,88,90] Static stress mode [89]
PSA	0.2 ng/ml-60 μg/ml [85] 10 pg/ml [91] 10 ng/mL - 1 μg/ml [92] 6 ng/mL - 60 μg/ml [90]	Optical [85,90] Piezoelectric [91] Piezoresistive [91]	Bending mode [85] Frequency [91] Resistance [92]
BSA	6 mg/ml [93] 2 mg/ml [94] 0.1 mg/ml [95]	Optical [93,95] Piezoresistive [94]	Static stress mode [93] Resistance [94] Bending mode [95]
C-reactive Protein	10 ng/ml - 1 μg/ml [92] 1 ng/ml [96]	Piezoresistive [92] Piezoelectric [96]	Resistance [92] Frequency [96]
Ligand-receptor force	Concanavalin A-yeast: 180 pN [97] Yeast to various surfaces [98] PGA: 100 pN - 600 pN [99] Antifluorescyl-IgG to MASFM probe: 120 pN - 400 pN [100] Vitronection receptors-MC3T3-E1 cells: 10^{-17} J/mm^2 [101]	Optical	Bending mode
IGg	0.195 mg/ml & 5.85 mg/ml	Optical	Static stress mode [93]
Lipoptotiens (LDL) &	LDL: 1.7 mg/ml oxLDL: 0.3 mg/ml	Optical	Static stress mode [93]

(oxLDL)			
Cystamine	1 mM	Optical	Frequency [102]
LPS/PMA to Collagen adhesion	Separation work:10^{-17} J/μm^2	Optical	Frequency [103]
Biotin-avidin	100 nM	Optical	Bending [104]
Phospholipid Vesicle	450 pg	Optical	Frequency [105]
E. coli O157:H7	1 × 10^6 cfu/mL	Optical	Bending mode [106]
Escherichia coli	140 pg/Hz	Piezoelectric	Frequency [107]
Yeast cells	400 ng/Hz ± 0.5 ng/Hz	Piezoelectric	Frequency [108]

Note: some data coming from reference [109]

Surface stress sensors are a new class of MEMS sensors that have immense potential to satisfy the demand for better quality sensors and have been investigated extensively in the recent years. “Surface stress” internationally either is represented by force per unit length (its unit is N/m), or by energy per area (J/m^2) [81, 82, 85, 110, 111], which is formally equaivalent by units (J/m² = Nm/m² = N/m), but neglects the character of dimensions: forces are vectors, energy is scalar. Since “Surface stress” in its histirical basics is a scalar thermodynamical term, it seems senseful to pont to the fact that mechanical stress is defined by vectorial force per area, in the unit N/m² = Pa. This kind of sensor uses a balance of free energy change, which is the underlying concept in any binding reaction, and hence offers a universal platform for biological and chemical sensing [6]. When bio/chemical reactions occur preferentially on one surface of such a sensor, changes in intermolecular forces create a surface stress that alters the curvature of the mechanical sensing element. The range of surface stress in such reactions was reported to be 5 mJ/m^2 to 50 mJ/m^2 [81, 85, 110, 111] or as high as 200 mJ/m^2 [80] or even 900 mJ/m^2 [82].

The detection principles commonly used in cantilever based biosensors are based upon changes in the deflection due to induced differential surface stress, resonant frequency shifts due to mass changes, thermal changes that cause bending, capacitance and resistance induced by the adsorption or attachment of analyte on

the cantilever's surface or the bending of cantilever. To the surface stress-based cantilever biosensors, it is possible to sensitize one surface of a cantilever differently than the opposing surface. When the target molecule of interest interacts with the sensitized surface, a surface stress is induced, and the cantilever bends due to the different surface stresses acting on both sides of the cantilever.

Cantilever sensors will develop a differential-induced surface stress upon the adsorption of analyte because the top and bottom surfaces of cantilever are different, for example only one side has a "recognition layer". The differential surface stress will cause the cantilever to bend or deflect [112-116]. The adsorption induced surface stress can be quantitated through measuring the curvature of the cantilever bending using the "Stoney's equation" [104,117]:

$$\frac{1}{R} = 6\left(\frac{1-\upsilon}{Et^2}\right)\left(\Delta\zeta_1 - \Delta\zeta_2\right) \qquad (1)$$

Where R is the radius of curvature, t the thickness, E the Young modulus, υ is the Poisson ratio, and $(\Delta\zeta_1 - \Delta\zeta_2)$ the differential surface stress. For a cantilever of length L that one end is fixed and the other is free, the tip deflection Δz can be expressed as:

$$\Delta z = 3L^2\left(\frac{1-\upsilon}{Et^2}\right)\left(\Delta\zeta_1 - \Delta\zeta_2\right) \qquad (2)$$

Therefore, the surface stress can be quantitated directly from the measured cantilever deflection.

The high sensitive surface stress-based cantilever biosensors have found a growing interest in the detection and quantification of biologics in the last decade. Cantilevers are used as the sensitive elements of biosensors due to their high sensitivity. However, surface stress based cantilever biosensors are not free from problems which include limitations imposed by the bulky size of the optical detection system, long term drift from non-specific adsorption on non-sensing side, loss of signal due to severe bending of the cantilever, and limited dynamic range. Moreover, the cantilever geometry is not the best for sensing in liquid media, which is most common in biological applications, because the entire cantilever is immersed in the fluid and

non-specific adsorption at the back side of the cantilever could drastically reduce the signal-to-noise ratio (SNR) [6]. The main other reason why micro and nano-sized cantilevers cannot be used to directly measure in liquids is that the liquid significantly dampens the sensor's dynamics at resonance, which can decrease substantially the quality of resonance and shifts resonance frequencies. The cantilever-based technique may not reflect the true state of the biologics when taking measurements because biological materials generally conform to their native state in a liquid environment [109]. Furthermore, salt from residual buffer solution on the cantilever will precipitate and increase the shift of measured resonant frequency and further enhance the cantilever's deflection. Also, there is the risk of breaking the cantilever in transporting it between different locations. In the application ranges that the binding and unbinding kinetics are needed and for real-time online monitoring of processes, detection in liquid is the desirable modality [109]. In addition, direct measurement in liquid will reduce false positive and false negative responses [109].

Membrane is another configuration of a sensitive mechanical element for detecting surface stress changes and using silicon polymer bimorph membranes such sensors have been developed for VOC and humidity sensing [118]. Membranes offer many advantages over cantilevers, some of which include easy electronic readout (capacitive detection [6,118]) and sample isolation from detection systems. But, for a given sensor dimension, membranes are less compliant than cantilevers and this results in lower sensitivity. Use of low stiffness materials like polymers, SU8, PMMA and PDMS instead of silicon or silicon nitride based materials can solve the problem of sensitivity.

The most widespread example of a commercial biosensor is the blood glucose biosensor; and cell-based biosensor is another main example of biosensor has been researched, popularized and applied in the biological and medical range.

1.2.1 Glucose biosensors

Glucose secreted by pancreas is of special interest due to its important function in human metabolic processes. If insulin can not be produced in a sufficient amount by pancreas, the glucose concentration of the blood will increase, leading to diabetes.

This is a worldwide problem. In 1921, F. G. Banting and C. Harbert discovered insulin, which can move the glucose from the blood into the cells of human body and then lowers blood glucose. Following its discovery, patients can be treated when insulin is injected into the body of patients. But therapists need continuous monitoring of glucose concentration in blood and the patients also need continuous monitoring at home to control diabetes. The American Leland C. Clark first developed a biosensor for monitoring glucose continuously in 1962, which is one of the most commercially successful products of its kind in the world (Afrin Sultana, ECE 730-13 Nanoelectronics, Course Project, 2004).

Blood glucose biosensor breaks blood glucose down through the enzyme glucose oxidase. For doing so, it first oxidizes glucose and the FAD (a component of the enzyme) is reduced to $FADH_2$ using two electrons. And then this is oxidized by the electrode which accepts two electrons from the electrode in a number of steps. The resulting current is a measure of the concentration of glucose. With the currently available glucose biosensors, the patient himself or herself can extract one small drop of blood and obtain a direct digital readout of the glucose concentration within one minute (Chris D. Geddes and Joseph R. Lakowicz, Glucose Sensing, 2006).

1.2.2 Cell-based biosensors

A cell constitutes the basic unit of not only body but also of disease, hence cells can be used to the analytes in biosensors as the target to measure the properties of cells and the pathology of diseases. Cell-based sensors can be divided into several classes. The first distinction may be made by the type of cells utilized in the system. For the past 25 years cells from bacteria and algae have been used, mainly in amperometric and potentiometric devices. In these sensors a cell layer is immobilized on the surface of an electrode. The quality of water can be probed by measuring the biological oxygen demand (BOD) by oxygen electrodes, and such sensors are already comercially available. New developments aim at fully automated systems [119]. Another parameter to monitor is the presence of herbicides which can be measured by using cyanobacteria together with a redox couple such as $[Fe(CN)_6]^{3-/4-}$. If the photosynthetic activity of the bacteria is reduced by the presence of herbicides the reduction of the iron complex is also reduced and hence the

response of an amperometric sensor device [120]. Other applications make use of the fact that some bacteria contain large amounts of a certain enzyme. The metabolic product is measured, e.g. by an ion-selective electrode (see, e.g., [121]) or an amperometric device (see, e.g., [122]). Examples also exist where the bioluminescence or a fluorescence signal were measured as a response to an enzymatic reaction (for a recent example see [123]). Another distinction may be made by the kind of connectivity the cells keep in the sensor system. One can either use single cells, cell layers, cell networks, tissue, or even whole animals/plants. Last but not least the measurement principle may be used to classify cell-based sensors. Three different approaches for whole cell sensors have mainly been applied: first, the mechanical contact between cells and between cells and substrates is measured via AC conductivity measurements in which the cells act as resistors; second, (bio-) chemical sensors are used to measure metabolic products delivered from cultured cells to the medium; third approach: the direct electrical response of electrogenic cells (neural cells, heart muscle cells, pancreas beta cells) or a neural cell network is measured [124].

Cells have also been studied for decades by using biochemical probes, efforts to transition their role from test subjects to that of sensor elements are relatively new [125]. Recent cell-based biosensor efforts have utilized a variety of secondary transduction methods just like illustrated in Figure 1-3, which can detect the responses of cells. Like reviewed in Bousse [125] and Pancrazio [126], these methods include monitoring metabolism [127], fluorescent probes and reporter genes [128], motility and adhesion [129], electrophysiology [130], and analyzing neuronal network signaling patterns [131].

Cell-based biosensors utilize whole cells as the primary transducer (analytes) to detect a biologically active agent as a cellular signal [132-134]. Figure 1-3 simply illustrates the process of one kind of biosensor [135]. The cellular signal is converted into an electrical signal (which can be processed and analyzed) by the secondary transducer. Thus, cell-based biosensors explicitly use cells in vitro (“in glass” = out of the body) to detect and classify cells by the response to cellular activity [135]. Manimaran *et al* designed a biosensor based microfluidic device as a deformation

assay to study the deformability and growth capability of cells through microgaps [136].

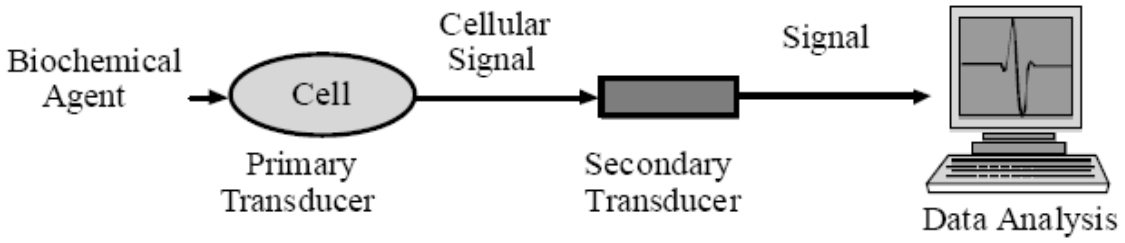

Figure 1-3: Signal transduction pathway of a cell-based biosensor [135]

In contrast to other kinds of biosensors, such as antibody- or enzyme-based biosensor to detect the binding of specific structural shapes in the method that get some biological information, cell-based biosensors have been developed to detect a broad range of biochemical agents each as a cellular response to specific stimuli. This cellular response is detected by a secondary transducer and converted into the mechanical or electronic signal suitable for measurement and analysis, which offer the advantage of a functional assay without requiring foreknowledge of the chemical structure. But to antibody- or enzyme-based biosensors, there is a problem resulting from false positives because binding alone is not always sufficient to evidence that an analyte will show the expected whole physiological effect. Subtle differences in the sensitive structures of biosensors may also allow binding but prevent functional activation. Hence, antibody-based and enzyme-based biosensors have limited application range. These advantages would be benefit from functional screening of unknown agents includes pharmacology, cell biology, drug discovery, toxicology, and environmental monitoring [109,118].

1.2.3 Mirofluidic devices or components for biosensors

Microfluidic devices or components have emerged in the beginning of the 1980s and were quickly used in the development of inkjet print heads, DNA chips, lab-on-a-chip technology and micro-thermal devices. Microfluidics can precisely control and manipulate fluids and analytes that are geometrically constrained to a small size, typically sub-millimeter, and scale. Typically, the mean of “micro” has the following features:

- the volumes are small (nl, pl, fl)

- the characteristic sizes are small
- energy consumption is low
- effects of the micro domain occur, esp. dominance of line and area (contact) effects to volume (mass inertia) effects

It is a multidisciplinary field intersecting engineering, physics, chemistry, microtechnology and biotechnology. To the design of practical systems, small volumes, channels and pumps of fluids can be used. Batch-fabricated microfluidic platforms that can mimic conventional sample handling techniques performed to enable both medical research and healthcare advances. Such miniaturized microfluidic devices or components have been termed “micro total analysis systems” (μTAS) or “biochips” combining with biosensors that work in sensing mechanisms (physical, optical, electrical, or chemical). These autonomous platforms have attracted considerable research interest due to the opportunity for fabricating a highly integrated system able to perform all necessary processing steps required for the specific application.

One of the most attractive applications of microfluidics has been in biomedical and life science diagnostics [137]. μTAS applications are attractive because of the potential of such systems to allow faster analysis of biological material. Further they can reduce the requirement to the amount of reagent and the number of processing steps. In addition, miniaturization of such systems can result in higher repeatability and precision of analysis, lower power consumption, and the potential to create portable diagnostic tools for on-site analysis. These advantages result not only in time and cost savings for diagnostic tests, but can also be life saving in time-critical environments such as critical medical diagnostics or biowarfare pathogen detection. A major research thrust in microfluidics has been the development of autonomous platforms for controlled microscale fluid transport allowing fluid flow rates ranging from nl/hrs to μl/min within compact fluid-handling and delivery systems — micropumps [138, 139].

Micropumps are a desired component of biosensors and microfluidic devices because of their wide application in surgery, drug delivery, drug discovery, and rapid diagnosis and treatment of disease [1]. Micropumps may be coupled with other microfluidic devices or components such as microfilters for particle [140] or molecular

filtration [141], microflow sensors for flow measurements [142], micromixers [143] for analyte and reactant dosing and reaction engineering, microneedles [144] and microdispensers [145] for precise fluid delivery, and microseparators [146] for biological component separations.

1.2.4 Detection method

The detection techniques used in biosensors can be broadly classified into label-free and label-based techniques [6]. The two methods can also be further classified as shown in Figure 1-4. Label-based techniques rely on the specific properties of labels like fluorescence, chemiluminescence etc. for detecting a particular target. However, the process of labeling and purification processes is associated with sample losses, which is critical when sample quantity is limited. Labeling processes can also have a detrimental effect on the functionality and stability of molecules like proteins. Mass spectrometry, surface plasmon resonance (SPR) and other optical method are label-free techniques, which can conquer these disadvantages. The following subsections are the detailed discussion to the respective advantages and disadvantages of every technique.

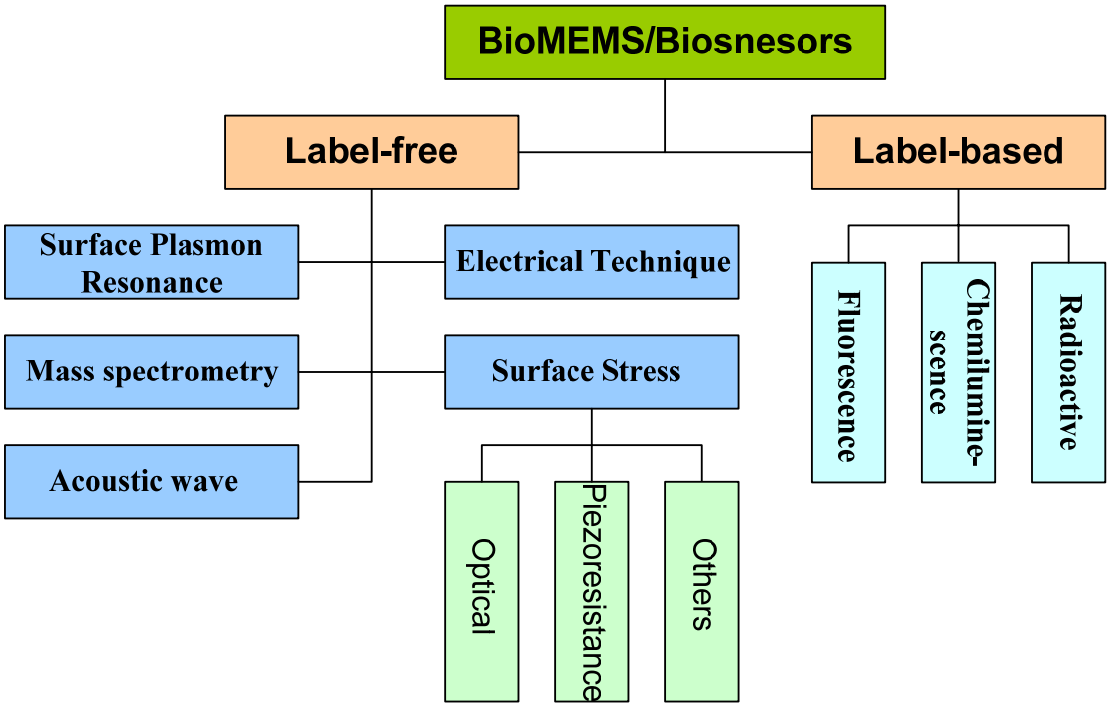

Figure 1-4: Classification of detection method of biosensors [6]

Label-free techniques

Surface Plasmon Resonance (SPR): SPR-based instruments measure the refractive index near a sensor surface through an optical method to for getting some information. When a light beam impinges onto a metal film at a specific (resonance) angle, the surface plasmons can be resonated with the light. As a result, it can induce the absorption of light. For the widely used Kretschmann configuration, a beam is focused onto the metal film. There is a range of incident angles provided focused light and the reflected beam will have the same range of the angles while the projection of the beam forms a band. A dark line will appear in the reflected band if the SPR occurs within the spread angles. An intensity profile of this band can be monitored and plotted against the range of angles as shown in Figure 1-5.

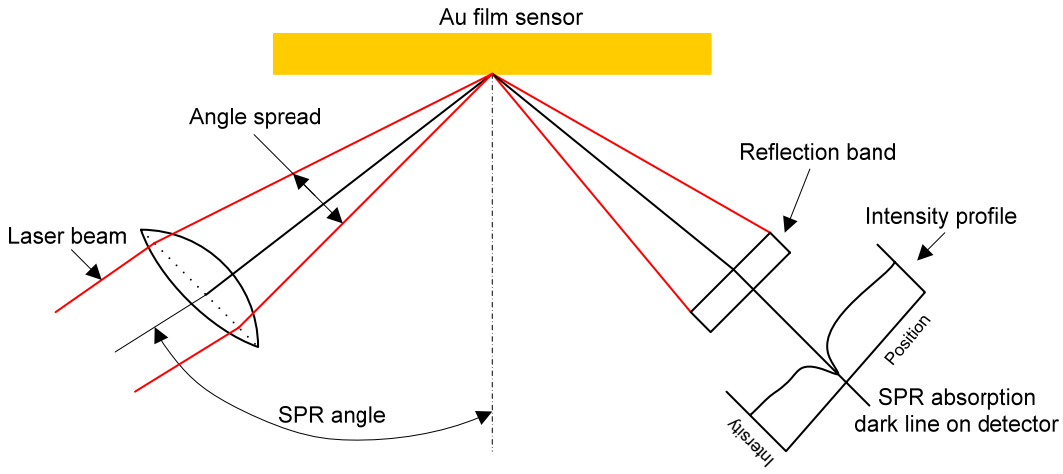

Figure 1-5: Principle of SPR detection in the mode of measuring the SPR angular shift [W1]

Many researchers have worked on developing SPR sensors for studying various kinds of biological reactions, and many reports have been published. The first application of SPR in biosensing was demonstrated in 1982 and the first commercial SPR sensor was introduced in 1990's [148,149]. Biosensing Instrument Incorporated uses a different approach to detect the SPR angle change, for example, using the position-sensitive detector. Only the position shift of the dip is measured, so it offers a highly sensitive detection scheme to measure extremely small angle changes of the SPR. In the range of the SPR angle spread, the system delivers exceptionally high angular resolution in its measurement [150]. Like Figure 1-6 illustrates, SPR is observed as a sharp shadow in the reflected light from the surface at an angle that is

dependent on the mass of material at the surface [150]. When biomolecules bind to the surface and change the mass of the surface layer, the SPR angle will shift (from I to II in the lower left-hand diagram). This change in resonant angle can be monitored non-invasively in real time as a plot of resonance signal (proportional to mass change) versus time [150].

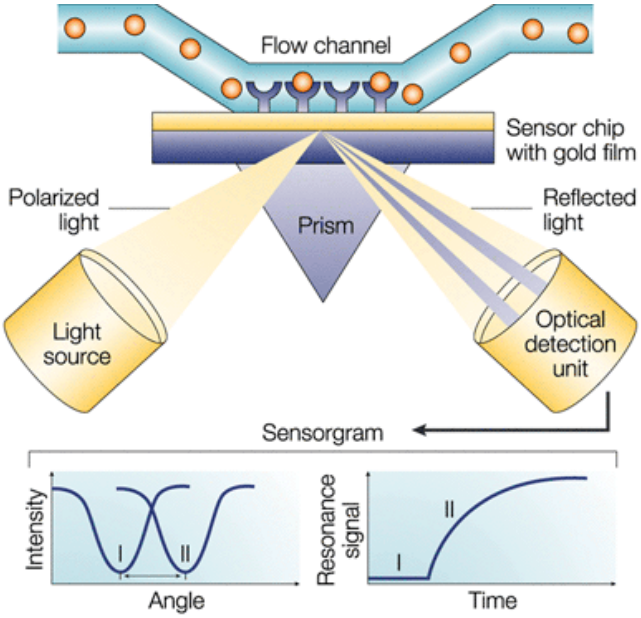

Figure 1-6: Schematic of SPR sensing method [147]

SPR has some advantages over other method, such as SPR can handle turbid or opaque samples and SPR sensor has the continuous monitoring capability which helps in studying the kinetics of the detection process. The main challenge in SPR is its poor sensitivity when dealing with low molecular weight analytes (less than 1000 Dalton) because the increase in the refractive index produced by the adsorption of these small molecules may not be sufficient to be detected directly (current direct SPR biosensors are limited to detection of about 1 pg/mm^2 surface coverage of biomaterial) [6].

Mass spectrometry: The mass spectrometry technique can be used for measuring the molecular mass of a sample. And structural information of the sample can be generated using certain types of mass spectrometers. The mass spectrometry can be applied to identify and, increasingly, to precisely quantify thousands of proteins from complex samples, which is believed to have a broad impact on biology and medicine [151]. But, the size of these equipments is large in general, which makes

them unfeasible for field applications which require portable devices, especially for biosensors.

Acoustic wave sensors: The detection mechanism of acoustic wave sensors is a acoustic (mechanical) wave. The velocity and/or amplitude of the acoustic wave can be affected by the changes of the characteristics of the propagation path when the acoustic wave propagates through or on the surface of the material [152]. Based on the sensor, the changes of velocity can be monitored by measuring the frequency or phase characteristics, and then it can be analyze based on the corresponding physical quantity being measured [152]. Virtually all acoustic wave devices and sensors use a piezoelectric material to generate the acoustic wave. The technology has been utilized in the commercial range for more than 60 years. And the high mass sensitivities of acoustic wave devices make them an attractive platform for monitoring immunochemical and other biomolecular recognition events. However, not all acoustic wave devices are suitable for liquid operation. If the sensor has surface normal deformations and the velocity of acoustic wave is greater than the compressional wave velocity of sound in liquid, then they can couple to compressive waves in the liquid and cause severe attenuation of the sensor signal. In contrast, devices in which surface particle motion is parallel to the sensor surface dissipate energy into the liquid primarily by viscous coupling, which does not produce severe losses and therefore are suited for liquid phase sensing.

Electrochemical techniques: Electrochemistry is to study the chemical reactions that take place in a solution at the interface of an electron conductor (a metal or a semiconductor) and the electrolyte. In the process, electrons transfer between the electrode and the electrolyte in solution. Macro scale electrochemical sensors have been used in chemical and biological sensing for a very long time. Electrochemical biosensors build a bridge between the powerful analytical methods and the recognition process of the biological specificity. Electrochemical sensors can be classified into amperometric, potentiometric or conductometric sensors based on whether current, potential or resistance is being measured during an electrochemical reaction (oxidation or reduction) between the analyte of interest and the electrode surface. Semiconductor field effect devices can also be used in biosensing either as

capacitors or as field-effect transistors (FETs). Binding of charged molecules to the gate electrode changes the capacitance or the I-V characteristics of these devices.

The main adverse problems is long term stability and reliability associated with incorporation of liquid electrolytes, life time and cycle time issues due to small amount of reactants (consumable electrodes like Ag/AgCl). Secondly, non specific reactions taking place between the electro active impurities on the surface and the sample also limit the sensitivity of these sensors. [153] is a good and detailed reference of microfabricated electrochemical biosensors.

Surface stress sensors: Microcantilever surface stress sensors have lots of applications in medical flied. Integrated microfluidics enabled individual cantilever addressing in the array for selective functionalization. Hansen *et al.* were able to show that microcantilevers are sensitive enough to detect single base-pair mismatch in DNA hybridization [154]. Wu *et al.* developed a PSA detection assay using a single microcantilever at clinically relevant levels in a large background concentration of human serum proteins – albumin and plasminogen [85]. Yue *et al.* [110] showed that passivation of the backside with inert coatings like PEG is absolutely necessary in order to make reliable protein interaction measurement. More detailed applications have been introduced in the fore section. But this kind of biosensor must associate with some detection methods to measure and analyse the usable information gotten from the analyte, for example, optical method, piezoresistance, and capacitive method.

Optical methods

The invention of the atomic force microscope (AFM) in 1986 [155] and its impact on the fields of biotechnology and nanotechnology has created a new modality of sensing: the cantilever. The most simple way of measuring cantilever deflection resulting from surface stress between the analytes with cantilever to get some measured information is by optical beam deflection as in most AFM instruments [156].

In the optical beam deflection technique, a laser diode is focused on the end of the free cantilever and the reflected laser beam is monitored using a position sensitive

photodetector, as shown in Figure 1-7 [9]. The typical displacement sensitivity achieved using this technique is on the order of 10^{-9} m [8]. Fritz *et al.* demonstrated DNA immobilization and hybridization using microcantilever measured by optical deflection detection [157]. And Yue *et al.* demonstrated a 2D cantilever array with integrated microfluidics using a single laser source and a CCD camera for simultaneous interrogation of several hundred cantilevers for DNA and protein sensing [158]. The advantages are its simplicity, linear response, and lack of electrical connections. However it suffers some limitations. A calibration is needed in order to obtain the recorded signal in terms of the actual cantilever deflection. Index of refraction changes of the surrounding medium of the cantilever can produce artificial deflection and the technique cannot be used in opaque media such as blood.

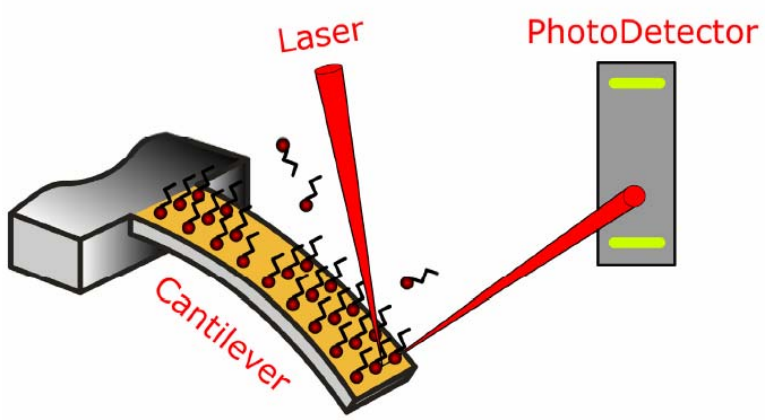

Figure 1-7: The optical beam deflection technique is used to monitor the deflection of the cantilever [9]

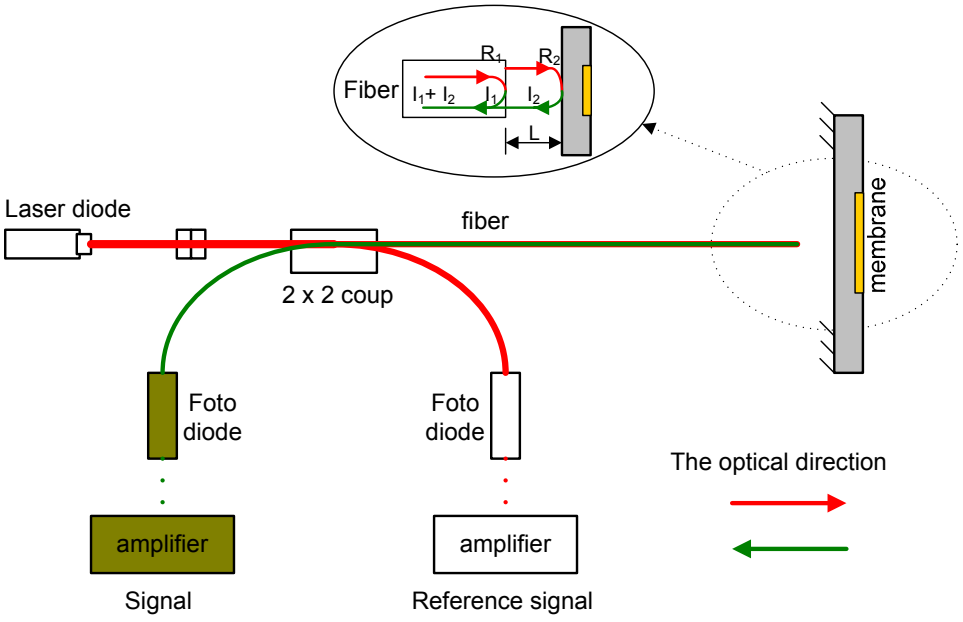

Figure 1-8: Schematic diagram of a fiber interferometer [160]

Another optical method which can attain better performance is interferometry [159]. When using a fiber optic interferometer [159,160], the interference signal from the reflected light of the cleaved end of the fiber optic and of the cantilever surface is a direct measure of the average cantilever displacement in the field of view. Deflection in the range of 10^{-11} m to 10^{-13} m can be measured [161]. Fiber optic interferometer is a mature technology and has many advantages, good performance, low loss, high bandwidth, safety and relatively low cost, for example, which is suitable for biosensors. The principle is as schematically shown in diagram Figure 1-8, the interference is formed inside an optical fiber. When the laser diode light passes at the fiber end-face, a portion is reflected off at the fiber/air interface (R_1) and the remaining light still passed through the air gap (L) with a second reflection occurring at the air/membrane interface (R_2). R_1 is the reference reflection named the reference signal (I_1) and the sensing reflection is R_2 called sensing signal (I_2). These reflective signals interfere constructively or destructively in the fiber due to the difference of the optical path length between the reference and sensing signals, which is called the interference signal [160]. Therefore, small deflection of the membrane causes a change in the air gap (L), which changes the phase difference between the sensing and reference signals producing fringes.

However, optical detection systems for cantilever arrays are still typically large and are more suited for bench-top applications than for portable handheld use. Nonspecific adsorption on the back side (non functionalized side) of the cantilever because of sensor immersion in liquid sample during measurement is a significant source of noise in these sensors.

Piezoresistance

Piezoresistivity is the variation of the bulk resistivity under applied stress. When a silicon cantilever is stressed because of its bending caused by surface stress, a highly doped region will change resistance in a sensitive way. The variation of cantilever resistance is typically measured using a DC-biased Wheatstone bridge. The advantage of piezoresistivity technique is that the sensor and the detection scheme can be easily integrated into lab-on-a-chip type devices. In addition it is more compatible with large array formats. Marie at al developed a cantilever system using

piezoresistive detection instead of optical deflection method for sensing DNA hybridization [162].

Nevertheless, this method possesses electrical connections which need to be protected for experiments performed in liquids and requires current to flow through the cantilever. This results in heat dissipation and thermal drifts which causes parasitic cantilever deflections.

Others

There are some less widely used and readout schemes existed methods [6], such as the capacitive method, piezoelectric method and electron tunneling. More recently, displacement detection methods for nanoscale cantilevers were implemented. Cleland *et al.* [163] developed a scheme based on capacitively coupling a nanobeam to a single electron transistor achieving sensitivity down to 10^{-14} m.

Label based techniques

Label based techniques use ‘tags’ or labels to detect a particular analyte in a background of other materials. Fluorescence, chemiluminescence and radioactive are three popular label based techniques in biosensors.

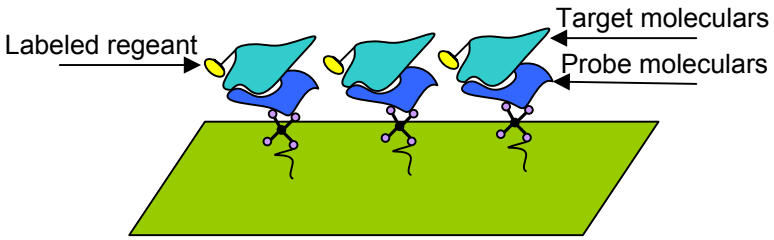

Figure 1-9: Schematic diagram of fluorescence: Surface with different probe molecules is exposed to solution with pre-labeled target molecules, presence of fluorophores on the surface indicates a specific binding reaction and the presence of a target molecule

Fluorescence: Fluorescence is the short-time (< 1 μs) category of luminescence, which is mostly exploited as an optical phenomenon in cold bodies. For doing this, the molecular component used absorbs a photon and can conesecutively emit a photon with a longer (less energetic) wavelength. Molecular rotations, vibrations or

heat can be produced because the absorbed photons have different energy; with the emitted photons, for example, the emitted light can be in the visible range even if the absorbed photon is in the ultraviolet range. The phenomenon depends on the absorbance and Stokes shift of the particular fluorophore.The fluorescence sensor's principle can be shown via an example in Figure 1-9: the probe molecules, such as antibodies, are immobilized onto the surface of probing microchamber using cross-linkers or covalent methods; the target moleculars with labelled reagent, such as antigens with fluorophore are loaded on the microchamber and they will bind to probes; and then the bound targets can be detected. Fluorescence is generally preferred and the most widely used detection method for reasons of sensitivity, stability, and availability of fluorescent scanners tailored for microarray use [164].

The disadvantage of this technique is that most fluorophores are bleached quickly upon exposure to light and are very sensitive to environment conditions such as solution's pH value. And both direct and indirect labeling methods have also their disadvantages. Indirect labeling is more complicated and time consuming, while fluorescence tags in direct labeling may be less stable and more disruptive to the labelled proteins as compared to small molecule tags in indirect labeling.

Chemiluminescence: Chemiluminescence or chemoluminescence is the phenomenon of light emission as the result of a chemical reaction, which leads to limited emission of heat (luminescence).

Chemiluminescence (CL) analysis promises high sensitivity with simple instruments and without any light source, so chemiluminescence has become an attractive detection method in μ-TAS in recent years [165-168]. On the other hand, many flow sensors based on CL reaction and molecular recognition using enzymes, which have great sensitivity in environmental, biomedical and chemical analysis, have been developed [169-174]. However, limited feature resolution because of signal bleeding and limited dynamic range is the reported drawbacks of this method [175]. Furthermore, sensing with chemiluminescence can be performed only once, unlike fluorescence-based methods which can be archived for future imaging.

Radioactivity: Radioactivity-based detection method is comparable to fluorescence method except that the labels are radioisotopes instead of fluorophores. Techniques using radioactive labels offer robust and reproducible protocols in applications that require ultimate sensitivity and/or resolution. Quantification of results is possible by the following exposure of signal to autoradiography film or reusable storage phosphor screens in automated imaging systems. However, automated liquid handling of radioactivity is difficult due to the need for safe handling and disposal of radioactivity, and is generally limited to manual, low-throughput applications.

Conclusions for development process

Surface stress-based micro membrane biosensor is a relatively new class of sensors, which holds a lot of promise because the technique is based on the universal concept of free energy reduction occurring from binding reactions. This kind of biosensor allows the detection in opaque media and the miniaturization of the sensor to incorporate it in portable devices for point-of-use sensing. The technique is advantageous since the process does not require any labeling of target molecules or the addition of redox probes.

Microfluidic devices are comprised of simple channels or chambers into complex components that can load the culture media and buffer, and perform digital logic, individually culture cells, and determine optimal reaction conditions, and much more. All these offer the advantages of small size for miniaturization and parallelization of devices. Furthermore, this small size opens the door to the potential of portable devices. With these advantages, the idea of biosensors can start to become a reality. Such devices would be very useful to researchers, clinical laboratories, and point-of-care clinicians in remote and/or resource-poor settings.

Labeling of biomolecules with fluorescent or other similar tags for detection can result in sample losses during the labeling and purification process and occasional loss of functionality, especially in proteins and other small molecules. Label-free detection technique can conquer the disadvantage, and the optical interference method is easy and simply to operate and high presicion to detect the deflection of membrane for getting the information/properties of the biological analytes.

Chapter 2 Biosensor Design

This chapter describes the detailed research to the design of the surface stress based micro membrane biosensor. Section 2.1 is on the biological environmental requirement for biological biosensors. The theory of surface stress utilized in the biosensor is introduced simply in section 2.2. Conceptual design of the whole biosensor is proposed in section 2.3. Section2.4 and 2.5 is on the biosensor design and on the microfluidic design respectively.

2.1 Biological environmental requirement

Mammalian cells or molecules, either from animasl or humans, require special environments for survival. The major environmental requirements include the substrate material, the temperature, the physiochemical properties of the medium, and the dissolved gas mixture [176] to be adequate. Additionally, the culture environment should be kept aseptic (free from invading microorganisms), and the media should be prohibited from contact with noncytotoxic materials. These requirements are discussed in more detail in the following subsections. And all of these must be considered for the design of the biosensor.

2.1.1 Substrate

To some biosensor, the analytes must contact with the interface of substrate to analyze them and thus require attachment to a substrate in order to survive, spread, and grow. Sometimes, cells typically attach to the extracellular matrix proteins that are either contained in the culture media or excreted by the cells, they do not directly attach to the substrate [135]. It has been demonstrated that cells adhere better to surfaces with high free surface energies than those with low free surface energies [177]. In general, the method used to test the biological suitability of a substrate is to test the cellular growth on its surface. Cells are plated onto a control surface and onto the tested film, and then it can be detected if there are any discernible

differences by monitoring and analyzing the growth rates and morphology of cells [135].

Glass and single-use disposable plastics (such as polystyrene) are the standard substrates used in standard tissue culture [176]. Glass has been used since the beginning of cell culture as the substrate because of the characteristics of good optical properties, low cost, ease of sterilization, and favorable surface charge [176]. Disposable plastics, such as tissue-culture treated polystyrene, provide an uniform and consistent substrate that helps achieve reproducible cultures [135].

To some cell-biosensors, the variety of possible substrates is constrained by the available thin films in the photolithographic process. Thin films that have been shown to support cell adhesion and growth include PDMS, some organic photoresists [178], silicon dioxide [179], silicon nitride [180], and silicon carbide.

2.1.2 Temperature

The suitable temperature for a cell culture varies according to cell type and origin, but most mammalian cells will grow satisfactorily at 37 °C. Cells can withstand considerable temperature drops for short periods of times and some cells can be stored for up to a month at 4 °C using hibernation media [181] or for years at cryogenic temperatures [182]. Mammalian cells cannot tolerate higher temperatures and will die rapidly at temperatures above 40 °C because protein enzymes denature (lose their active conformational shape) although temperatures a few degrees below optimal do not affect viability [176]. Thus, it is important to keep the constant temperature or to regulate the temperature of biosensors to keep the cells living for performing cell related experiments. Because both the metabolism and growth rate of cells is temperature dependent, it is better for the regulation to maintain temperarture within ±0.5 °C [176].

2.1.3 Medium

For a normal mammalian cell, the culture medium should contain salts, glucose, amino acids, and vitamins. Some cells also require the addition of a serum (blood

component) that contains polypeptide growth and adhesion factors that promote cell growth and division. Further more, pH and osmolarity are another two important properties of the media. Cellular metabolism and electrophysiology are sensitive to changes in pH [183]. The carbon dioxide (CO_2) gas phase regulates the pH through the bicarbonate buffer system to a typical value of 7.4 [135]. The importance of osmolarity arises in sample injection, as care must be taken to adjust the osmotic strength of the sample to limit osmotic stresses across the cell membrane [176]. Consistency to within ±10 mOsm/l should be maintained although most cells are tolerant of osmolarities in the range of 260 mOsm/l to 320 mOsm/l [176].

2.1.4 Gas phase

There are two most significant constituents of the gas phase for living cells: one is oxygen, a metabolite, another is carbon dioxide, a metabolic waste product. Oxygen is necessary for the metabolism of eukaryotic cells and consumption rate of human cells is approximately 20 amol/cell/sec to 100 amol/cell/sec (Table 2-1) [135]. Carbon dioxide is not only a waste product of cellular metabolism but is also required for most cell types to regulate the pH through the bicarbonate buffer system.

Table 2-1: Type cellular oxygen consumption rates [135]

Cell Origin	Oxygen Consumption Rate [amol/(cell·s)]	Reference
Human Skin	18 – 27	[184,185]
Human Heart	27	[184]
Human Lung	66	[184]
Human Conjunctiva	48	[184]
Human Liver	83 – 123	[184,185]
Human Intestine	36 – 110	[184,185]
Chick Heart	50 – 150	[184]

Oxygen partial pressures *in vivo* for blood leaving the lungs is approximately 13 kPa, and this value drops to approximately 5 kPa after passing through tissue capillaries [186]. Although the optimal oxygen partial pressure for maximum growth *in*

vitro varies with cell type, a range of 5 kPa to 20 kPa is satisfactory for the metabolic requirements of most cells [187]. At lower oxygen tensions, the impaired cellular function and activity can be activated because the cell's metabolism may more depend on the anaerobic metabolic pathways under the condition. When oxygen tensions above approximately 35 kPa (varies by cell type), the inhibition of cell growth and cellular degeneration can occur after 48 hours of exposure [188].

The carbon dioxide pressure of the medium is also important due to its involvement in the bicarbonate buffer system (Equation 1 [135]). The bicarbonate buffer system is used to regulate the pH of the blood, and bicarbonate itself has been proved that it is a necessary metabolite for the long term growth and survival of most cells [135]. The range of 5 kPa to 6 kPa versus an atmospheric value of ≈ 0.1 kPa is the typical partial pressure for carbon dioxide in blood. A decrease in carbon dioxide partial pressure from typical blood values to atmospheric would result in a shift of the equation to the left, resulting in the depletion of carbonic acid (H_2CO_3) and bicarbonate (HCO_3^-) [135] .

$$CO_2 + H_2O \Leftrightarrow H_2CO_3 \Leftrightarrow HCO_3^- + H^+ \qquad (1)$$

Because bicarbonate plays an important role in the cellular metabolism, the combination of bicarbonate and a regulated carbon dioxide headspace (air volume above the culture media) is used as the buffer system of most culture media. The pressure from 5 kPa to10 kPa is the typical carbon dioxide partial pressure range and the appropriate concentration of bicarbonate is added to regulate the pH within the range of 7.4 ± 0.2 [135].

However, the timescales of bicarbonate depletion is not deleterious or in bicarbonate-independent cells, it can use the carbon dioxide independent buffer in reality which may be preferable since bicarbonate can form precipitates with heavy metals and other compounds [135]. For the bicarbonate buffer system, there are several carbon dioxide independent alternatives. Each celluar buffer must be tested because the sensitivity of cells to different buffers varies. The most commonly used is HEPES (N-2-hydroxyethylpiperazine-N'-2-ethanesulfonic) acid which has a pK_a of 7.31 at 37 ºC [135].

2.1.5 Aseptic environment

It needs the order of twenty hours to grow a typical mammalian cell, which is ten times longer than that of yeasts. The shorter cycle microorganisms can exponentially outgrow if not prevented, such as bacteria, yeasts, mycoplasmas, and fungi. Viruses and phages can cause disruption to the normal function and activity of the cells. Aseptic techniques including the careful use of sterilized equipment in a sterile environment are necessary to prevent unwanted microorganisms from access to the culture during the operational lifetime.

2.1.6 Cytotoxicity

Cytotoxic materials leach physiologically significant amounts of toxins over the duration of the biosensor's lifetime. Hence, an additional important requirement to all contacted materials with the culture medium is the absence of cytotoxicity. Namely, the materials of the biosensor must not dissolve in media nor leach more quantity of other substances; otherwise it will produce some effect on the metabolism, growth rate, or viability of the cells.

2.2 Theory of surface stress

Surface stress [189, 190] is a macroscopic quantity that is governed by microscopic processes. Although being a macroscopic quantity, the measurement of the surface stress involved in a system can lead to insight into the microscopic mechanisms basic for the generation of surface stress without detailed knowledge of the atomistic processes involved. Recent investigations of surface reconstruction, interfacial mixing, and self-organization at solid surfaces have renewed interest in the study of surface stress [191-195]. Now the surface stress existing between biological molecules, cells and some special functional materials has been used in the biosensors for biological and medical research based on the surface stress analysis.

Biological sensing of numerous analytes based on surface stress can be achieved using cantilever or membrane as the sensitive element of sensors. It is possible to

sensitize one surface of the sensititive element differently than the opposing surface. When the analytes of interest interact with the sensitized surface, a surface stress is induced, and the cantilever or membrane bends due to the different surface stresses acting on both sides of the cantilever or membrane. The sensor's specificity, i.e. the sensitivity of the sensor to a specific analyte, is determined by the chemical functionalization of the sensitized surface of biosensors. Very specific surface functionalizations can be achieved using molecular self-assembled monolayers (SAMs) as sensing layers assembled on the surface of biosensor sensitive element. Thiol-chemistry has been favored as a versatile method of sensitizing a surface.

Alkanethiol [$HS(CH_2)_nCH_3$] SAMs are one of the most widely studied self-assembled systems because of their versatility and stability [196-198]. Alkanethiol SAMs for long time have been viewed as a simple model system whose properties can be applied to more complex self-assembled systems. Alkanethiol SAMs provide stable and ordered structures on surfaces, which are envisaged to be useful in a broad range of applications, including protective coatings, wetting control, friction and adhesion control, electronics [197, 199, 200], improve biocompatibility and provide sufficient bending stiffness.

The functionalized SAMs used as the sensing layer on the cantilever surface is both receptive (sensitized to react with analytes) and responsive (by allowing the transduction of the surface stress to the cantilever beam) [201-204]. This functionalized SAMs can be formed on a gold-coated cantilever, for example, turning it into a sensor sensitive to specific analytes. Functionalized alkanethiol SAMs used as the sensing layer when formed on the gold-coated cantilever surface is depicted in Figure 2-1 [9], receptor groups can be immobilized on a gold surface using thiol chemistry. In this case, the receptors only interact with 'green triangular' bio-targets, and nothing else. When these thiolated species bind to a gold-coated cantilever, the induced surface stress will vary as a function of the analyte concentration or structual characteristic. In any case, an understanding of the origins of the surface stress in these thiolated systems will lead to better design and optimization of this class of sensors.

The self-assembly of alkanethiol SAMs onto gold surfaces is driven by the molecule's thiol head group's high affinity for gold. This sulphur atom forms a strong covalent bond (~185 kJ/mol) with gold surface atoms [205], following dissociation of the S-H bond, just like in Figure 2-2 [9].

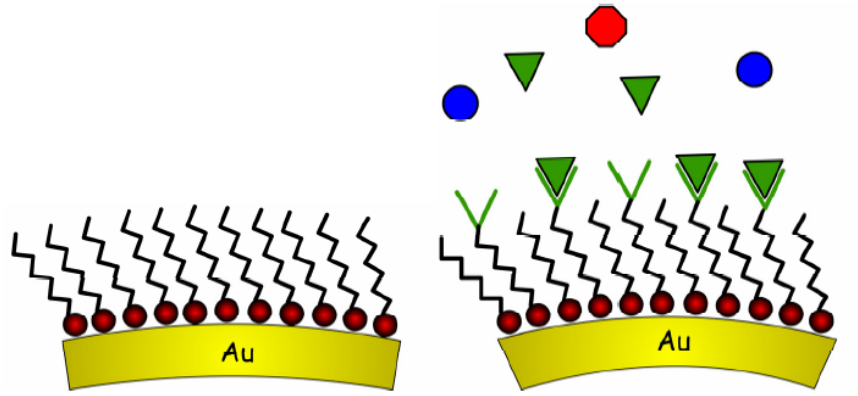

Figure 2-1: Depiction of an alkanethiol SAM and a functionalized SAM used as a sensing layer [9]

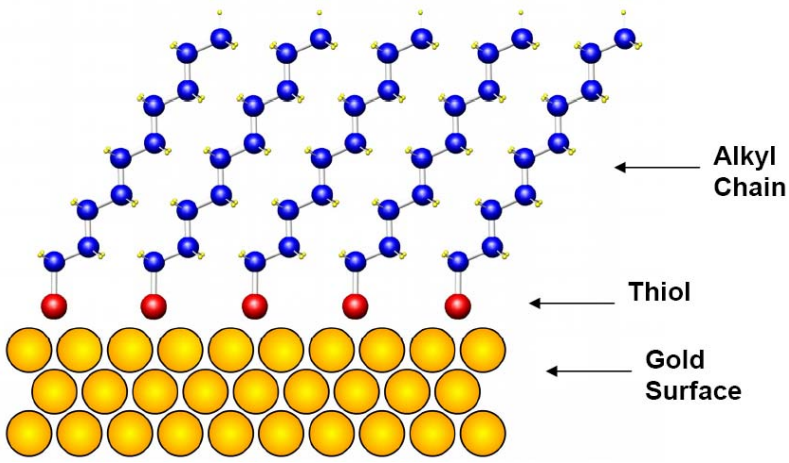

Figure 2-2: Side view of an alkanethiol SAM on gold [9]

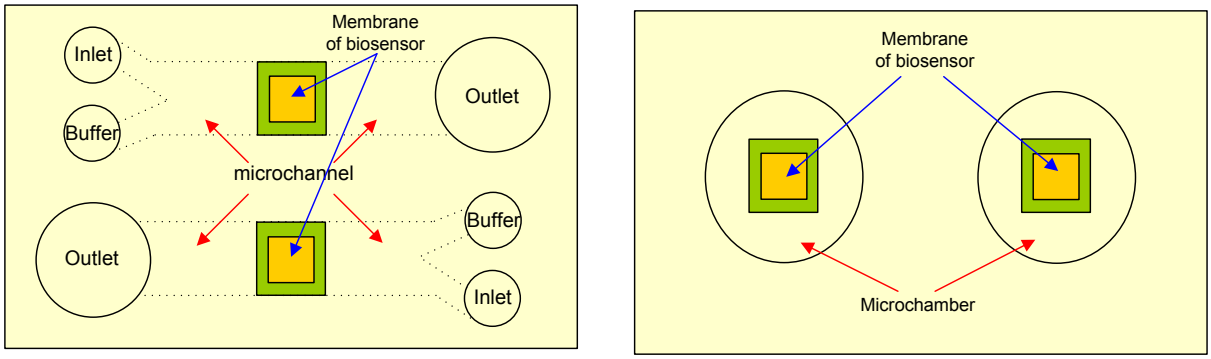

Figure 2-3: The schematic diagram of two kinds of structure in one wafer

2.3 Conceptual design

The conceptual design of biosensor in this thesis is illustrated in Figure 2-3; two kinds of biosensor structure are located on one wafer to make sure the later experiments can be done easily and successfully. For the first biosensor chip, the microfluidic structure is made of inlets, outlets, buffers and microchannels: the inlets are used to load medium and analytes; the buffers are to clear chip after experiment; the waster is drained from outlets. The mcirofluidics of second biosensor chip consists of only two chambers over the membranes and all the manipulations will be realized in vertical direction.

From the conceptual design it can also be seen that each biosensor chip contains two micro-membranes, one acts as the active membrane and the other as reference. Figure 2-4 illustrates the operational concept of the biosensor. The active membrane is sensitized to react with specific analytes. The selective biochemical reactions between the analytes and the membrane will induce a surface stress change that causes the membrane to deflect. The analytes will not present on the reference membrane, it is only used to remain sensitive to other environmental factors that can also result in a deflection of the active membrane, such as temperature variations (bimetallic effect), laminar or turbulent flow around the membrane, vibrational (including acoustic) noise, non-specific binding (including the swell induced by solution) and so on. The differential signal is solely due to the interaction of the analytes with the membrane. This design has very sensitive surface stress measurements for analytes detection, which is one main novelty of the biosensor.

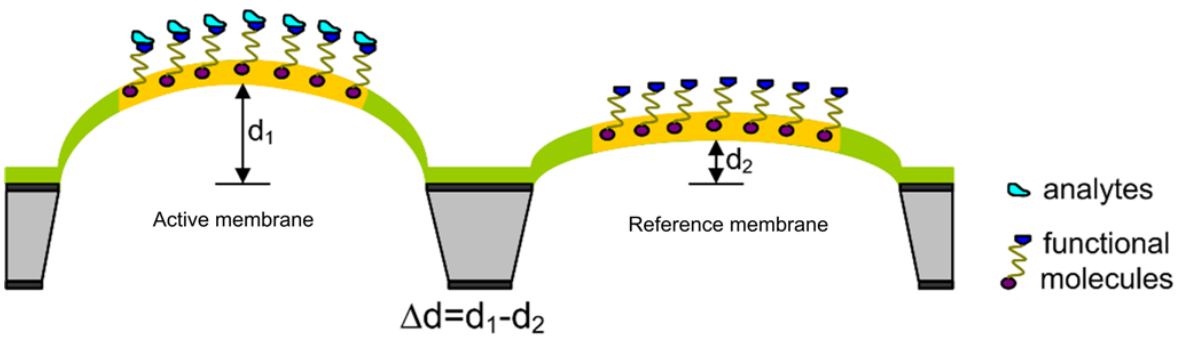

Figure 2-4: The operational concept of the PDMS membrane biosensor

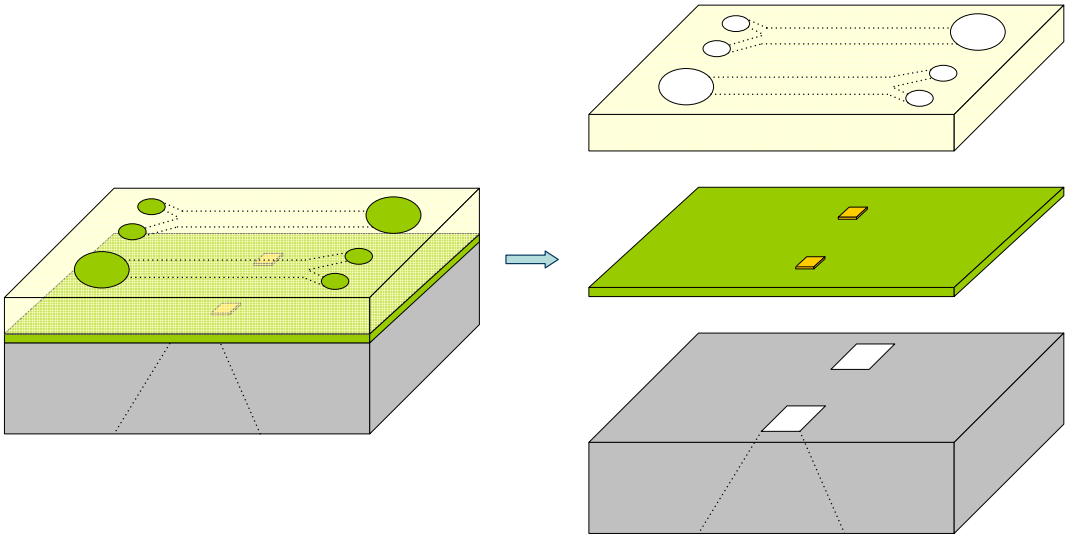

(a) The 3D schematic diagram of the first biosensor structure

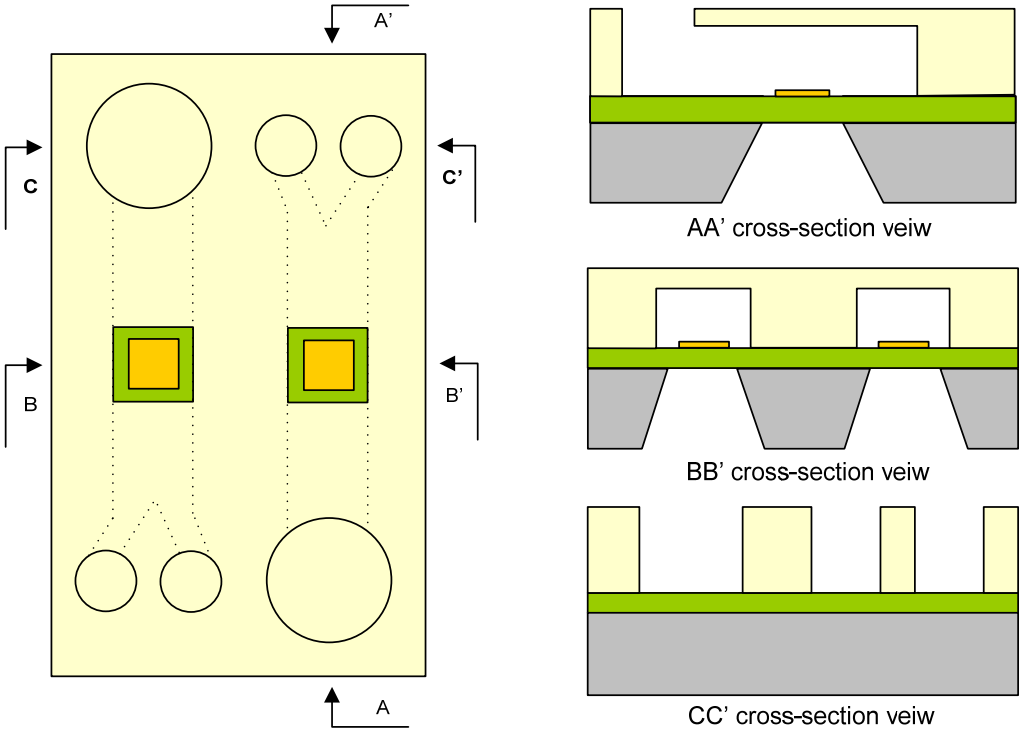

(b) The top view and cross-section view of the first chip

Figure 2-5: The illustrated diagram of the first kind of biosensor

Figure 2-5 shows the three-dimensional (3D) schematic diagram and cross-section view of the first kind of biosensor. It consists of two layers: microfluidic layer and sensor layer made of thin film layer and substrate. The thin membrane as the crucially sensitive element of the biosensor is formed by the thin film, partly gold coated on its surface, and the trapezoidal structure in substrate. The trapezoidal

holes in substrate can be etched using standard microfabrication techiques. The gold layer is essential to form the SAMs (the formation of SAMs will be introduced in chapter 5) to react with special analytes. The SAMs can improve the biocompatibility of the biosensor and provide sufficient bending stiffness. There are two microfluidic systems in each microfluidics, which contains inlets, outlets, buffers and microchannels.

The second kind of biosensor is equal to the first kind, illustrated in Figure 2-6, except the arrangement of biosensor membranes and microfludics. There is no inlet, outlet and microchannel in the microfluidic layer, only two chambers over the membranes. All the manipulations will be realized in vertical direction.

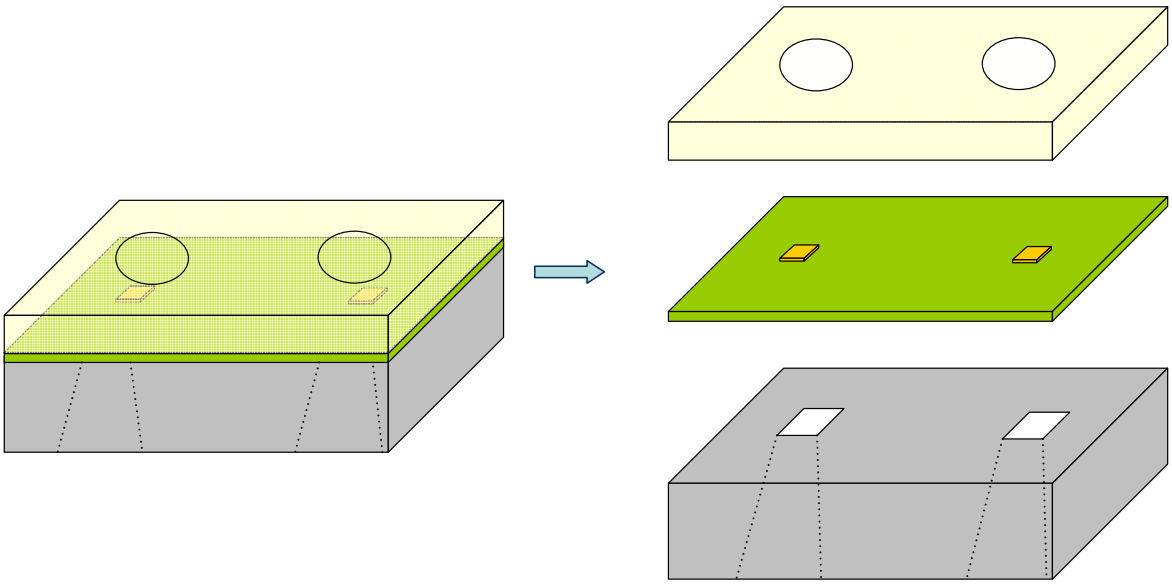

(a) The 3D schematic diagram of the third chip

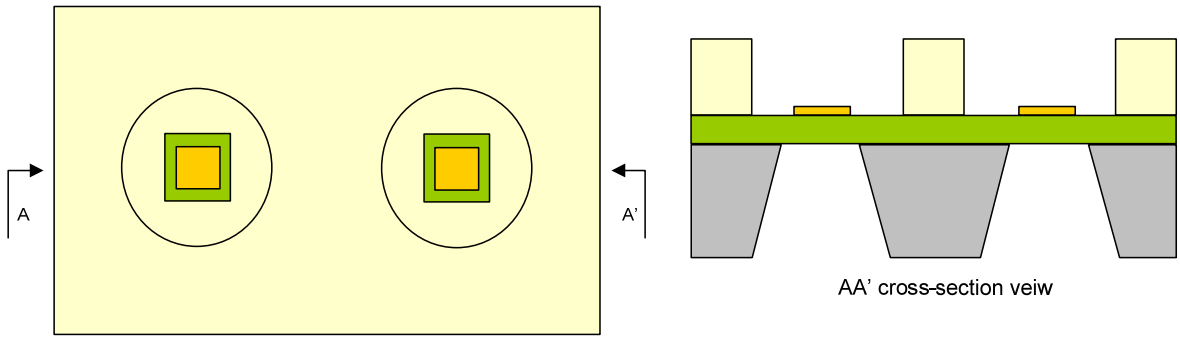

(b) The top view and cross-section view of the third chip

Figure 2-6: The illustrated diagram of the second kind of biosensor

2.4 Biosensor design

The sensitive element of biosensor plays a decisive role in the whole biosystem. Hence, the prime work is the design of this sensitive element, including the structural selection, the material selection and the parameter optimization.

2.4.1 Theory of the sensitive element model

Cantilever, beam and membrane are the three structures most commonly used as the sensitive element of a sensor. Each structure is described by its own deflection theory.

The typical cantilever is that one end is fixed and another end is free, it is shown in Figure 2-7a. The load exerted on the cantilever can be classified into concentration load (Figure 2-7b) and uniform load (Figure 2-7c). Based on the theory, the deflection is dissimilar to the two different kinds of load, theoretical formulas (1) (2) for concentration load and formulas (3) (4) for distribution load [206].

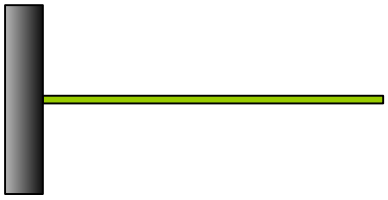

(a) The schematic diagram of cantilever

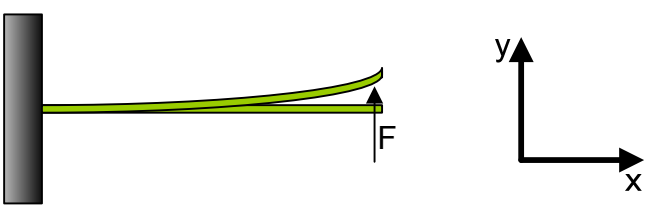

(b) The schematic deformation caused by concentration load

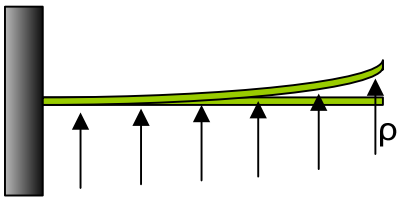

(c) The schematic deformation caused by distribution load

Figure 2-7: The sketch-map of cantilever structure

$$y(x)=\frac{F}{6EI}\left(3x^2L-x^3\right) \quad (1)$$

$$y(x)=\frac{\rho x^2}{24EI}\left(6L^2-4Lx+x^2\right) \quad (3)$$

$$y_{\max} = \frac{FL^3}{3EI} \quad (2) \qquad y_{\max} = \frac{\rho L^4}{8EI} \quad (4)$$

Where:

L = the length of cantilever

t = the thickness of cantilever

I = the moment of inertia of cantilever and $I = \frac{1}{12} wt^3$ (5)

w = the width of cantilever

E = the Young's modulus of cantilever

F = the force

ρ = distribution load (N/m)

When the stress is surface stress, the microcantilever sensor response (y), i.e. microcantilever tip deflection, for a surface stress change (ζ) is given by Stoney's formula (Equation 6).

$$y = \frac{3\zeta(1-\nu)}{E}\left(\frac{L}{t}\right)^2 \quad (6)$$

Where:

L and t is the length and thickness of microcantilever;

E is theYoung's modulus;

υ is the the Poisson ratio.

The cantilever can become the beam structure when its other end is also fixed, like shown in Figure 2-8a. To the two kinds of load, concentration load (Figure 2-8b) and uniform load (Figure2-8c), reference [206] has deduced the deflection formulas (7) (8) for concentration load and (9) (10) for distrubition load.

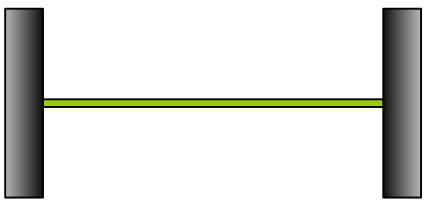

(a) The schematic diagram of cantilever

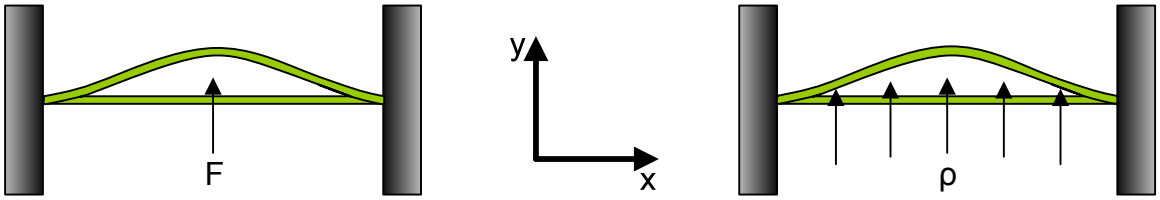

(b) The schematic deformation caused by concentration load

(c) The schematic deformation caused by distribution load

Figure 2-8: The sketch-map of beam structure

$$y(x)=\frac{Fx}{48EI}\left(3Lx-4x^2\right) \quad (7)$$

$$y_{\max}=\frac{FL^3}{192EI} \quad (8)$$

$$y(x)=\frac{\rho x^2}{24EI}(L-x)^2 \quad (9)$$

$$y_{\max}=\frac{\rho L^4}{384EI} \quad (10)$$

Where:

L = the length of beam

t = the thickness of beam

I = the moment of inertia of beam and $I=\frac{1}{12}wt^3$ (5)

w = the width of beam

E = the Young's modulus of beam

F = the force

ρ = distribution load (N/m)

When all the edges of the structure are fixed, it becomes membrane: rectangular membrane (Figure 2-9a), or square membrane (Figure 2-9b) and or round membrane (Figure 2-9c). Figure 2-9d illustrates the cross-section view of the membrane structures. Deflection formulas (11) [206] and (12) [207] can be deduced when the load is uniform load, such as pressure.

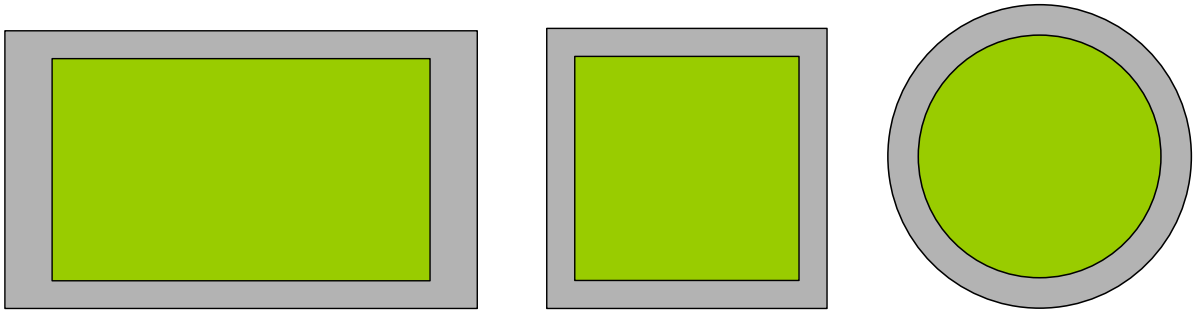

(a) Rectangular membrane (b) Square membrane (c) Round membrane

(d) The cross-section view of membrane (e) The schematic deformation due to uniform load

Figure 2-9: The sketch-map of membrane structure

To the round membrane

$$y_{\max} = y_{center} = \frac{3pr^4(1-\nu^2)}{16Et^3} \quad (11)$$

To the square membrane

$$y_{\max} = y_{center} = \frac{12pL^4(1-\nu^2)}{Et^4} \quad (12)$$

Where:

r = the radius of round membrane

L= the half length of square membrane

t = the thickness of membrane

v = Poisson's ration

E = Young's modulus

p = the pressure (N/m^2)

Based on the deflection theory, the cantilever is easiest to deflect (most compliant), the beam under this aspect takes the second place and the membrane is last when their basic parameters are same. But the cantilever and beam geometry is not optimal for sensing in liquid media, which is common in biological applications, just like noted in chapter 1. The main limiting reason is that the entire cantilever or beam is immersed in the fluid and some non-specific adsorption on the back side of the cantilever or beam drastically reduces the signal to noise ratio (SNR). Hence the membrane is selected as the sensitive element of the biosensor that is designed and fabricated for the work of this thesis. The sensitivity problem can be solved by using material with lower elasticity modulus, such as SU8, PMMA and PDMS. For easy fabrication and manipulation, the square membrane is the chosen geometry.

2.4.2 Material selection of the membrane

One intention of the design process is to select the best material to optimize the sensor signal, i.e. to maximize the deflection for a given surface stress change, when the basic parameters of membrane are same. PDMS, silicon, aluminium nitride, silicon nitride and PMMA are the commonly used membrane materials. The deflection comparision of different membranes by the simulation method can intuitively show which material is better as the membrane material. According to the front discussion, a surface stress-based structure has two basic layers in addition to SAMs: submaterial layer and contact, i.e. gold layer. Figure 2-10 illustrates the schematic diagram of surface stress-based square membrane.

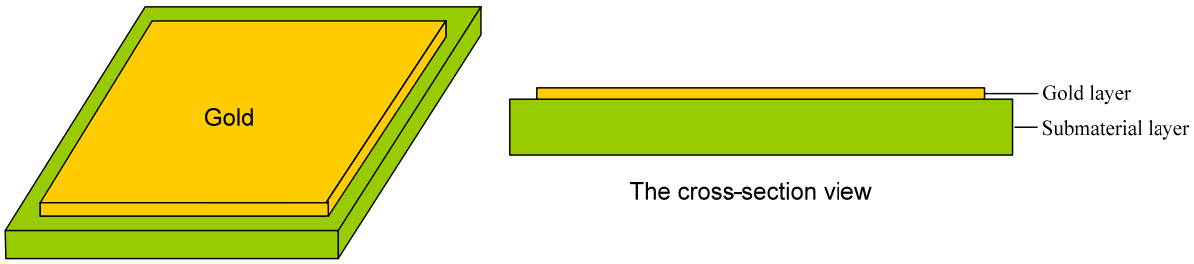

Figure 2-10: The surface stress-based square membrane

From basic membrane theory, it is obvious that the deflection of a composite membrane is a function of the mechanical stiffnesses of both the gold and the submaterial, and the membrane stiffness for surface stress loading is directly proportional to $(l_m/t_p)^2$, where l_m is the membrane length and t_p is the membrane thickness. The gold layer on top of the membrane increases the membrane stiffness and, hence, should be as thin as possible. During the research, the submaterial thickness and the gold thickness is temporarily set 100 nm and 30 nm respectively to simulate which material is better for optimal deflection.

Finite element (*FE*) analysis software ANSYS® was used to modelize the mechanical behaviour of composite membranes. The details of material and *FE* model properties are listed in Table 2-2. The *FE* model built in ANSYS® software is illustrated in Figure 2-11, and the simulation program is given in Appendix I. In the ANSYS® *FE* analysis software, there is no direct method to apply the surface stress load. Hence, an equivalent temperature load instead of surface stress load was applied to the

membrane. The equivalent temperature load (T) for a surface stress load (ζ_s) was evaluated using Eq. (13).

$$T = \frac{\zeta_s}{E_g \alpha_g T_g} \qquad (13)$$

E_g, α_g and T_g are the *E*, *CTE* and thickness of gold, respectively.

The material coefficient of thermal expansion (*CTE*) except the gold layer was set to zero for the analysis [208], since the temperature changes here represent surface stresses, and "real" thermal effects in the application on cells will be avoided by homoeostasis, which beneath other aspects means constant temperature. It has to be pronounced that under any application of the model results constant temperature of the membrane has to be assured, to avoid that the membrane serves as a thermometer. Based on (13) formula, $\Delta T/\Delta\zeta$ is around 45, which means that the membrane deflection induced by the change of surface stress is greater than by the change of environmental temperature.

Table 2-2: Material and *FE* model properties [P1]

Material / Parameters	Si	AlN	SiN	PMMA	PDMS	Gold
E (GPa)	165	308	310	5	0.007	78
Poisson ratio	0.22	0.28	0.27	0.43	0.48	0.44
Length×Width (um)	200×200	200×200	200×200	200×200	200×200	variable
Thickness (nm)	100	100	100	100	100	30
Element type	Solid186	Solid186	Solid186	Solid186	Solid186	Shell93

Once a typically compressive surface stress (vectorial, but unconventional unit, cp. Chapter 1) of 10 mJ/m^2 [208] is loaded on the model geometry based on (13) formula, the deformation of the membrane can happen as a result of the surface stress load. One deformed shape of the membrane is shown in Figure 2-12. The center deflections of the membrane with different submaterials are plotted in Figure 2-13.

Figure 2-13 shows that the center deflection of membrane is one function of the geometry of coating gold. With the decrease of submaterial's *E*, the deflection of membrane becomes larger and the ratio ($P_{gold}/P_{submaterial}$, P : the side length of the square geometry) making the membrane reach the maximal deflection becomes larger too, from 0.65 to 0.9. The blue short dot line indicates the upward tendency. However, the size of gold making the deflections reach maximum is equal in some certain range of *E*, just like the first three black round dots.

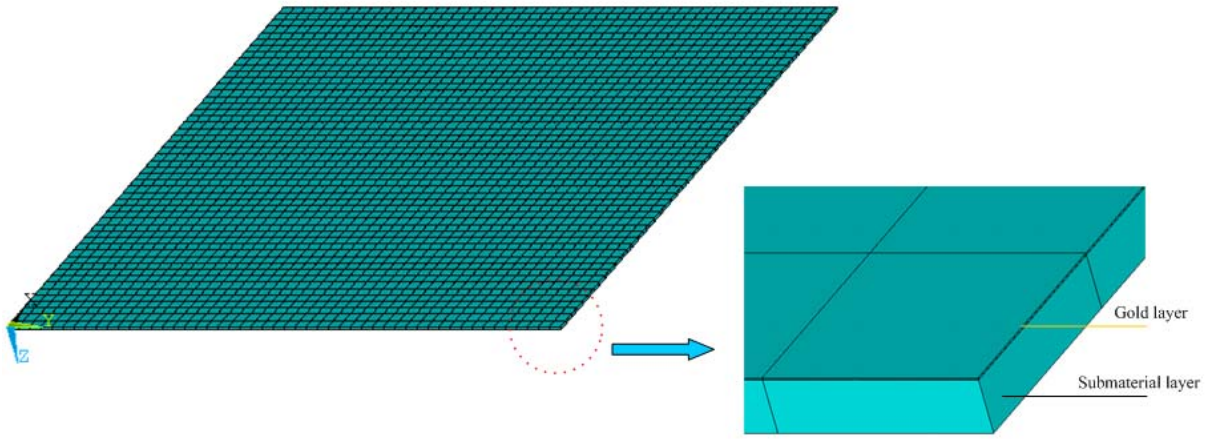

Figure 2-11: *FE* model (1/4 symmetry) of the membrane with submaterial layer and gold layer

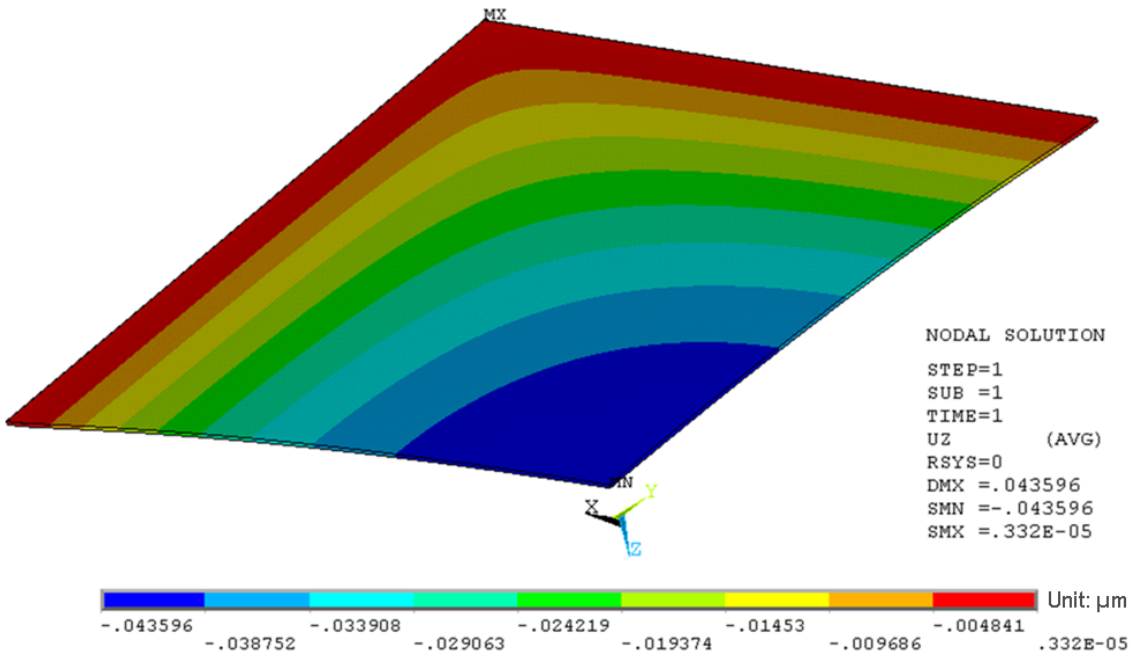

Figure 2-12: Simulation diagram of the deflection of the membrane introduced in fig. 2-11 due to surface stress

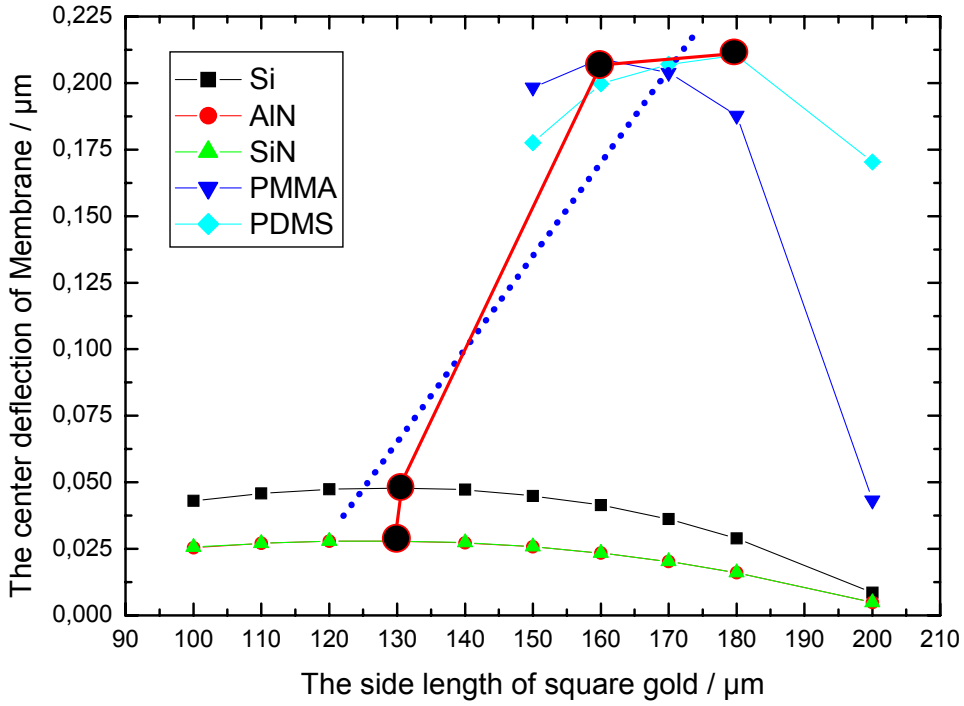

Figure 2-13: The center deflection of membrane with different submaterial as the function of geometry of coating gold [P1]

PDMS is the best material selected as the sublayer of membrane based on the simulations. Further, PDMS has the characteristic of biocompatibility and ease of processing [209-213]. PDMS can also be easily processed to have a range of Young's modulus values that are physiologically relevant [214]. Table 2-3 gives the total properties of PDMS material. In the following section, detailed simulation will be done to decide the parameters of membrane for the optimation of the biosensor and the feasibility of fabrication.

Table 2-3: Material properties of PDMS

(The raw material of PDMS consists of two parts: base and hardener. The ratio (e.g. 5:1) represents the ratio of base to hardener.)

Property		Numerical value and unit	Reference
Mechanical Properties	Density ρ	0.918 g/cm^3 — 0.987 g/cm^3 5:1 0.952 g/cm^3 7.5:1 0.918 g/cm^3 10:1 0.920 g/cm^3 12.5:1 0.927 g/cm^3 15:1 0.987 g/cm^3	[215]

	Specific Gravity	1.05 at 25℃	[216]
	Young's Modulus *E*	8.7 ×10^5 Pa — 3.6 ×10^5 Pa 5:1 8.68 ×10^5 Pa 7.5:1 8.26 ×10^5 Pa 10:1 7.50 ×10^5 Pa 12.5:1 5.49 ×10^5 Pa 15:1 3.60 ×10^5 Pa	[215]
	Shear Modulus *G*	1000 kPa — 3 MPa ≈ 205kPa at RT 1.1 kPa/K change of *G* with T	[217]
	Poisson ratio υ	0.5 $\nu = \frac{E}{2G} - 1$ with E = 750 kPa and G = 250 kPa	[218]
	Tensile / Fracture Strength	2.24 MPa	[219]
	Dynamic Viscosity	3.9 Pa·s at 25℃	[219]
Electrical Properties	Volume Resistivity ρ	2×10^{14} Ω/cm	[216]
	Electric Conductivity κ	4×10^3 Ωm	[216]
	Dielectric Strength	14 V/μm	[217]
	Dielectric Constant	2.3 — 2.8	[219]
	Arc Resistance	115 *s*	[216]
	Loss Tangent δ	« 0.001 0.0009 at 100 Hz 0.001 at 100 kHz	[217] [216] [216]
Thermodynamic Properties	Expedient Service Temperature	-55 ℃－+200 ℃ -100 ℃－+100 ℃	[216] [217]
	Boiling Point	> 100 ℃	[220]
	Melting Point	-49.9 ℃－-40 ℃	[219]
	Thermal Expansivity a	20×10^{-5} K^{-1}	[217]
	Glass Transition Temperature T_G	≈ -125 ℃	[217]
	Specific Heat *c*	1.46 kJ/(kg•K)	[219]
	Thermal Conductivity	0.15 W/(m•K)	[219]
Chemical	Chemical Formula	$(H_3C)[SiO(CH_3)_2]_nSi(CH_3)_3$	[220]

Properties	Contact Angle with Water (H_2O) Contact Angle with Isopropanol (C3H8O) Contact Angle with Acetone (C3H6O)	90°－120° 18° 30°	[215]
Optical Properties	Transparency	transparent within the visible spectrum	[220]
	Index of Refraction *n*	1.4	[219]
Others	Wet etching method	Tetrabutylammonium fluoride ($C_{16}H_{36}FN$) + n-methyl-2-pyrrolidinone (C_5H_9NO) 3:1	[221]
	Plasma etching method	CF_4+O_2	
	Biocompatibility	Nonirritating to skin, no adverse effect on rabbits and mice, only mild inflammatory reaction when implanted	[222]

2.4.3 Decision of the square membrane parameters

For the optimal and practical purpose, a series of PDMS membranes with different parameters were studied using the *FE* analysis software ANSYS® based on the prior works and the simulation program in Appendix I. The value of surface stress applied in these simulations is still 10 mJ/m^2. Table 2-4 lists a serial of membrane parameters and their corresponding simulation results. The PDMS membrane deflections induced by surface stress are also plotted as a function of geometry of coating gold based on Table 2-4, shown in Figure 2-14.

Figure 2-14 illustrates the change tendency of membrane. The membrane deflection caused by surface stress becomes larger with the increase of PDMS size. For each defined set of PDMS parameters, the deflection changes along with the coating gold size and reaches its maximum at a special gold size, which were marked using the big green round point in Figure 2-14. But the ratio (P_{gold}/P_{PDMS}) that makes the membrane reach maximal deflection varies with the parameters describing gold and PDMS. Figure 2-15 shows clearly the ratio variation when the the gold has a fixed

thickness (20 nm) and PDMS thickness is 0.5 μm and 1 μm respectively. When the size of PDMS is 200 μm, 300 μm and 500 μm, the ratios are same even though the PDMS thickness is different. But, the ratios are different when the size of PDMS is 400 μm. Hence, the simulation is a very important process to obtain the optimal parameters for each defined membrane.

Table 2-4: The membrane parameters and the corresponding simulation results

The size of PDMS / μm	The thickness of PDMS / μm \ The size of gold / μm (length = width) \ Deflection / nm	The thickness of gold = 20 nm				
200		160	170	180	190	200
	0.5	50.358	52.361	53.955	55.155	48.189
	1	26.057	26.939	27.644	28.194	27.593
300		260	270	280	290	300
	0.5	119.57	122.13	123.975	124.66	105.451
	1	61.4	62.433	63.29	63.817	60.82
400		360	370	380	390	400
	0.5	217.797	220.852	223.172	222.928	180.638
	1	111.151	112.314	113.259	113.475	106.659
500		460	470	480	490	500
	0.5	344.45	347.039	349.137	346.952	280.067
	1	175.47	176.728	177.613	177.376	162.089

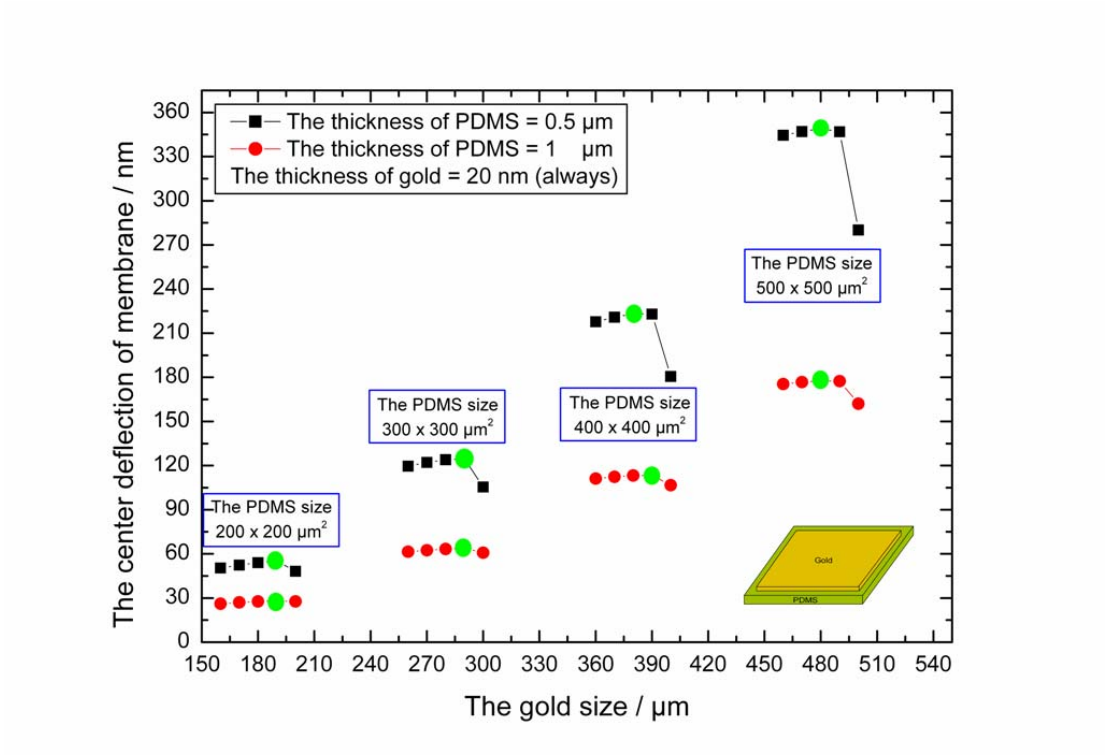

Figure 2-14: Membrane deflection caused by surface stress to different PDMS membrane parameters as a function of geometry of coating gold

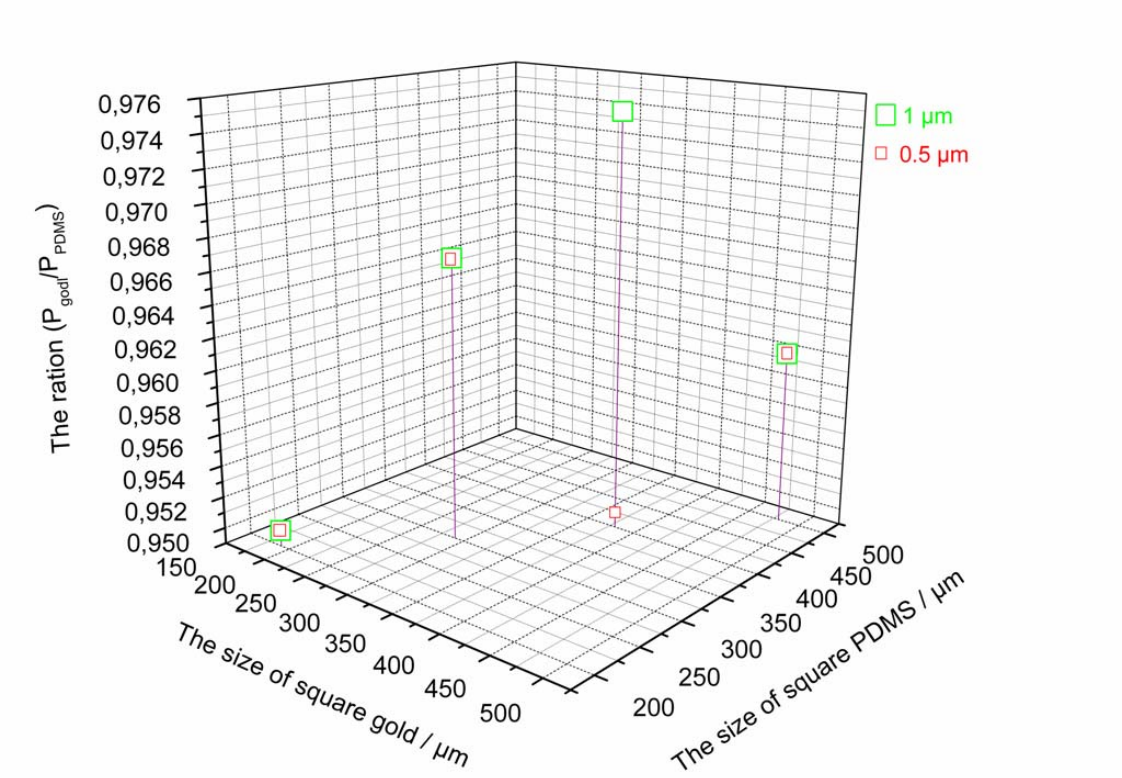

Figure 2-15: The ratios making the membrane reach maximal deflection according to the parameters of gold and PDMS

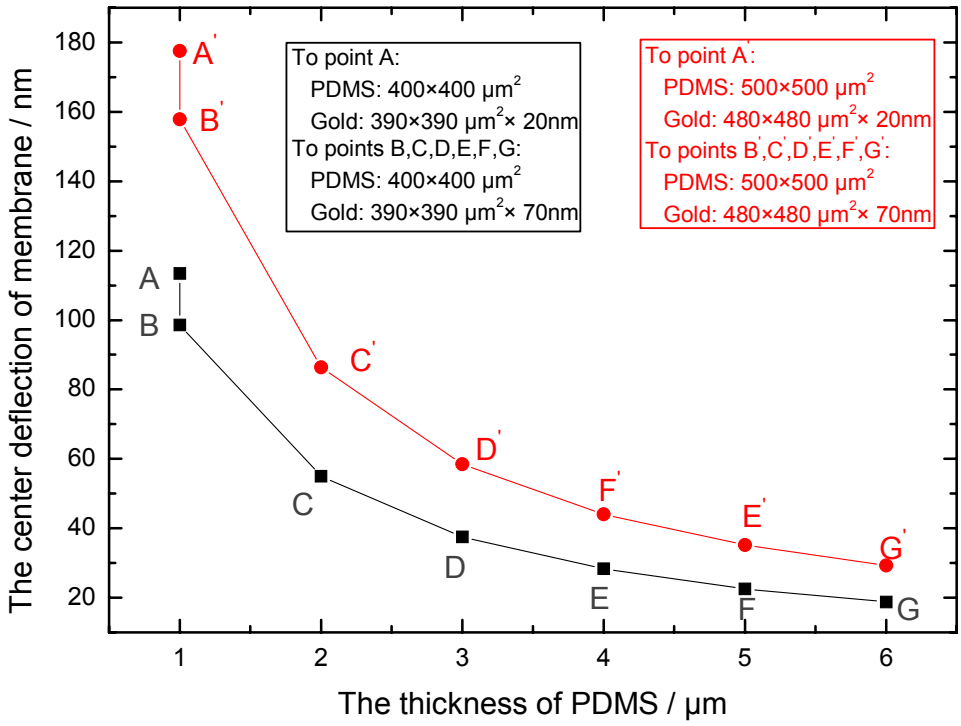

Figure 2-16: The center deflection of membrane as a function of PDMS thickness at the point of maximum deflection

At the points of maximal deflection shown in Figure 2-14, the center deflection of membrane still has a big change with the increase of membrane thickness, just like the simulation results shown in Figure 2-16 when the size of membrane is 400 x 400 μm^2 and 500 × 500 μm^2 respectively. The deflection decreases directly if gold thickness increases and PDMS thickness is fixed. The membrane deflection also exponentially decreases with the increase of PDMS thickness when the gold thickness is fixed. The simulation results clearly show that the signal enhances when the membrane size is changed from 400 × 400 μm^2 to 500 × 500 μm^2.

Founding on the simulation results and the real permission of fabrication techniques, two types of membrane parameters can be selected to be fabricated, Table 2-5.

Table 2-5: Summary of the membrane parameters selected for further design process

		Length / μm	Width / μm	Thickness
Type 1	PDMS	400	400	1 μm
	Gold	390	390	20 nm
Type 2	PDMS	500	500	1 μm
	Gold	480	480	20 nm

2.4.4 Material and parameters of the substrate

The carrier and basic function substrate of the biosensor is silicon (525 μm, 4' silicon wafer) not only because silicon allows to release the membrane and the membrane device to be handled easily, but the silicon fabrication is one of best developed technologies in the MEMS field. Since the beginning of semiconductor engineering, silicon is one important material used to fabricate most integrated circuits for the consumer electronics. The economies of scale and ready availability of cheap high-quality materials make silicon attractive for a wide variety of MEMS applications. Further, it can incorporate electronic functionality. The basic techniques to produce the silicon-based MEMS devices include: material layers deposition, structure patterning by photolithography, and etching to deposited layer or silicon for producing the required shapes. Many BioMEMS technologies have also been developed based on the silicon technologies.

The decision on parameters of the trapezoidal frames in silicon substrate is ruled by the parameters of membrane and the silicon anisotropic etching technique using KOH, as shown in Figure 2-17.

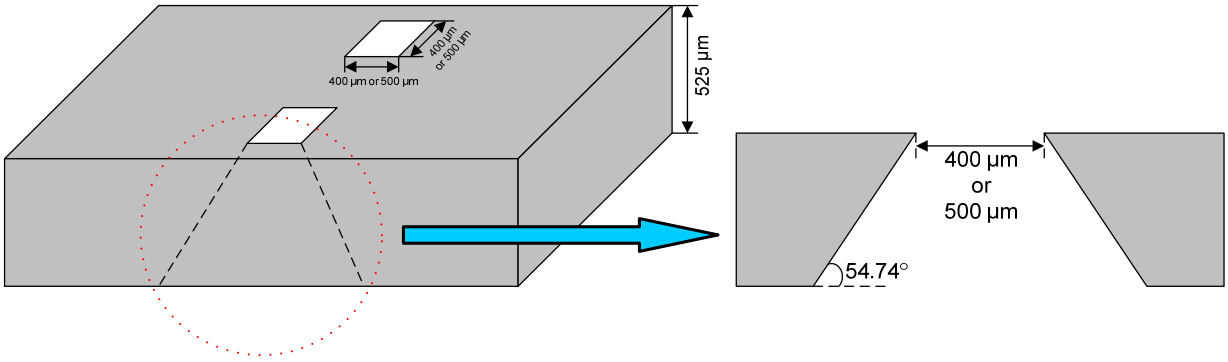

Figure 2-17: The structure in silicon substrate and its parameters

2.5 Design of the microfluidic devices or components

2.5.1 Material selection

To date, many substrates, such as silicon [223-225], glass [226-229], ceramic [230], polydimethylsiloxane [231], polymethyl methacrylate [232,233], and SU-8 [234] have been used to fabricate microfluidic devices for biological and medical micro system, micro total analysis system (*μ*TAS) applications, etc. Among them, glass is a widely used substrate material in microsystem technology, especially in the manufacturing of microfluidic devices for biological analyses and biotechnical applications [235-237] as it provides beneficial structural and functional material properties. With comparison to silicon, the use of glass in *μ*TAS applications is advantageous with regard to its optical transparency which allows for visual inspection and on-line optical detection (good fluorescence properties) as well as its good dielectric properties used in a number of applications which allow it to withstand the high voltages used in electrokinetically driven flows and separations (e.g. capillary electrophoresis). Other beneficial properties of glass are its good chemical resistance, high thermal stability, chemical inertness and established schemes for

surface modification and functionalisation (silane modification) [236] which make glass the most widely used substrate for the fabrication of DNA arrays. The use of glass substrates may also improve the long-term chemical stability of the devices in comparison with silicon-based systems. Many applications also require the high mechanical strength and the good mechanical stability of glass. Therefore, the glass is selected as the microfluidic material in the thesis.

2.5.2 Parameters decision

It is known from the conceptual design that the first kind microfluidic device is made of inlet, outlet, microchannel and buffer, the second kind microfluidic device consists of only two chambers over the membrane. The thickness of glass substrate available and used in the biosensor is 700 μm based on a discussion with Little Things Factory GmbH at Ilmenau. The key parameters mainly refer to the membrane size and some other factors, such as the fabrication techniques, the experimental manipulation, and the normal size of analytes. Figure 2-18 shows the size of some cells and molecules. The chosen parameters for microfluidic device or component are illustrated in Figure 2-19 and Figure 2-20.

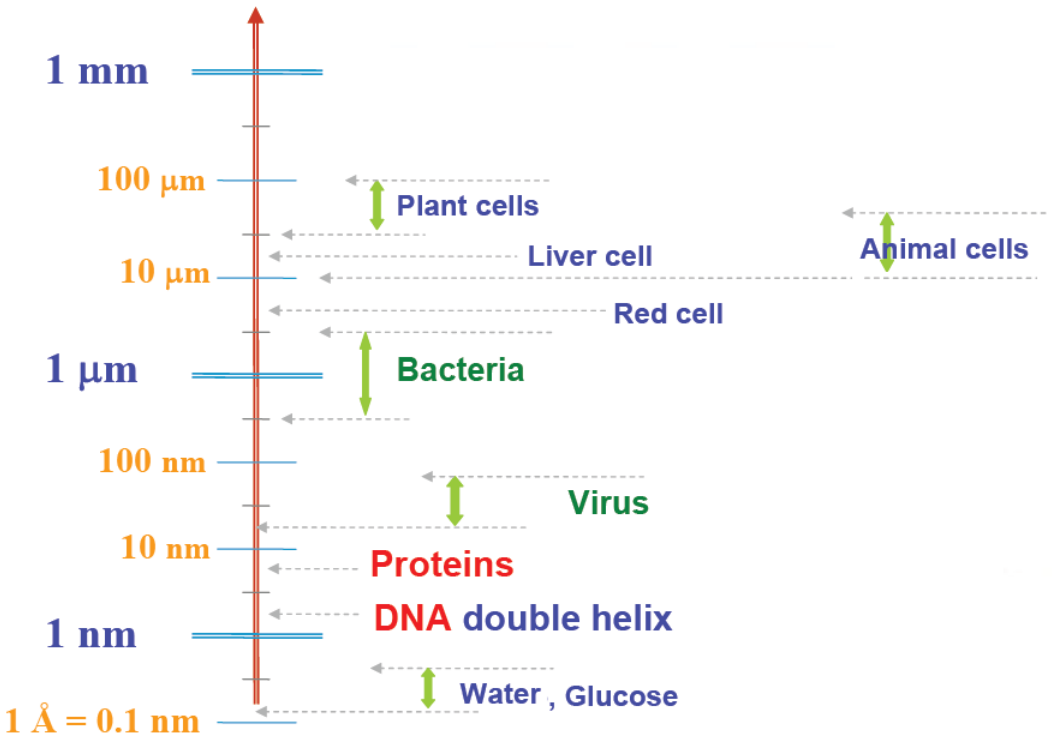

Figure 2-18: The size of normal analytes

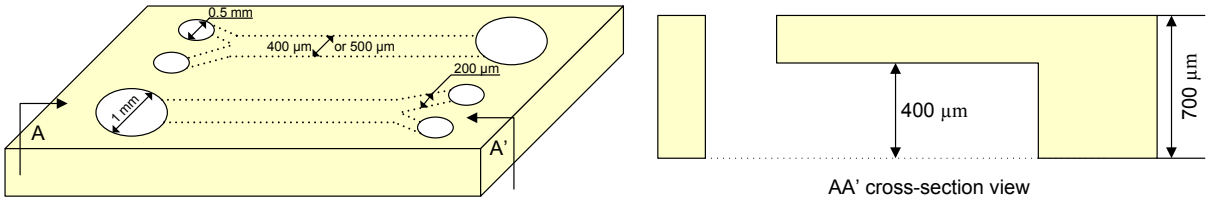

Figure 2-19: The main paramerers of first microfluidics

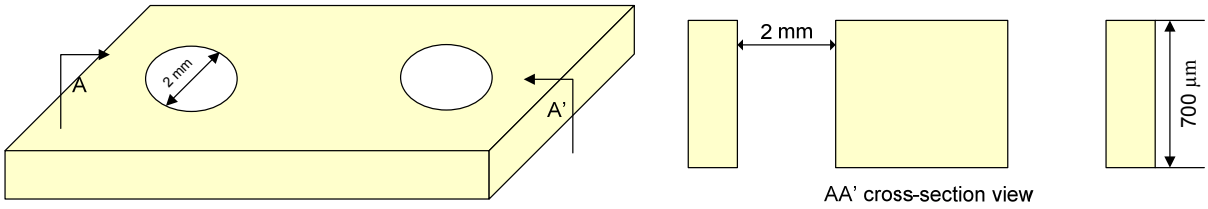

Figure 2-20: The main parameters of second microfluidics

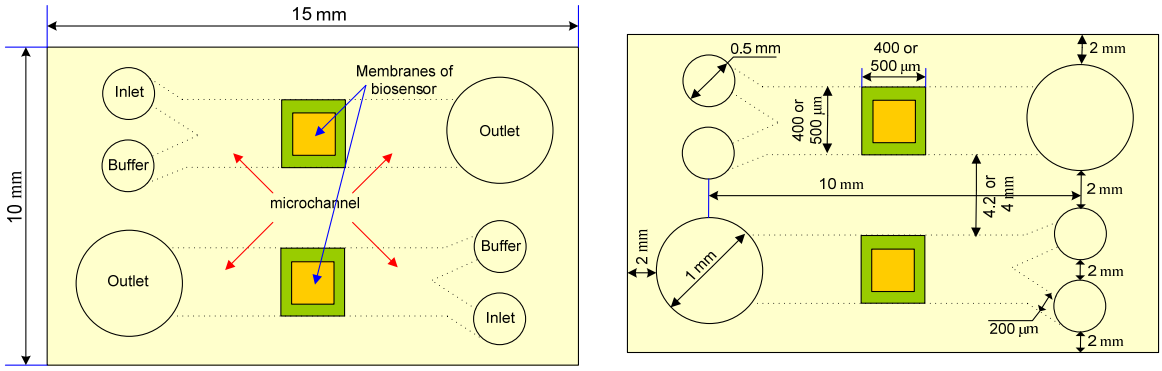

(a) The parameters of first biosensor

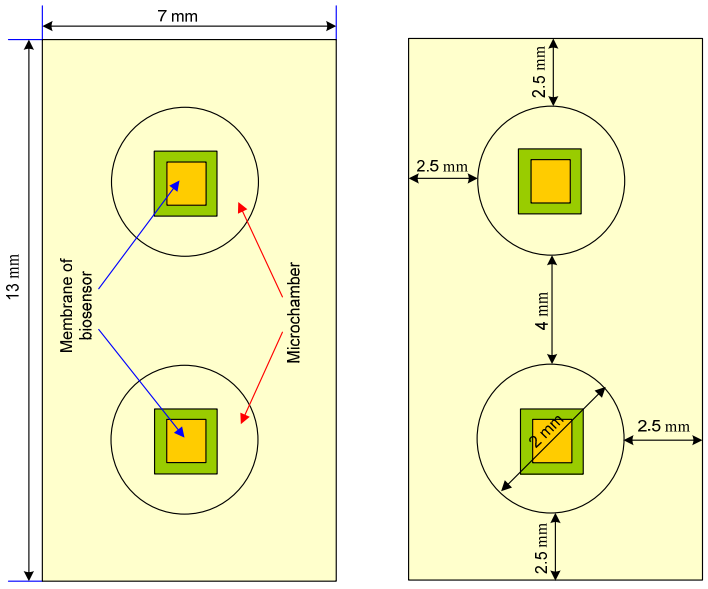

(b) The parameters of second biosensor

Figure 2-21: The detailed parameters of one biosensor chip

Summary

PDMS, glass and silicon were selected as the material of membrane, microfluidics and substrate respectively based on fundamental and/or simulation researches. Two kinds of biosensor structures were designed and will be fabricated. Each structure contains two layers: microfluidic layer and sensor layer. To each kind of biosensor, the sensor layer is similar, it consists of two membranes, one acts as the active membrane and the other as reference. But the microfluidic structure is different, one is made of inlets, buffers, microchannels and outlets, and the other has only two chambers. The key parameters of membrane and microfluidics were chosen based on the *FE* method, fabrication techniques, and experimental manipulation, and so on. The detailed parameters of each kind of biosensor chip are shown in Figure 2-21.

The design of the novel micro membrane surface stress-based biosensor is feasible and exploits the low elasticity modulus of PDMS, which will be fabricated (chapter 3) and applied to typical cells (chapter 4).

Some simulation work has been published under the the title “Finite Element Analysis of the Membrane Used in a Novel BioMEMS” in Journal of Biomimetics, Biomaterials and Tissue Engineering (2009) 3:51-57 [P1].

Chapter 3 Biosensor Fabrication

3.1 Fabrication techniques

Microfabrication or micromanufacturing is the technique for the processes of fabrication of the structures with micrometer sizes and smaller. The microfabrication technique was earliest applied for semiconductor devices in integrated circuit fabrication. These microfabrication processes have been named by the term "semiconductor device fabrication," "semiconductor manufacturing," etc. The general methods of MEMS process flows can be classified into two primary categories: surface micromachining and bulk (also called substrate) micromachining. Surface micromachining is a method of producing MEMS by depositing, patterning and etching a sequence of thin films, typically 1 μm – 100 μm thick. One of the most important processing steps required for dynamic MEMS devices is the selective removal of the underlying film named as sacrificial layer, without attacking an overlying film, referred to as structural layer. Commercial examples of components made from surface micromachining include airbag accelerometers and micromirror projection arrays. Bulk micromachining is different from surface micromachining because the substrate material, which is silicon, glass or other substrates, is used for patterning and shaping to form an important functional component of the resulting device. Many high-precision complex three-dimensional shapes, such as V-grooves, channels, pyramidal pits, membranes, vias and nozzles, can be formed by exploiting the predictable anisotropic etching characteristics of single-crystal silicon [238, 239]. It is most widely known commercially in production of membranes for pressure sensors and nozzles for inkjet printing. In addition to surface and bulk micromachining, there is in fact a third type of micromachining called “mold” micromachining. To the technique, the part is formed by filling a mold which was firstly defined through photolithographic methods. Micromachining molds can be formed in some photopolymer with X-ray lithography (“LIGA”) or more conventional UV lithography [206], with the aim of producing piece parts.

In the actual microfabrication, the main typical processes include:

1. Substrates: Microfabricated devices are not generally freestanding devices but need usually a thicker substrate to support such as silicon wafer.

2. Deposition or Growth: Microfabricated devices are typically constructed using one or more thin films by deposition techniques. Examples of deposition techniques include [206]: 1) thermal oxidation, 2) sputtering, 3) evaporative deposition, 4) epitaxy, 5) Physical Vapor Deposition (PVD), and 6) chemical vapor deposition (CVD), the two most important CVD technologies in MEMS are Low Pressure CVD (LPCVD) and Plasma Enhanced CVD (PECVD).

3. Patterning: It is often desirable to pattern a film into distinct features or to form openings in some of the layers. Examples of patterning techniques include: 1) photolithography and 2) shadow masking.

4. Etching: The technique used to remove of some portion of the thin film or substrate is called etching [206]. Etching techniques include: 1) Dry etching or Plasma etching such as Reactive-ion etching (RIE) or Deep reactive-ion etching (DRIE) [206] and 2) wet etching or Chemical Etching [206].

5. Others:
1) Wafer cleaning, also known as "surface preparation";
2) Thermal diffusion or ion implantation, named as doping;
3) Chemical-mechanical planarization (CMP);
4) Wire bonding and substrate bonding: Silicon, glass, metal and polymeric substrates can be bonded together through several methods [239,240] (for example, fusion bonding [241], anodic bonding [242], eutectic bonding [243] and adhesive bonding [244]);
5) Nonsilicon microfabrication: The development of MEMS has contributed significantly to the improvement of nonsilicon microfabrication techniques. LIGA and plastic molding from micromachined substrates [206] are two prominent examples;
6) Integration of circuits: the integration of circuits can make the performance of many MEMS improvement greatly.

In this chapter, the fabrication techniques of PDMS micro membrane-based biosensor are developed based on surface and bulk microfabrication techniques.

3.2 Fabrication

The process started with a flat, 4 inches silicon wafer (525 μm thickness). Ten main processing steps were designed and used for the fabrication of biosensor according to the biosensor structure and practical fabrication techniques, as shown in Figure 3-1: (1) depositing Si_3N_4 on both sides of silicon wafer ([001] orientation); (2) spinning coat PDMS thin film on the surface of the front Si_3N_4 layer; (3) depositing and exposing the photoresist to form the gold layer pattern; (4) depositing gold using Edwards Auto 306 (E306.CO.UK); (5) lift-off; (6) depositing and exposing the photoresist on the backside of substrate; (7) etching Si_3N_4 using RIE (Reactive Ion Etching) method; (8) KOH-etch silicon; (9) etching Si_3N_4 using RIE method to release the membrane; (10) microfluidic bonding with sensor array. The detailed description of the biosensor fabrication will be introduced in the following sections. Section 3.2.1 is the fore fabrication of membrane, i.e. the fabrication of PDMS thin film; the next section 3.2.2 and 3.2.3 is the fabrication of sensor structure and microfluidic devices or component respectively. The last section 3.2.4 is the bonding techniques to form the later experimental biosensor.

From the fabrication flow it can be derived that one key point is to get the planned thickness of PDMS thin film, which plays a crucial role in the whole fabrication and to the function of biosensor itself. Hence, lots of experimental fabrications have firstly been done to know under which conditions an 1 μm thick PDMS thin film can be fabricated reproducibly.

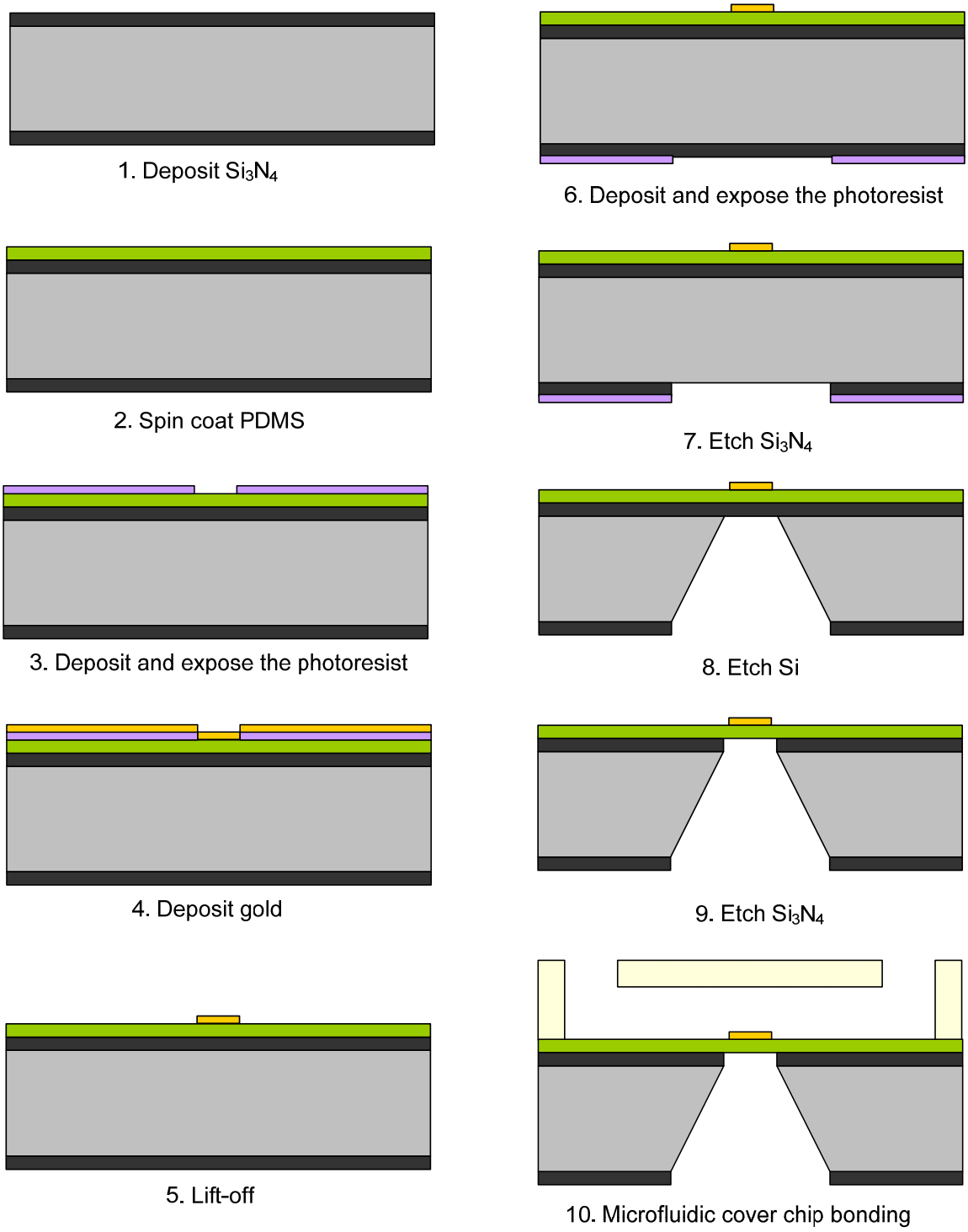

Figure 3-1: Fabrication process flow of the biosensor [P2]

3.2.1 Fabrication of PDMS thin film

Sylgard 184, Dow Corning (DOW CORNING CORPORATION Midland – Michigan USA) is the raw material of PDMS thin films, which have two components: base and hardener. Different ratio of these two parts can be used to get different characteristic thin film. A ratio of 20:1 for thin layer and 5:1 for thick layer was found to work

best [245]. Without diluting the PDMS, the thickness of thin film could only be reduced down to about 3 µm [246]. Hence, it must be diluted to get the thinner thin film, 1 µm for the aims of this thesis. Three materials, hexane, toluene and silicon oil can be employed. In our fabrication, Sylgard 184 was diluted with hexane (CHEMOS GmbH, Germany), which allowed the fabrication of membranes as thin as ~70 nm [247].

The PDMS thin film was spun on the silicon substrate using spin-coater (Photo Resist Spinner Model 5000-1, Electronic Micro Systems Ltd., UK). Four kinds of ratios, 10:1 and 20:1 (Base : Hardener), 10:1:1.5 and 10:1:3 (Base : Hardener : Hexane), and two spin-coating fabrication programs, only one step (6200 rpm / 130 s) and three steps (1. step: 620 rpm / 120 s, 2. step: 1500 rpm / 120 s, 3. step: 4300 rpm / 110 s), were employed. Figure 3-2 is the optical micrograph of one PDMS thin film on silicon substrate.

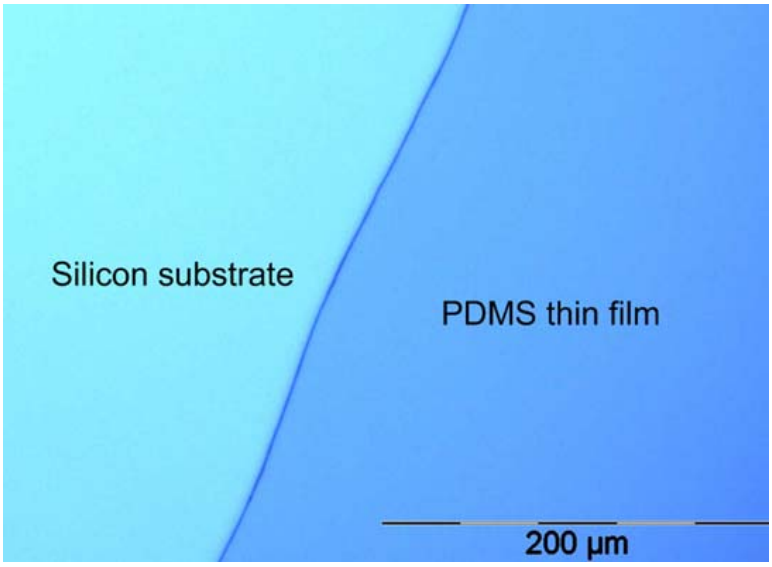

Figure 3-2: Optical images of PDMS thin film on the Si substrate [P2]

Profilometer (AMBIO Technology XP-2, Ambios Technology, Inc., USA) and Tactile Sensor (Institute of PMS, TU-Ilmenau, Ilmenau / Germany) were used to measure the thickness of PDMS thin films that have been fabricated accoding to different ratios and different programs. Figure 3-3 is one measurement result of a same PDMS thin film using the two different measuring methods. The comparative thickness of PDMS membranes based on different fabrication conditions and measuring mehods is shown in Figure 3-4.

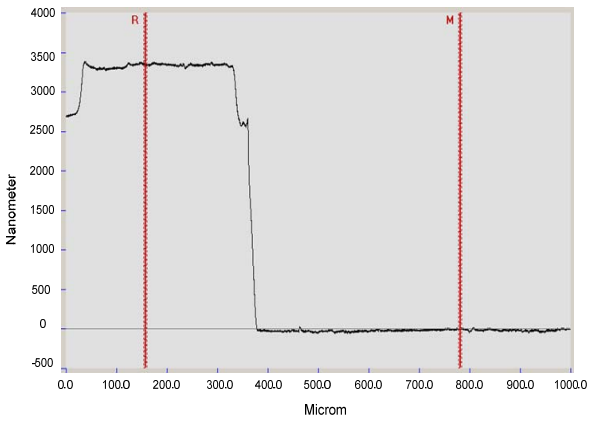

Figure 3-3(a): Measuring result for thickness of PDMS membrane from profilometer

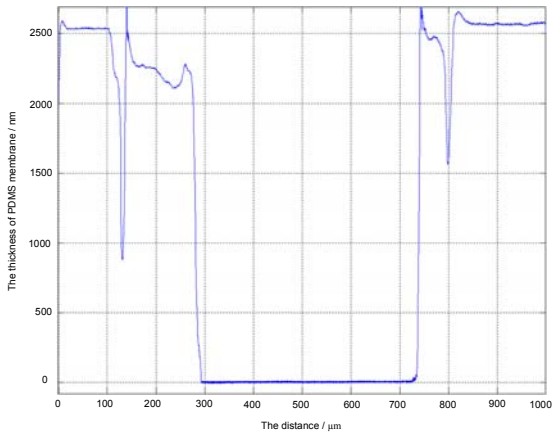

Figure 3-3(b): Measuring result for thickness of PDMS membrane from tactile sensor

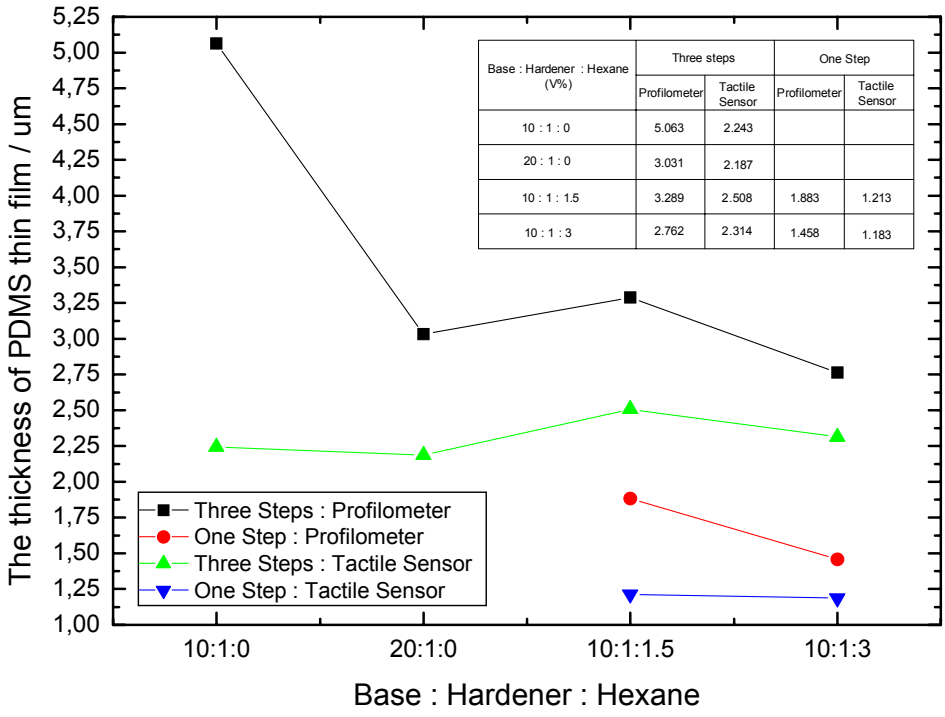

Base : Hardener : Hexane (V%)	Three steps		One Step	
	Profilometer	Tactile Sensor	Profilometer	Tactile Sensor
10 : 1 : 0	5.063	2.243		
20 : 1 : 0	3.031	2.187		
10 : 1 : 1.5	3.289	2.508	1.883	1.213
10 : 1 : 3	2.762	2.314	1.458	1.183

Figure 3-4: The comparative thickness of different thin films [P2]

From the analysis of Figure 3-3 and 3-4, the following information can be derived:

(1) The measuring result from tactile sensor is “thinner” than that from profilometer to one same thin film. The possible reason is that the tactile sensor is not easy to control and the needle may stick into the thin films during measurement, which effect can be inforced by repeated measurement at the same place: the thickness “became thinner” with the increase of measurement time.

(2) The thickness of undiluted PDMS thin film is thicker than that of the diluted thin film. The thickness of undiluted PDMS thin film becomes thinner with the increase of base component in the mixture. The thickness of diluted PDMS thin film also becomes thinner with the increase of Hexane in the mixture.

(3) The PDMS thin film thickness is thicker than the reference [247], Figure 3-5, even though the ratio is same, the potential reasons may be:

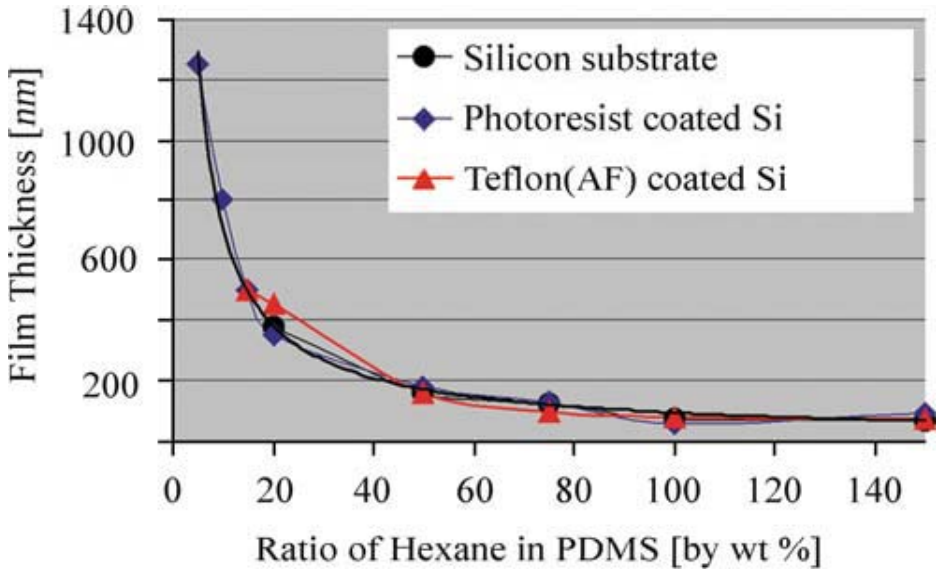

Figure 3-5: The reference thickness of PDMS thin film related to the ratio of Hexane in mixture [287]

- 3.1) Cutting the PDMS around the place where the thickness was measured will definitely influence the measuring results since the film may detach partially from the substrate while cutting.

- 3.2) The spinning method or the process control is different between our measurements and the reference [10], which are two important factors to affect the thickness of PDMS thin film.

- 3.3) Evaporation of hexane from mixture is the most important reason. Hexane is well known as a pretty volatile liquid. It takes long time from mixing the mixture, removing the bubbles of mixture to spinning coat. The whole time may be too long for the hexane to volatilize from the mixture and the viscosity of mixture becomes higher.

Hence, the evaporation rate of hexane must be calculated, and the amount of evaporation into the beginning mixture for getting the uniform 1 μm thickness PDMS membrane must be added. An evaporation rate is the rate at which a material will vaporize relative to the rate of vaporization of a specific known material.

The reference material must be stated whenever a relative evaporation rate is given. Sometimes n-butyl acetate (commonly abbreviated BuAc) is chosen as the general reference material for evaporation rates. When the relative evaporation rate of butyl acetate is set to 1.0, other materials are then classified as Table 3-1 [W2] reports. But such a number would presumably be relative to some variables, temperature, atmospheric pressure, humidity, air flow, viscosity etc, for example.

Table 3-1: The evaporation rates of general reference material [W2]

Speed	Evaporation Rate (BuAc = 1.0)	Examples
Fast	> 3.0	Methyl Ethyl Ketone = 3.8 Acetone = 5.6 Hexane = 8.3
Medium	0.8 to 3.0	95% Ethyl Alcohol = 1.4 Naphtha = 1.4
Slow	< 0.8	Xylene = 0.6 Isobutyl Alcohol = 0.6 Water = 0.3 Mineral Spirits = 0.1

The evaporation rate of any solvent can be calculated based on the following formula [W3]:

$$R_{solvent} = \frac{R_{water} \times 2.26}{H_{solvent}} \qquad (1)$$

$R_{solvent}$: Evaporation rate of solvent (g/h)

R_{water} : Evaporation rate of water (g/h)

$H_{solvent}$: Heat of vaporization of solvent (J/g)

For example, when using a 20-liter Industrial Rotary Evaporator and if the vapor pressure temperature is 40°C and the bath temperature is set to 60°C, the evaporation rate of Hexane can be gotten [W3]:

$$R_{Hexane} = \frac{R_{water} \times 2.26}{H_{Hexane}} = \frac{2000 g/h \times 2.26}{371 J/g} = 12.183 g/h \qquad (2)$$

$$V = \frac{R_{Hexane}}{\rho_{Hexane}} = \frac{12.183 g/h}{0.659 g/cm^3} = 18.487 cm^3/h \qquad (3)$$

Evaporation rate of water with (t = 20°C, rpm = 225) = 2.0 L/h or 2000 g/h
Heat of vaporization of hexane = 371 J/g
Density hexane = 0.659 g/cm^3

In the fabrication, the process of removing bubbles of the mixture in the vacuum glass vessel takes most time, so the evaporation speed in the vessel must be evaluated too. First, 6 ml hexane was put into the vessel. ~4.2 ml and ~3.2 ml hexane was left 20 min and 30 min later respectively. Hence, the evaporation speed during the process is:

$$v = \frac{6 - 4.2}{20} ml/\min = 0.09 ml/\min \sim 0.1 \ ml/min \qquad (4)$$

Considering these comprehensive factors, the relatively better PDMS thin films (about 1 μm) were fabricated after adding the evaporated hexane into the first mixture and improving the process control. Figure 3-6 illustrates the measuring results of two PDMS thin films measured based on Profilometer (AMBIO Technology XP-2, Ambios Technology, Inc., USA) and Tactile Sensor (Institute of PMS, TU-Ilmenau, Ilmenau / Germany) respectivley. The thickness of PDMS thin film meets the requirement.

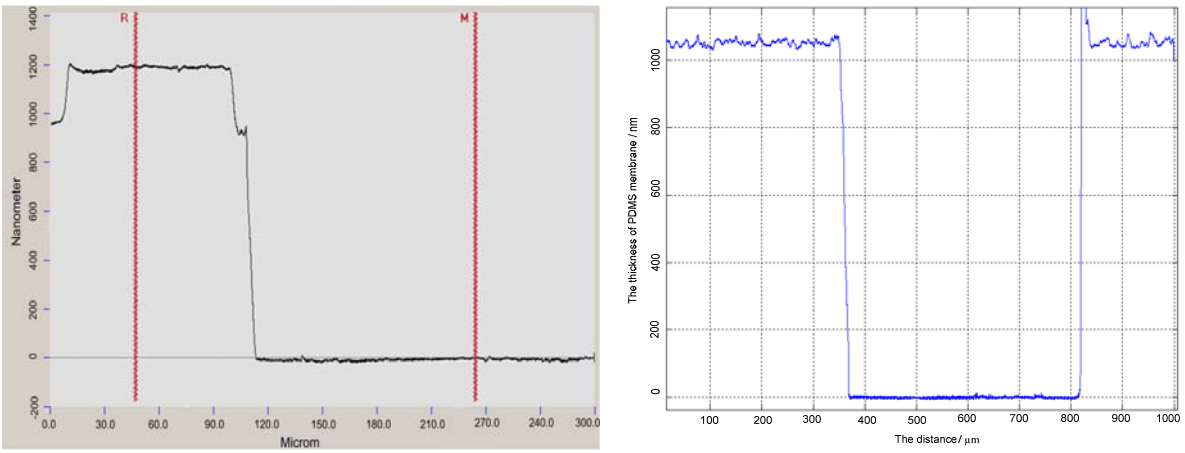

(a) The measuring result from Profilometer (b) the measuring result from Tactile Sensor

Figure 3-6: The thickness measurement results of PDMS thin films fabricated based on the "improved method" [P2]

3.2.2 Sensor fabrication

The sensor layer can be fabricated after gaining the relatively better PDMS thin film. Two chromium masks are required to finish the fabrication of sensor layer, one is used to form the gold pattern, and the other is for the pattern to release the membrane. The two mask layouts were designed using AutoCAD® software based on the basic parameters designed in chapter 2. Figure 3-7 shows the mask layouts, the blue layout is for the gold mask to form the gold pattern during the fabrication, and the green layout is membrane mask for membrane pattern.

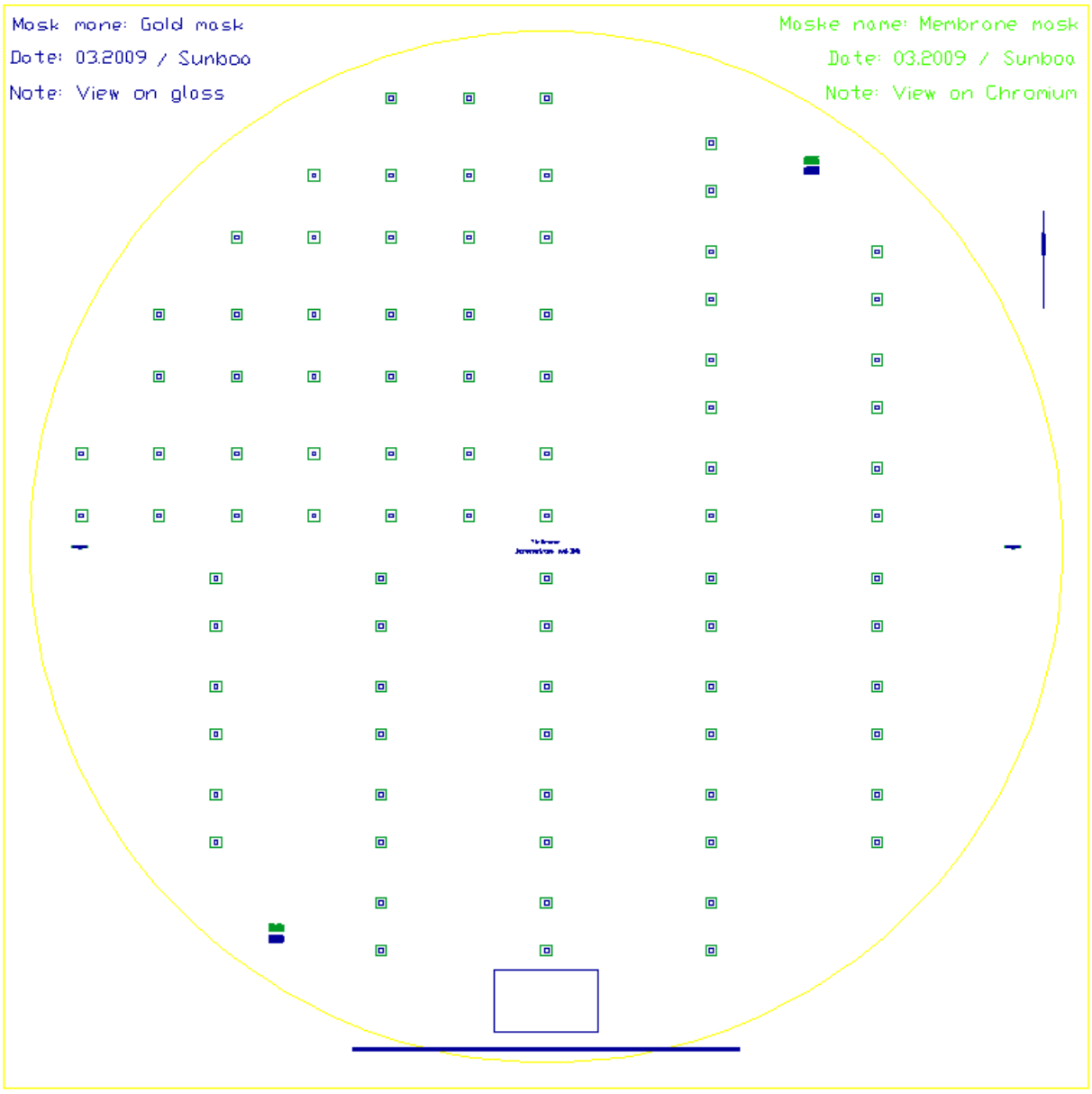

Figure 3-7: The masks to fabricate sensor: the blue is gold pattern and the green is membrane pattern

Briefly, four key steps can be summarized to form the sensor layer based on the front fabrication flow shown in Figure 3-1. It is illustrated in Figure 3-8: (1) deposit nitride silicon (Si_3N_4); (2) 1 μm thickness PDMS thin film patterning; (3) 20 nm thickness gold patterning (Edwards Auto 306); (4) membrane release (KOH etching and reactive ion etching). Appendix II is the detailed process plan of the biosensor fabrication. Two Si_3N_4 layers were firstly deposited on both sides of the silicon substrate ([001] orientation). The layer on the back face was used as the mask to KOH anisotropic etching of silicon, and the other layer was as the etch-stop layer to protect the PDMS thin film. After the spin-coat of PDMS (~1 μm) thin film and the Au pattern (390 μm × 390 μm × 20 nm), the PDMS micro membranes were last formed

by the removal of supporting Si_3N_4 with reactive ion etching (RIE) from the backside. During the whole process, the PDMS thin film/membrane should be avoided contacting with KOH and Acton long time to protect PDMS. The thin film/membrane might swell if it contacts with KOH and Acton long time, especial for KOH. The arrangement of fabrication flow and each fabrication step must be based on the basic point.

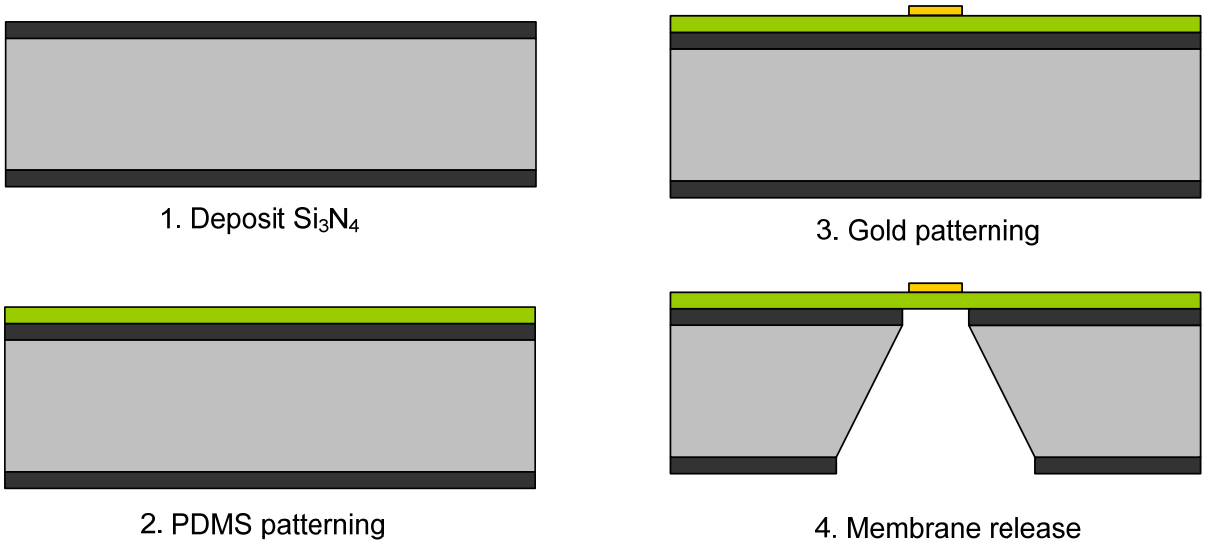

Figure 3-8: Simple fabrication process sequence of sensor layer

The last wafer with sensor structures was gained after the whole fabrication, as shown in Figure 3-9a, two membranes constitute one sensor unit. Figure 3-9b and 3-9c illustrates the optical micrograph of the front side and the back side of one sensor unit respectively. Figure 3-10 shows the view of two kinds of sensor compared with one Euro coin and the profile of dome shaped Au-PDMS membrane. Figure 3-10b is the SEM (Scanning Electron Microscope) image of the PDMS membrane. The 3D profile was measured to estimate the curvature characteristics of the fabricated membrane utilizing the white light interferometer (Gesellschaft für Bild- und Signalverarbeitung (GBS) mbH, Ilmenau Germany). The central curvature was about 1 µm as illustrated in Figure 3-10c. The possible reason induced the curvature is the weight of PDMS membrane and gold layer.

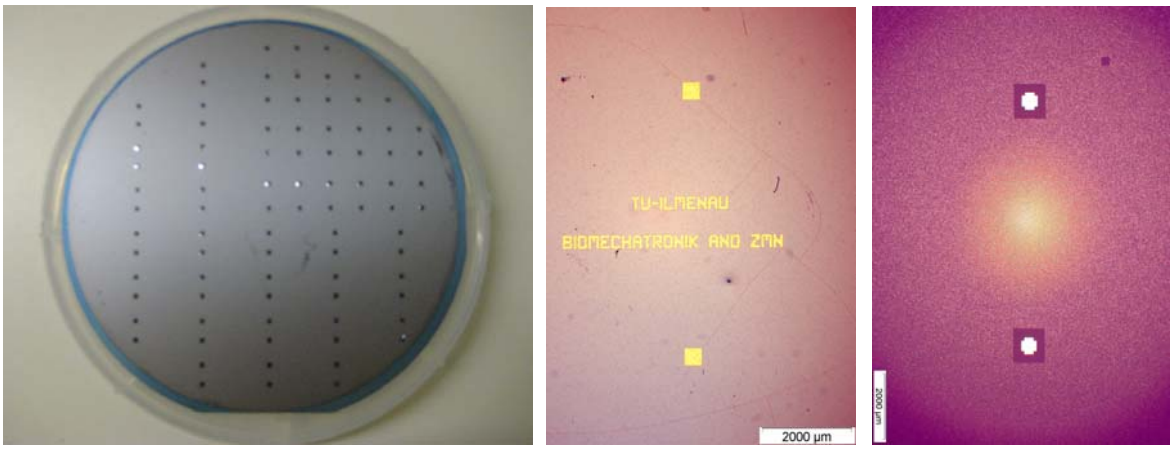

(a) Whole sensor wafer before dicing (b) Front side of one sensor (c) Back side of one sensor

Figure 3-9: The fabricated sensor structure

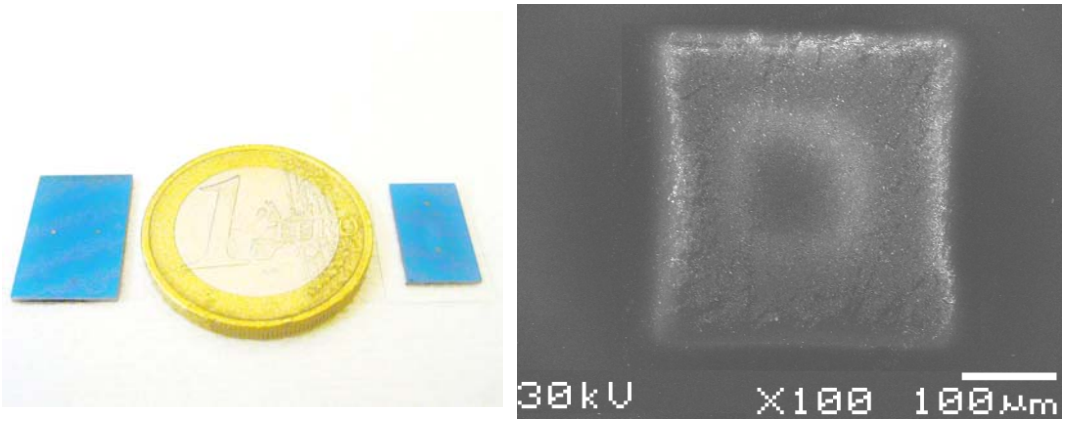

(a) The size of two kinds of biosensors compared to an one Euro coin

(b) SEM image of the dome shape membrane with Au

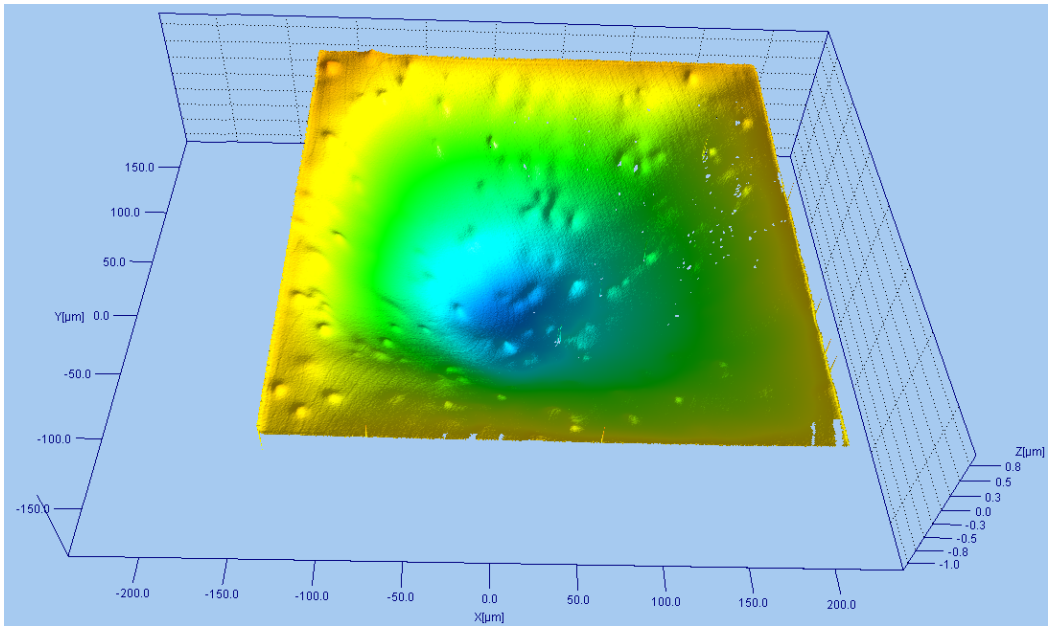

(c) 3D profile of the dome shape membrane with Au

Figure 3-10: The photo of sensor and profiles of the dome shaped Au-PDMS membrane

3.2.3 Microfluidic fabrication

Two kinds of microfluidic structures are planed to be fabricated based on the design in chapter 2, as shown in Figure 3-11. One is made of two microfluidic systems; each consists of inlet, mcirochannel and outlet for the input, transportation and output of medium and analytes respectively, and a buffer for the clearing of biosensor system. Another is composed of only two chambers; all the manipulations will be realized in the vertical direction.

The microfluidic fabrication also needs two masks, one is used to fabricate the holes as the inlets, outlets, buffers or chambers in the glass wafer, and the other is for the fabrication of microchannels. The mask layout was designed using the AutoCAD® software based on the parameters chosen in chapter 2. It is shown in Figure 3-12, the pink layout is the structure for the fabrication of channels, and the wine layout is for the fabrication of holes. The microfluidic masks must be consistent with the sensor masks, especially for the positions of every structure. Figure 3-13 illustrates the whole mask design of the biosensor, including sensor layer and microfluidic layer.

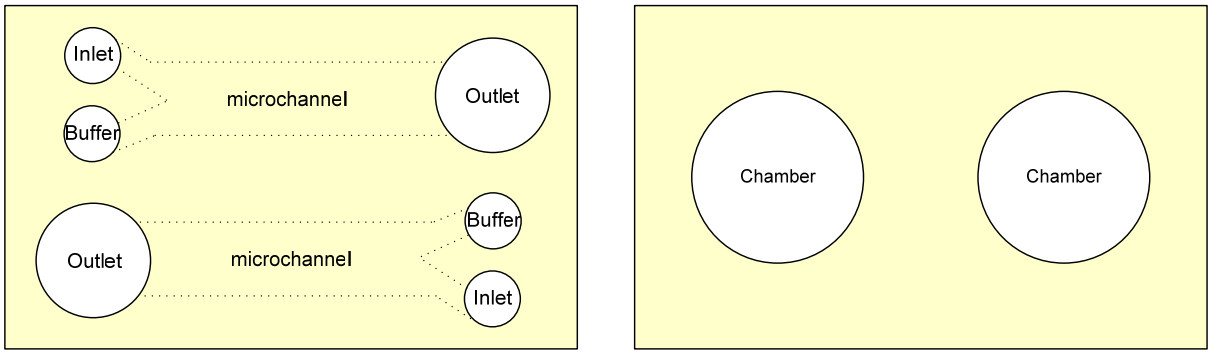

Figure 3-11: Two kinds of microfluidic structure

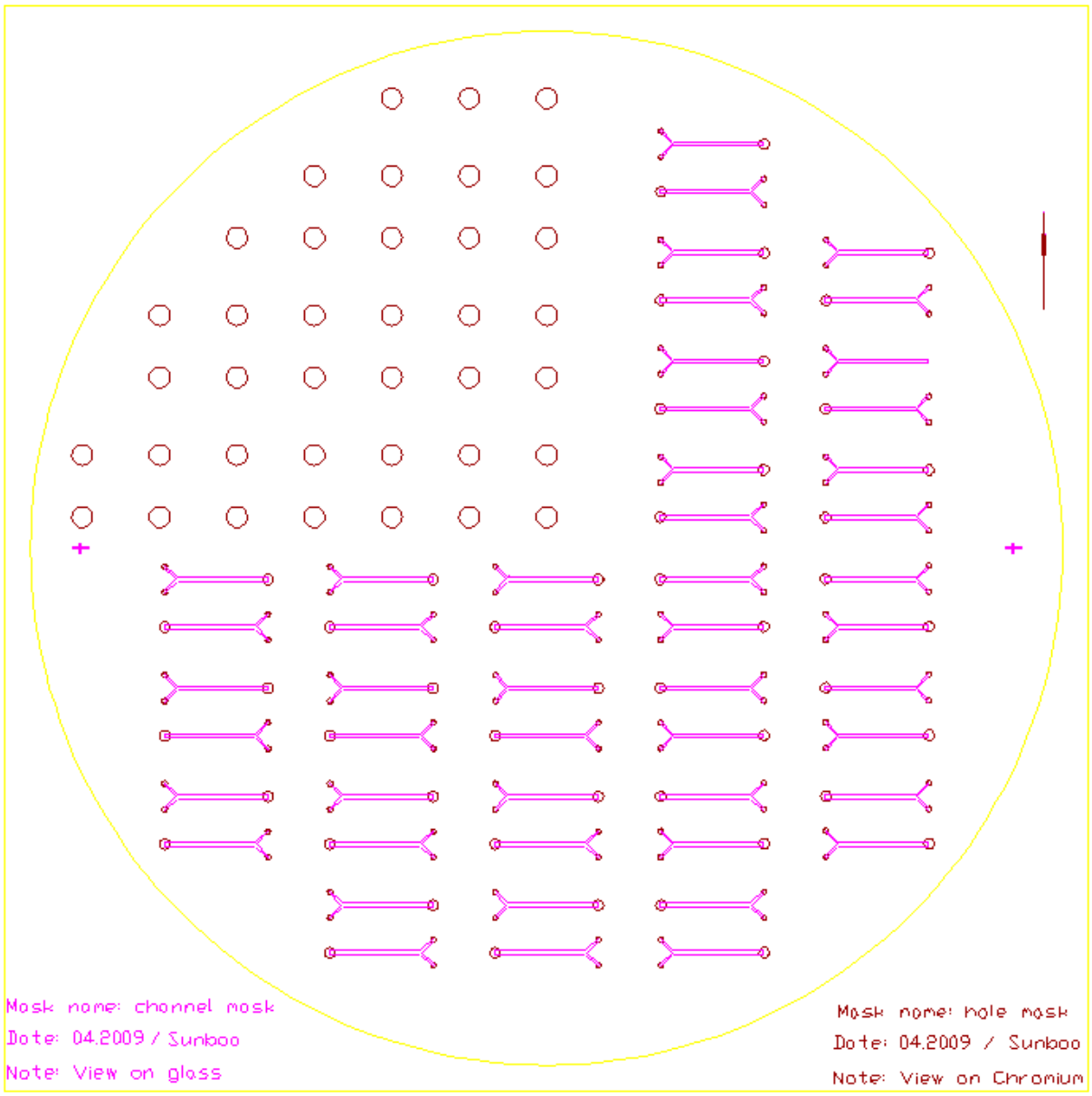

Figure 3-12: The masks for the microfluidic fabrication: the wine is the hole pattern, the pink is the channel pattern

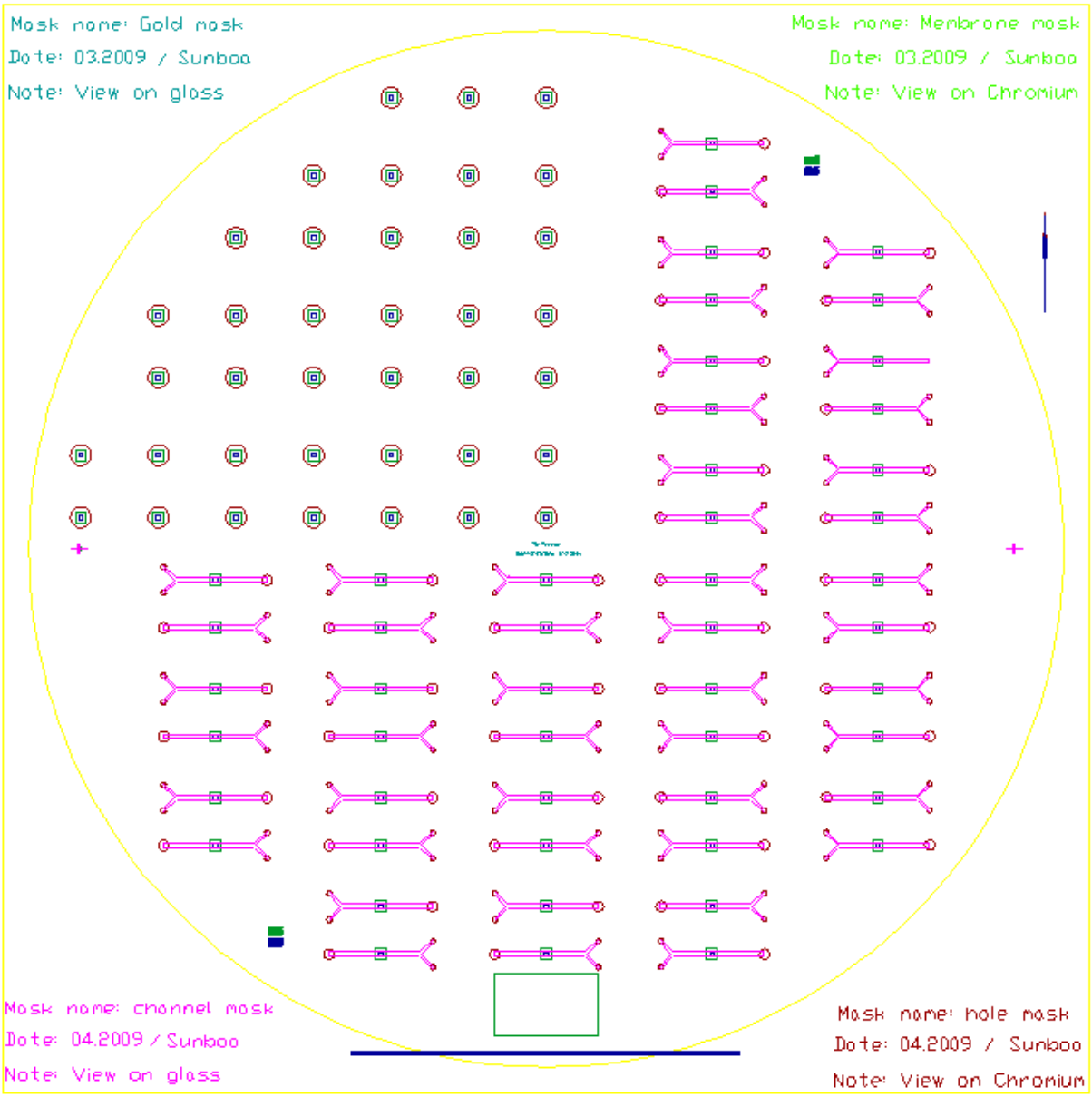

Figure 3-13: The assembled mask, blue: gold pattern, green: membrane pattern, wine: hole pattern, pink: channel pattern

3.2.4 Bonding technique

To build the later experimental biosensor structure, a bonding step is required to assemble the microfluidic elements to the silicon wafer containing the sensor array. The bonding technique plays a crucial role to the biosensor because it makes sure that the microfluidic layer will not separate from the sensor layer during the dicing process of fabrication and the later experimental process.

In general, bonding techniques can be briefly classified into two major categories –

direct bonding and bonding with an intermediate layer.

Fusion bonding [241], anodic bonding [242] and activated surface bonding [248, 249] belong to direct bonding. Fusion bonding relies on the attractive forces existing between flat surfaces to form a strong bond. The process of fusion bonding requires extensive precleaning to the bonding surface, and bonding process is usually performed under vacuum with external pressure to help form good contact. By applying a high contact force the substrates are first forced into intimate contact. The substrates hold together once in contact due to atomic attraction forces (van der Waal) [241], which are strong enough to allow the bonded substrates to be handled. After which a solid bond is formed between the substrates, the substrates are then placed in a furnace and annealed at high temperature, the bonding strength is higher by a thermal cycling process. Fusion bonding is special suitable for bonding silicon wafers. For anodic bonding, also called electrostatic bonding, the wafers are cleaned extensively, aligned and brought into pressure contact [242]. An irreversible bond can be formed between the substrates by high voltage (> 1 kV) and high temperature (> 400°C). The bonding technique is well suitable for bonding glass or glass coated substrates with silicon and nitride substrates. In the case of surface activation bonding, the substrates are pre-treated with oxygen plasma, hydration processes or other chemicals to increase the reactivity, and then brought into contact to form an irreversible bond with or without the condition of external pressure and high temperature [248, 249]. The effect of surface treatment processes lasts only for a small time interval and the bonding processes including alignment need to be completed within this time window. Activation with oxygen plasma has been used extensively for bonding PDMS devices with PDMS or glass [250], which are commonly used materials in prototyping microfluidic devices. Liu *et al.* have bonded PDMS to PDMS and glass by incubating the device with the two surfaces to be bonded in contact at 80 °C [251].

Bonding with an intermediate layer includes adhesive bonding, eutectic bonding, solder bonding and thermo-compression bonding and so on. Adhesive bonding [248, 249] does not require high temperatures or voltages, but requires a thin adhesive layer between bonding structures, which is usually obtained by spin coating. This process is very useful for bonding different materials that can not be welded. There

are many kinds of adhesives made from various natural and/or artificial compounds to be used in bonding. A hindrance to this process is that it takes more time to finish the adhesive bonds for curing, such as welding or nailing. Eutectic bonding uses a thin gold layer as an adhesive to bond silicon wafers [252]. The reflow of the eutectic material requires precise force delivery and uniform temperature. The wafers to be bonded contact each other closely and the temperature is raised to gold-silicon eutectic point, an irreversible bond can be formed last. Which bonding technique is used in advanced MEMS packaging and 3D integration technologies [252]. Lin and others [253-255] improved this process to bond locally using patterned gold lines and in situ electrical heating. Localized bonding overcomes the high temperature problem but requires one or more additional bonding layers (gold, silicon) by depositing and patterning. Hence the bonding technique may not be suitable for some device materials like polymers or with some fabrication processes. Solder bonding and thermo-compression bonding again involve the deposition and patterning of additional layers like solder or other soft metals and to form bonds between substrates through either heat and/or pressure method. Detailed analyses of these bonding processes and additional references can be read in the review paper by Schmidt [252]. Recently, Noh *et al.* [283] demonstrated a conformal bonding process where intermediate parylene layers, deposited on the wafers to be bonded, were selectively heated using variable frequency microwave to form a bond. Parylene deposition is conformal and it is also a biocompatible polymer, but additional lithography steps are required to make sure the bonding on special selective regions of the chip.

A room temperature bonding technique is used in our biosensor due to its special characteristics. The bonding technique uses an intermediate adhesive layer like UV curable polymer or uncured PDMS. UV curable adhesive was found to be more suited for silicon, glass and nitride surfaces [6]. Alternatively, PDMS can also be used as the adhesive layer; the technique is particularly practical for bonding PDMS devices [6]. When the glass wafer with microfluidic devices is bonded with the sensor layer in our design, the two contacted materials are glass and PDMS. Hence, the uncured PDMS method is suitable for our biosensor.

One structure for testing the PDMS bonding process consists of two components: a

glass slide and a silicon wafer with the PDMS thin film. The glass slide was bonded on the silicon substrate, which had been spun to a 1 μm PDMS thin film, by the transfer bonding technique using uncured PDMS as the adhesive layer. It is shown in Figure 3-14: (a) 3 ml of freshly mixed PDMS (10:1 ratio) was poured on another glass slide, which was then spun at 8000 rpm for 8-9 minutes. This resulted in a thin layer of uncured PDMS of thickness 1 μm - 1.5 μm [6]. (b, c) The glass slide which will be bonding with the PDMS thin film was cleaned with isopropyl alcohol (IPA). It was then placed on the glass slide (about 15 minutes after spinning) and lifted off, leaving a layer of uncured PDMS on it. (d) The previously fabricated PDMS thin film was prepared for bonding by cleaning with IPA. The glass slide with the thin layer of uncured PDMS was then placed on the PDMS thin film and cured at room temperature for 24 hours or 110 °C for 15 minutes to obtain the final testing structure.

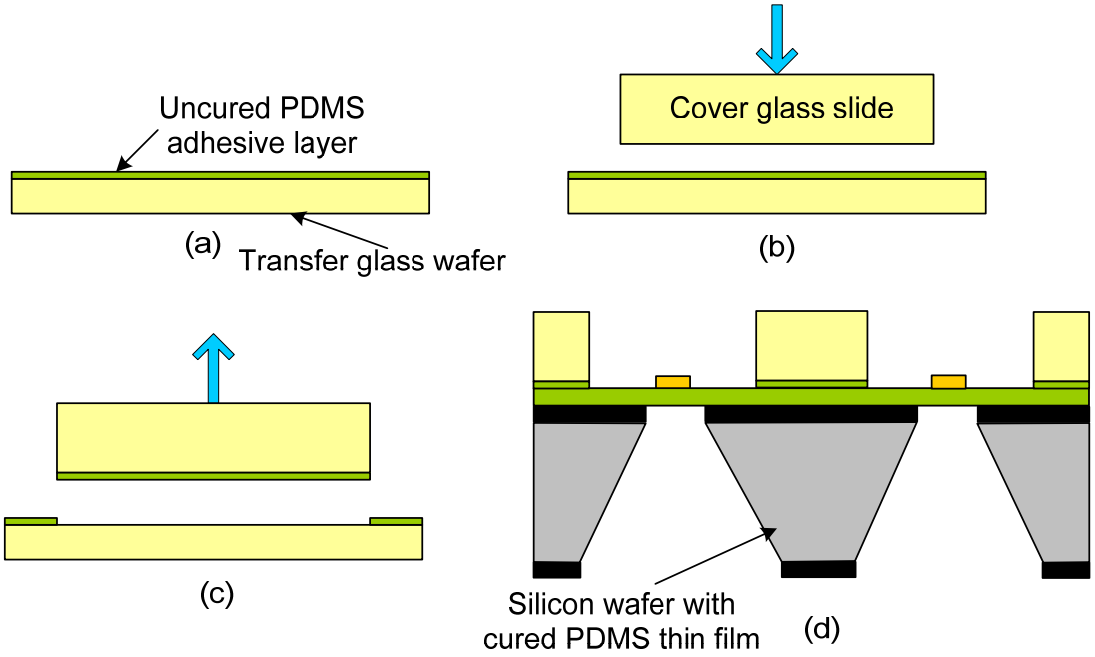

Figure 3-14: Bonding process. (a) uniform uncured PDMS adhesive layer on a glass wafer by spinning, (b) the cover glass wafer brought into contact with the adhesive, (c) selective transfer of the adhesive to the cover glass wafer, (d) the cover wafer aligned with a cured PDMS thin film on the biosensor, brought into contact and bonded. [P2]

The whole bonding wafer was firstly diced to 10 × 10 mm^2 chip for testing the bonding strength between glass and PDMS thin film using the uncured PDMS method, as shown in Figure 3-15, which is easy to assemble with test set, and to calculate the bonding strength. And then the chips were glued onto Al-cylinders using epoxy resin and cured 24 hour at room temperature to form an assembly, as shown in Figure 3-16. Last, the assembly was fixed with a flexible mechanism into a

commercial pull tester (zwick GmbH & Co. KG) and pulled the sample under controlled conditions, as shown in Figure 3-17.

Figure 3-15: The test bonding chip [P2]

Figure 3-16: The assembly of Al-Cylinder and chip for bonding test [P2]

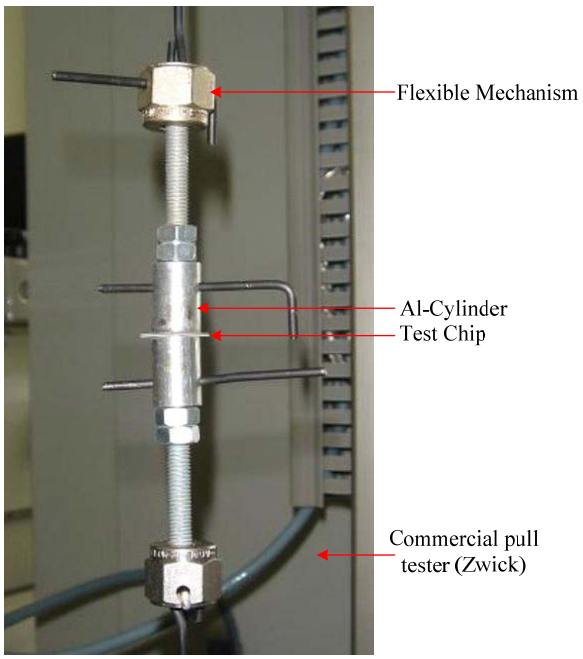

Figure 3-17: Experimental set-up for the bonding test [P2]

Through several repeated test experiments, the devices could withstand the pulling forces (tension) of 4 MPa to 5 MPa. One of the test results is presented in Figure 3-8, the glass wafer was separated from the PDMS thin film on silicon wafer when the pulling force is around 500 N. Based on the optical micrograph of separated interfaces, Figure 3-19, it can be known that the PDMS tears instead of separating at some places of the interface, which suggests that the bond strength is close to the

bulk PDMS. Hence, the bonding technique using an intermediate adhesive layer of uncured PDMS is suitable for our biosensor fabrication.

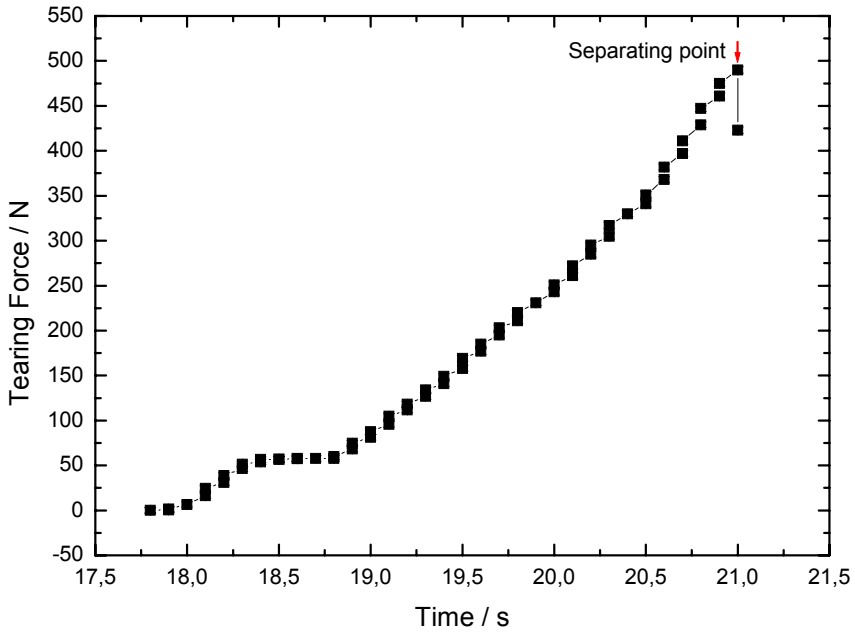

Figure 3-18: The bonding strength between glass and PDMS thin film using uncured PDMS method [P2]

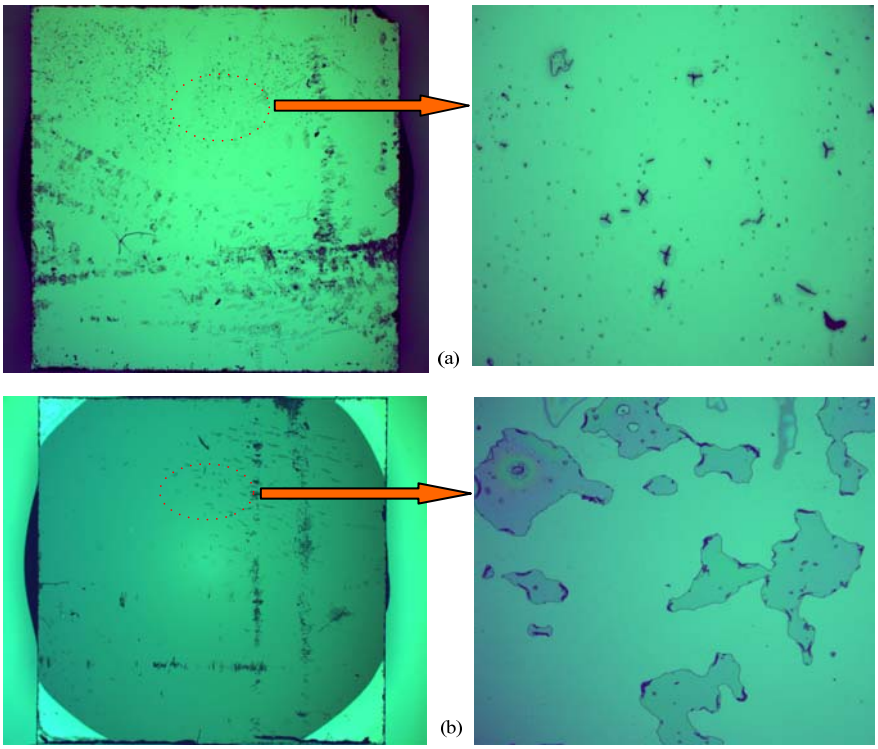

Figure 3-19: The optical micrograph of separated interfaces (a) the PDMS thin film part, (b) the glass part. Note the piece of PDMS torn from one of the bonded components and stuck to the other indicating that the bond strength is comparable to that of bulk PDMS. [P2]

Summary

The new biosensors with two relatively perfect thin PDMS micro membranes were fabricated based on the surface and bulk microfabrication technology. Many challenges in the fabrication, such as realization of PDMS processing based on conventional microfabrication processes, fabrication of relatively perfect PDMS thin film and release of PDMS membrane, were successfully overcome to form the biosensor. The microfluidic fabrication layout with two different structures was also designed using the AutoCAD® software. The bonding technique, uncured PDMS as the intermediate layer, was tested and the bond strength is close to the bulk PDMS, which is suitable for bonding the biosensor with the glass microfluidic devices or components.

The fabrication work has been published under the title “Fabrication of a surface stress-based PDMS micro-membrane biosensor” in Journal of Microsystem Technologies (2010) 16:1001–1008 [P2].

Chapter 4 Biosensor Testing and Application

In this chapter, the test and application of the surface stress-based PDMS micro membrane biosensors is discussed. First, the experimental solution chambers were designed and superimposed on the thin film surrounding the micro-membranes using the uncured PDMS as intermediate layer introduced in chapter 3. Then, two biosensor test systems were set up based on a smart white light interferometer (smartWLI) and a fiber optic interferometer (FOI) respectively, and debugged for the later test and application. Last, biosensors were functionalized using different functional materials and testing experiments using *Escherichia coli* (*E. coli*) were performed based on the biosensor test systems.

4.1 Design of the solution reservoirs

The small experimental solution reservoirs were created using a biochemical plastic pipe with ~4 mm diameter and bonded together with biosensors using uncured PDMS method according to the following program.

1. 2 ml of freshly mixed PDMS (10:1 ratio) was poured on glass slide, which was then spun at 1200 rpm for 40 second.
2. The plastic reservoirs which will be bond with the PDMS thin film were cleaned with isopropyl alcohol (IPA). They were then placed on the glass slide (about 15 minutes after spinning) and lifted off, leaving a layer of uncured PDMS on it.
3. The surface of previously fabricated biosensor was prepared for bonding by cleaning with IPA. The reservoirs with the thin layer of uncured PDMS was then placed on it surrounding the micro-membranes and cured at 60 °C for 5 minutes to prevent the uncured PDMS moving on the PDMS membranes.
4. And then, structures are cured at room temperature for 24 hours to obtain the final test structure, as shown in Figure 4-1.

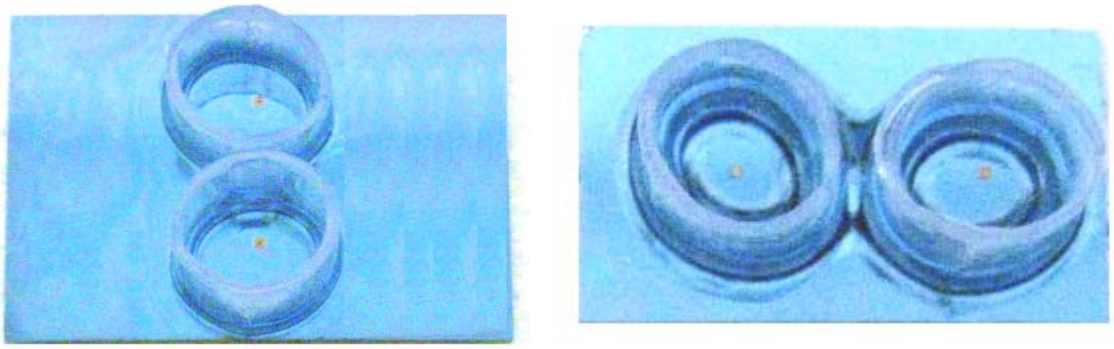

Figure 4-1: The biosensors with medium chamber surrounding the micro-membranes

4.2 Biosensor test system

4.2.1 SmartWLI-based biosensor test system

White-light interferometry (WLI) is an optical measurement technique for recording 3-D topographies with depth resolution in the nanometre range. The height information can be gathered over a large area in a very short time because the measurement points are acquired and processed in parallel. Typical applications in research and in quality management are to nanometer-accurately quantitate the surface roughness values (wafer structures, membrabe, mirrors, glass, and metals) and to precisely measure the curvatures of surfaces, such as microlenses, the deformation of micro membranes or cantilevers. The smartWLI (Gesellschaft für Bild- und Signalverarbeitung (GBS) mbH, Ilmenau Germany, as shown in Figure 4-2) was employed to set up the experimental test system to measure the membrane deflection of biosensor caused by surface stress.

Figure 4-3 illustrates the principle scheme and the real test system of the smartWLI-based biosensor test system built by us. The test system has a better spatial resolution (1 nm) and the membrane deflection information can be read nanometre-accurately and directly, but its time resolution is relatively low (~1 min.).

Figure 4-2: The smartWLI system composed of light system, camera system, piezoelectric control system and computer software control system (GBS mbH)

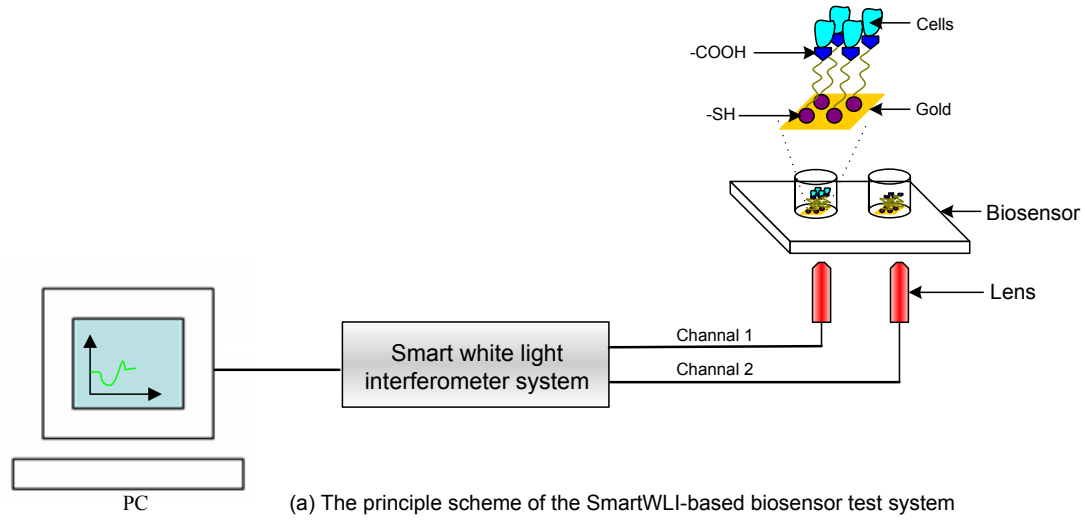

(a) The principle scheme of the SmartWLI-based biosensor test system

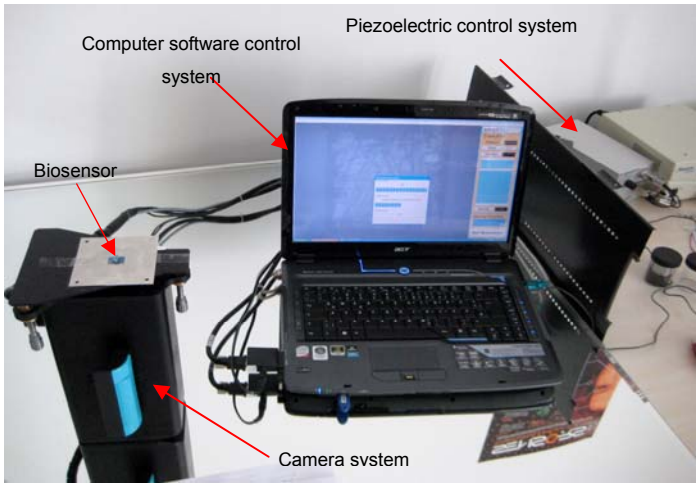

(b) Photograph of the test system

Figure 4-3: The smartWLI-based biosensor test system

The system error of the smartWLI-based biosensor test system was firstly measured to evaluate the system stability when nothing was imposed on the membranes of biosensor. Figure 4-4 illustrates three test signals measured by the test system corresponding to three biosensors. The maximal test error is about 4 nm for the system during the whole test time (16 minutes), which is quite smaller than the the deflection caused by the surface stress according to the theoretical simulation. Hence, the error from environment and system itself is small and the smartWLI-based biosensor test system is stable.

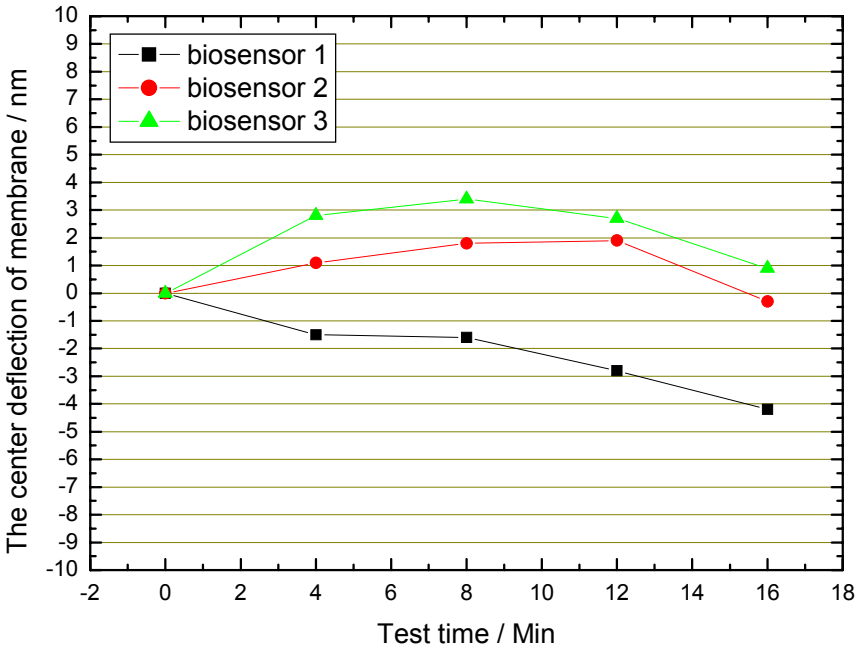

Figure 4-4: The test lines of smartWLI-based biosensor test system when nothing is on the membrane

4.2.2 FOI-based biosensor test system

Fiber optic interferometer is a mature technology and has many advantages in comparison to other methods for distance measurements, just like cited in the introduction in chapter 1: better performance, low loss, safety and so on. In theory, a deflection in the range of 10^{-11} to 10^{-13} m [161] can possibly be measured. The analog fiber optic sensor system TETRA® (TETRA Gesellschaft für Sensorik, Robotik und Automation mbH, Ilmenau Germany, Figure 4-5) was applied to build our FOI-based biosensor test system. Light emitted from a transmitting fiber is reflected by the surface under test. The reflected light is collected by the receiving fiber and is

transformed to electrical signals by an optoelectronic converter. The variable transmission of the light beam at the receiving fiber influences the receiving optical fiber.

Figure 4-5: The fiber optic sensor system

The signal-distance characteristics, as shown in Figure 4-6, are governed by the optical transmission behaviour and by the photometric distance law. It can work in two measuring ranges. The first measuring range (MR1, near range) is a very strong rise of voltage at a small displacement between the sensor tip and the target surface, which has better resolution. In the second measuring range (MR2, far range) the signal rise goes over a long distance. The signal maximum is described as a peak.

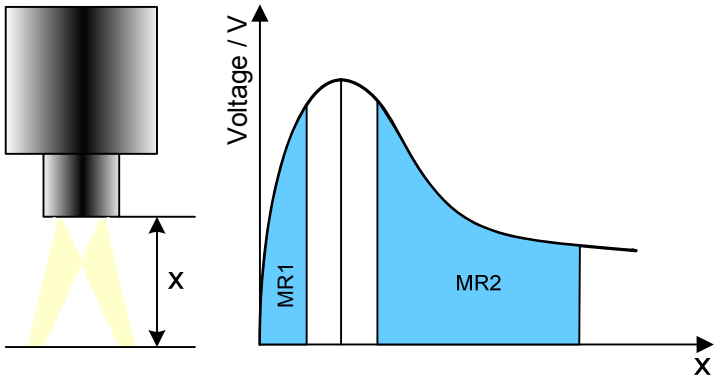

Figure 4-6: Signal distance characteristics

Figure 4-7 shows the principle scheme and the real test system of the FOI-based biosensor test system built by us, where the average membrane deflection signal is converted to an electric signal (voltage) through the fiber optic sensor system and monitored by the computer using software. NI USB-6210 I/O (NATIONAL

INSTRUMENTS®, National Instruments Corporation) is the adapter between computer and interferometer system. The FOI-based biosensor test system has a higher time resolution (< 0.5 sec.) than the smartWLI and can monitor signals continuously.

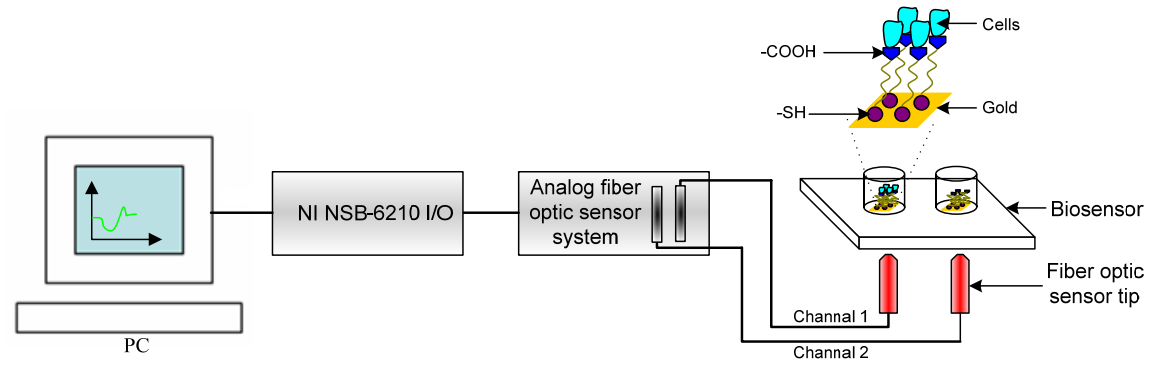

(a) The principle scheme of the FOI-based biosensor test system

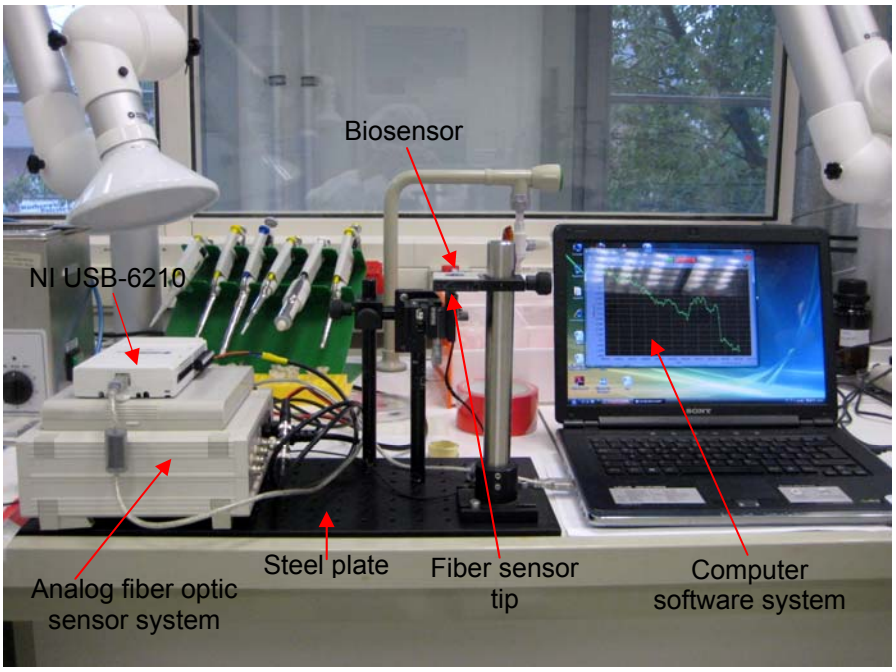

(b) The real photo of the test system

Figure 4-7: The FOI-based biosensor test system

The test software was edited based on the LabVIEW® software. It was finished under the help of Dipl.-Ing. Steffen Schneider in Department of Physical Chemistry and Microreaction Technology, Faculty of Mathematics and Natural Sciences, TU Ilmenau, Germany. Figure 4-8a shows the logic schematic diagram of test software, which has the accuracy of five-digit number after the decimal point, for getting more precise signals. Figure 4-8b illustrates the interface of the test software.

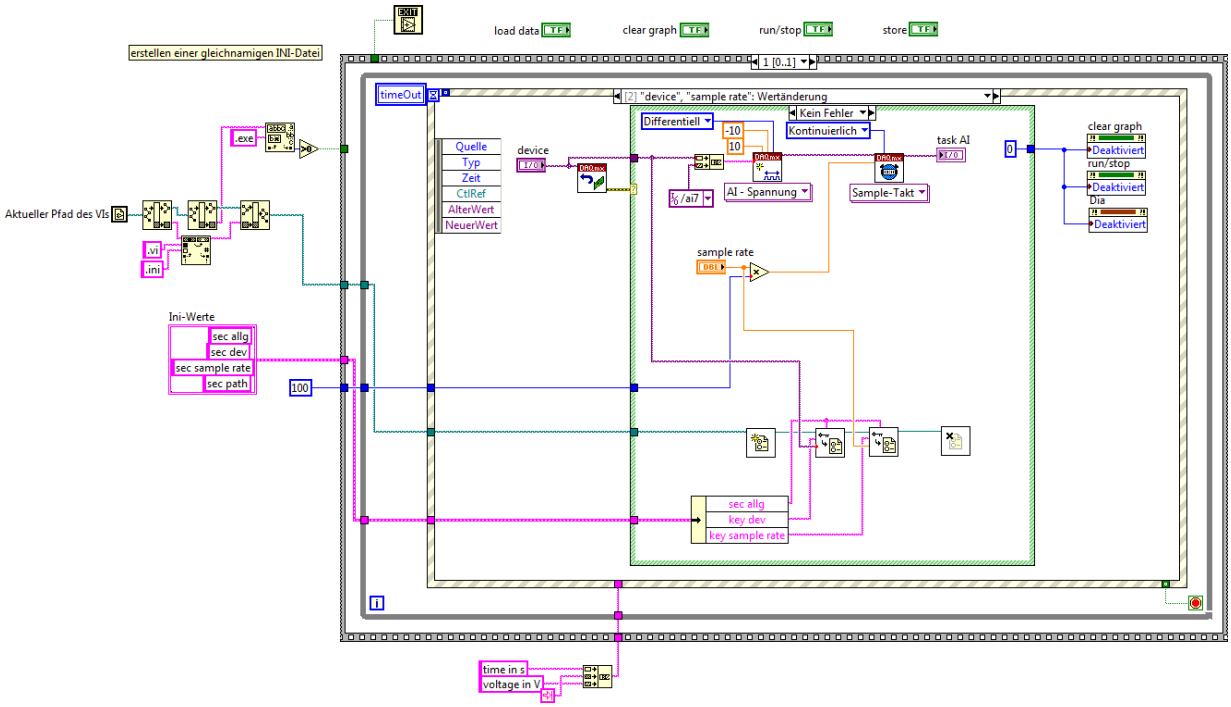

Figure 4-8a: The logic schematic diagram of FOI-based biosensor test system software

Figure 4-8b: The software interface of FOI-based biosensor test system

After the assembly of the FOI-based biosensor test system, the system error was evaluated when nothing was on the membranes. The maximal test error is about 0.003 V during the whole test time (about 2 hours), as shown in Figure 4-9, which is quite smaller than the equivalent of deflection caused by the surface stress based on the theoretical analyses. Hence, the error from environment and system itself is small and the test system is quite stable.

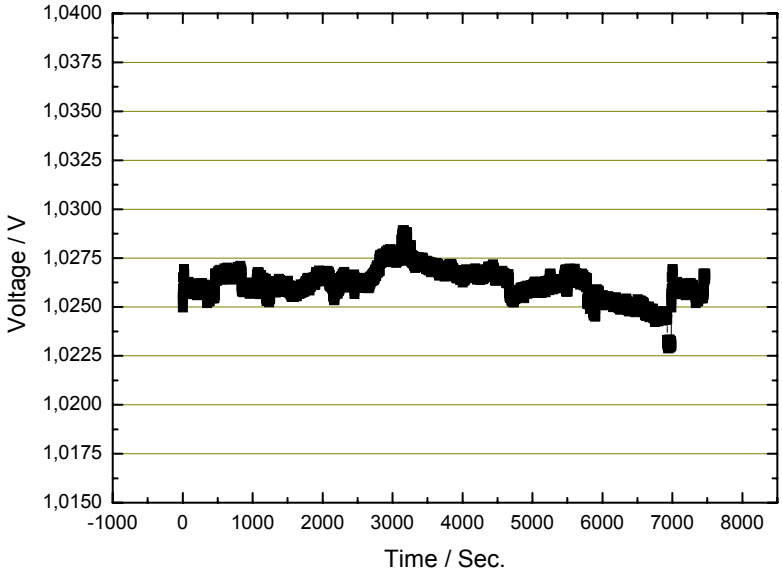

Figure 4-9: The test line of FOI-based biosensor test system when nothing is on the membrane

However, the main disadvantages of the test system are that: (1) Its spatial resolution is relatively low (min. 20 nm) because the resolution is affected easily by some factors, such as the topography of biosensor membranes, and the distance between the fiber sensor tip and the membrane. (2) The sensor signal depends on the reflection characteristic of the biosensor membranes, too. For example, the reflective quantity of light depends on the micron structure of the color of the surface; and the surface qualities have in restricted size an influence on the location of the peak distance and on the quantity of the peak signal. Hence, the characteristic curve is different if two biosensor membranes have some difference, as shown in Figure 4-10, the different characteristic curves of two different biosensors.

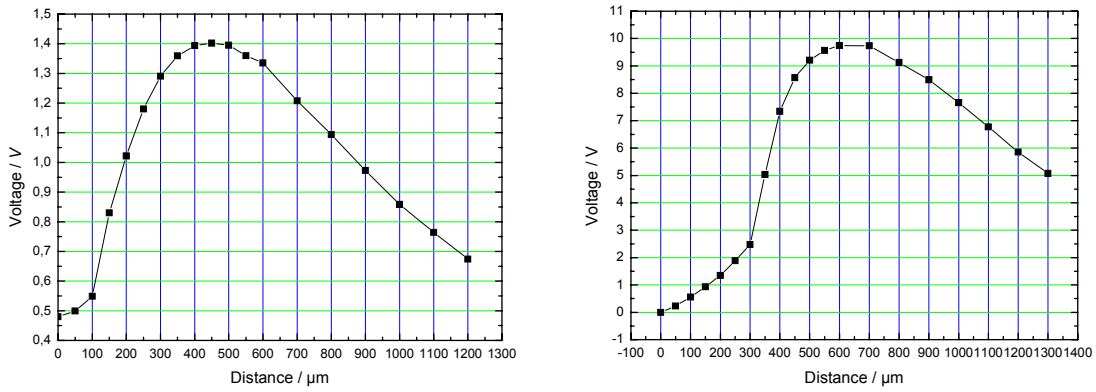

Figure 4-10: Real characteristic curves to different biosensor membranes

4.3 Functionalization

Three alkanethiol molecules with different functional end groups: 11 Mercapto 1 undecanoicacid (MUA: SH-$(CH_2)_{10}$-**COOH**), 11 Mercapto 1 undecanol (MUO: SH-$(CH_2)_{11}$-**OH**) and Dodecane thiol (DOT: SH-$(CH_2)_{11}$-**CH_3**) were selected as the biosensor coating layers for the *E. coli* detection.

4.3.1 Introduction of the three functional end groups

Carboxyl group, as shown in Figure 4-11

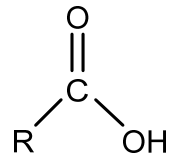

Figure 4-11: Model of carboxyl group

A carboxyl group is a set of four atoms bonded together and has two functional groups: carboxylic acids and amino acids (Bruce Alberts et al., Molecular Biology of the Cell, 2008). In every carboxyl group there is a double bond between the carbon atom and oxygen atom and a single bond between the carbon atom and hydroxyl group (OH). In this way a carboxyl group is equivalent to a carbonyl group bound to a hydroxyl group. The acidic nature of a carboxyl group arises from its H atom. Specifically, in aqueous solution the H atom can be transferred as H^+ to H_2O molecules, forming H_3O^+ and leaving behind a COO^- group. The COOH group has only a separate fleeting existence when not bound to a fifth atom. It is called the carboxyl radical and symbolized as •COOH in such cases [257]. The reference can be read in the study by Milligan and Jacox [257]. The acid dissociation constant of •COOH has been measured using electron paramagnetic resonance spectroscopy [258].

Hydroxyl group, as shown in Figure 4-12

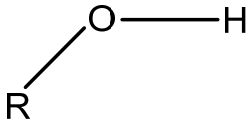

Figure 4-12: Model of Hydroxyl group

The functional group -OH is named as hydroxyl group, it is a substituent in an organic compound. C_nH_{2n+1}-OH is the simple formula of alcohols which are molecules containing in organic compound.

Hydroxyl group has the characteristic of hydroxyl radical. The hydroxyl radicals are very reactive and so have a short-timed life. They are the important components of radical chemistry.

Methyl group, as shown in Figure 4-13

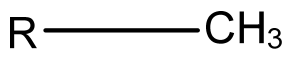

Figure 4-13: Model of Methyl group

The methyl group is named based on methane (CH_4) and it is a hydrophobic alkyl functional group. There are many such hydrocarbon groups in organic compounds. Due to the S_N2 reaction on iodomethane or the reaction of methyl lithium or MeMgCl with a carbon atom, the methyl groups can be incorporated into organic compounds.

The methyl groups as substituent of a compound usually have the characteristics of increasing lipophilicity and reducing solubility. Hence it is easy to absorb into biological membranes and difficult to release into aqueous surroundings. Incorporating a methyl group into a molecule can have three effects:

- by oxidizing the methyl group,
- by demethylation
- by reduction, reducing the analogue.

The reactivity of a methyl group is different when it attaches different substrates. The methyl radical is induced by the unpaired electron on the substance CH_3.

4.3.2 Functionalization of the biosensor membranes

The three functional materials were firstly deployed standard solution (concentration: 0.1mM) using ethanol as basic solution. The three standard functional solutions (20 µl, 0.1mM) were then loaded into different biosensor reservoirs using

micropipettes. The membranes were incubated in thiol solutions for the coating formation of SAMs until evaporation of all solutions. The functionalization process can be detected using the FOI-based biosensor test system due to its continuity, as shown in Figure 4-14. Once the membranes were functionalized, the entire chips were washed in ethanol to remove the non-specifically bound thiol molecules. The last membranes consist of three layers: PDMS layer, gold layer and SAM, as shown in Figure 4-15.

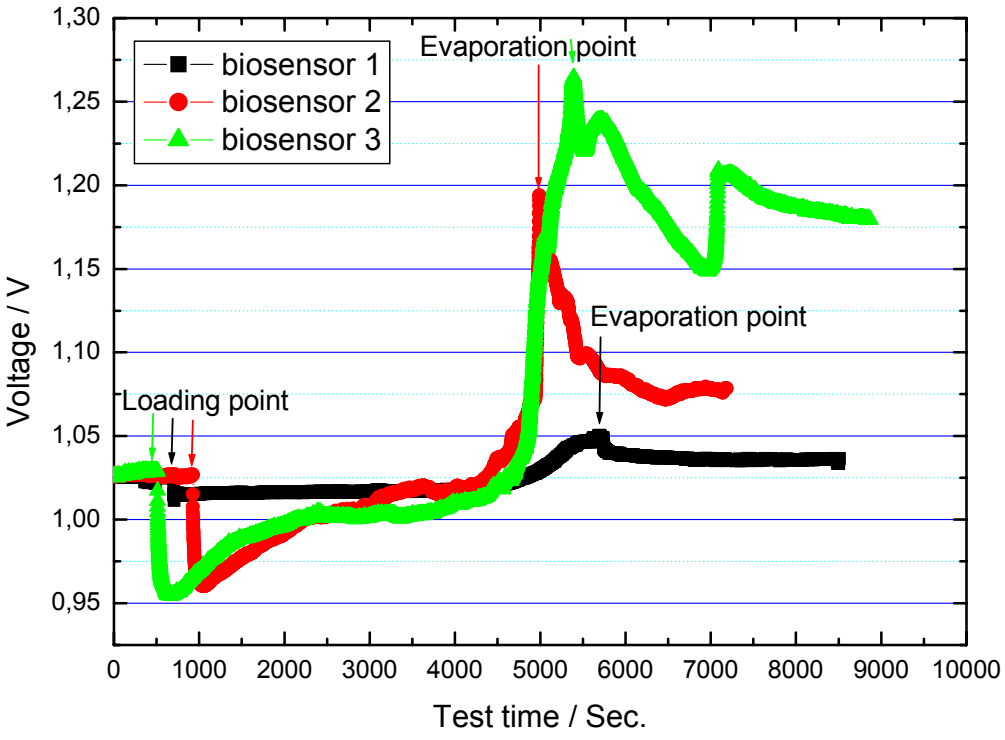

Figure 4-14: The functional process to the membrane of biosensor, observed by fiber-optic interferometer [P3]

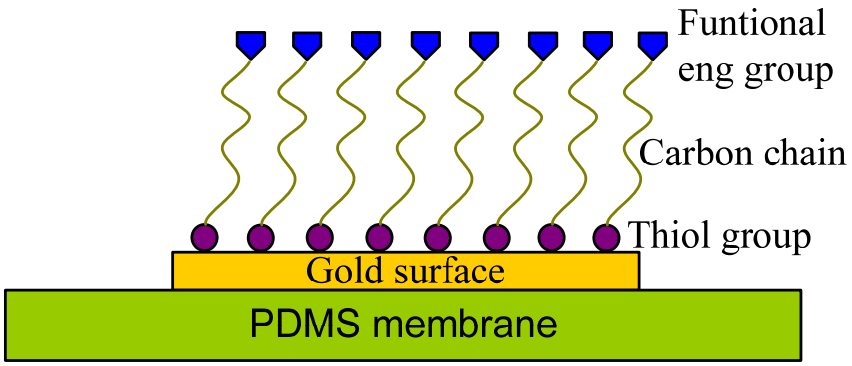

Figure 4-15: The schematic diagram of last biosensor membranes

Figure 4-14 shows the deflection characteristics of the membranes during the functionalization process. At the first stage, the weight of functional solution was the main factor for the membrane deflection, which made the membrane deflect in –Z direction. The voltage also became small as a result of the reflex of functional solution to laser. With the evaporation of functional solution, the surface stress resulting from the bond between gold and thiol group became the main influence factor. The surface stress to form a strong covalent bond between these sulphur atoms with gold surface atoms is equivalent to around 185 kJ/mol, hence the voltage became larger during the later stage until one stable level. It can also be concluded that the direction of membrane deflection caused by the weight of solution was opposite to the one caused by the surface stress, which is consistent with the theoretical prediction.

4.3.3 Testing of the Functionalization

SAMs on gold substrates can be characterized by various analytical techniques including Fourier transform infrared spectroscopy (FTIR) [259-261], X-ray photoelectron spectroscopy (XPS) [260, 262], surface plasmon resonance (SPR) [259, 261], ellipsometry [259], and quartz crystal microbalance (QCM) [263, 264]. Furthermore, the evaluation of functionalization can be tested by the alteration of the induced surface stress before and after SAMs. The smartWLI-based biosensor test system was employed in the test due to its advantage of nanometer resolution. First, 35 µl distilled water was loaded respectively on the no functionalized membranes and functionalized membrabes to measure the basic line. After the recovery of membranes, 35 µl *E. coli* medium (concentration: 1.7×10^3 cells/µl, Institute of Physics, TU Ilmenau, Germany) was loaded to measure the deflection caused by the surface stress. Figure 4-16 illustrates one comparative result of the not functionalized biosensor and the biosensor functionalized by MUA. The deflection has an obvious alternation when the membrane is functionalized or not. The reason is that the surface stress is different when the cells are absorbed on the not functionalized membrane and on the functionalized membrane. These phenomena will be explained in detail in the section 4.5.

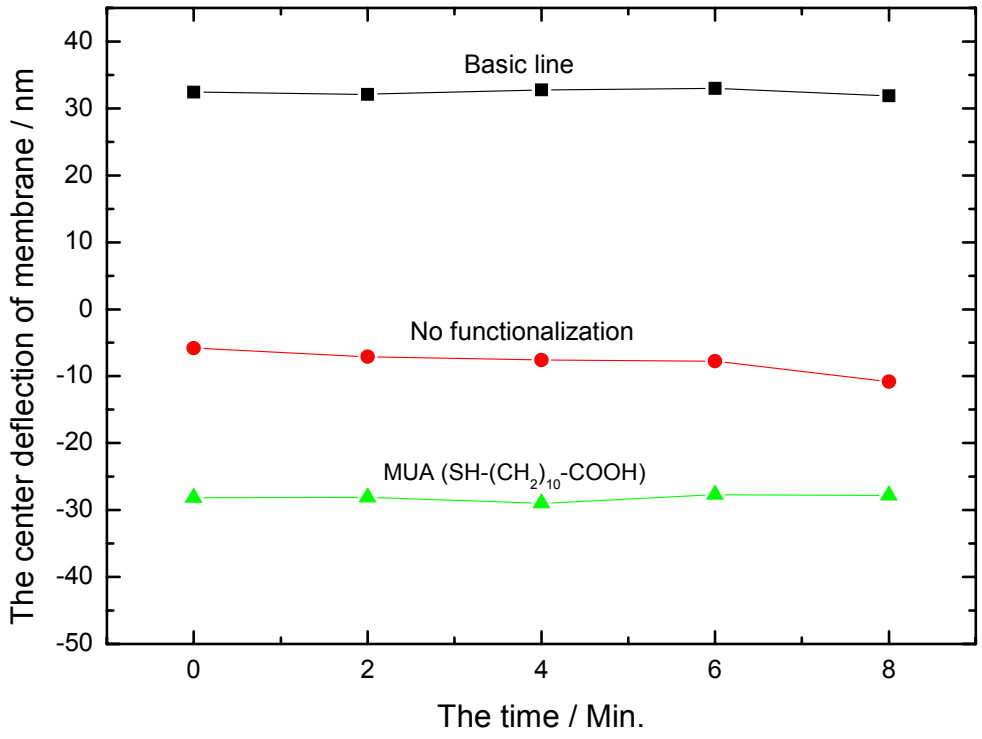

Figure 4-16: The membrane deflection before and after functionalization

4.4 Repeatability of the biosensor and test system

The repeatability of the biosensor and the two test systems was measured to evaluate the practicability of the biosensor and the test systems. In the experiment, lots of biosensors were measured once each day during a continuous five day period based on the two test system.

Figure 4-17 illustrates the test results of two biosensors based on the smartWLI-based biosensor test system. One biosensor was loaded with 25 µl of distilled water and the other was loaded with 35 µl for each measurement. Figure 4-18 shows the difference values between the measurements of each day.

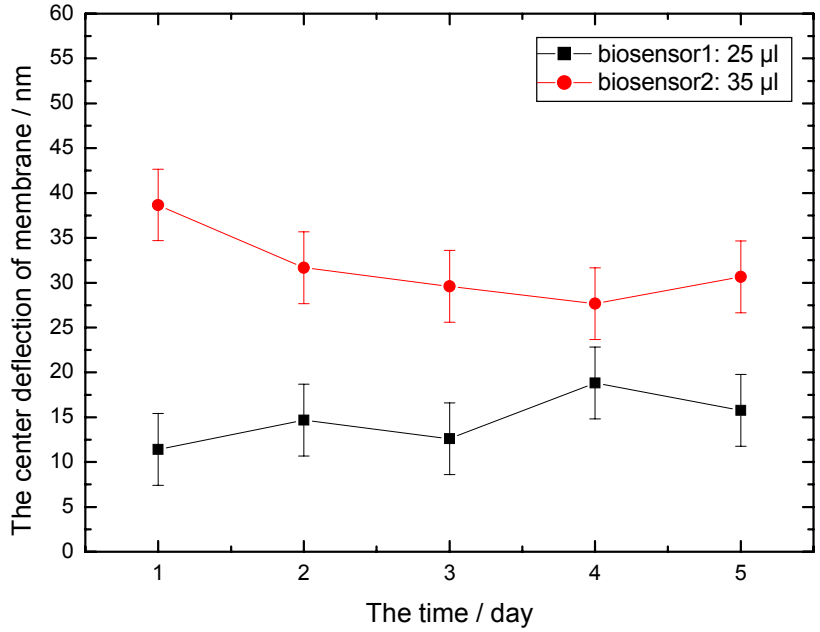

Figure 4-17: The test results of two biosensors during five days based on smartWLI

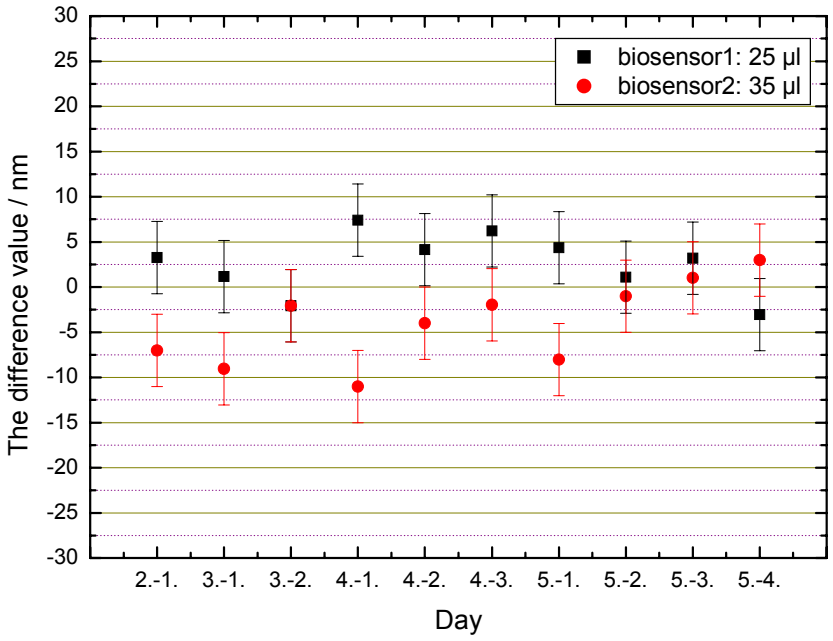

Figure 4-18: The difference values of biosensors during five days based on smartWLI

From Figure 4-17 and 4-18, it can be derived that the deflection has an obvious change when the amount of solution is different. The deflection measured at each day shows a little alteration. The maximal difference occured on fourth day, it is 7.39 nm for biosensor 1 and 11.01 nm for biosensor 2. After the system error (4 nm) is

subtracted, the maximum is about 3.39 nm and 7.01 nm, which may be induced by the environmental factor, such as the temperature or pressure. However, the difference value is smaller than the membrane deflection caused by the surface stress based on the theoretical simulation. Hence, biosensors and the test system show good repeatability.

For the FOI-based biosensor test system, 35 µl distilled water was loaded on the biosensor membranes for each day's measurement. Figure 4-19 shows the test results of two biosensors during a continuous five days period. The deflection curves of biosensors show good repeatability. Figure 4-20 illustrates the difference values between the measurements. The maximal difference value of biosensor 1 occured between the first day and the fifth day, and between the second day and the fourth day for biosensor 2, about 0.0075 V, 0.0045 V after subtracting the system test error, which is also quite smaller than the membrane deflection caused by the surface stress. Hence, the biosensor test system shows good repeatability. The bigger difference at the loading point was mainly induced by the operation factor for the load of distilled water.

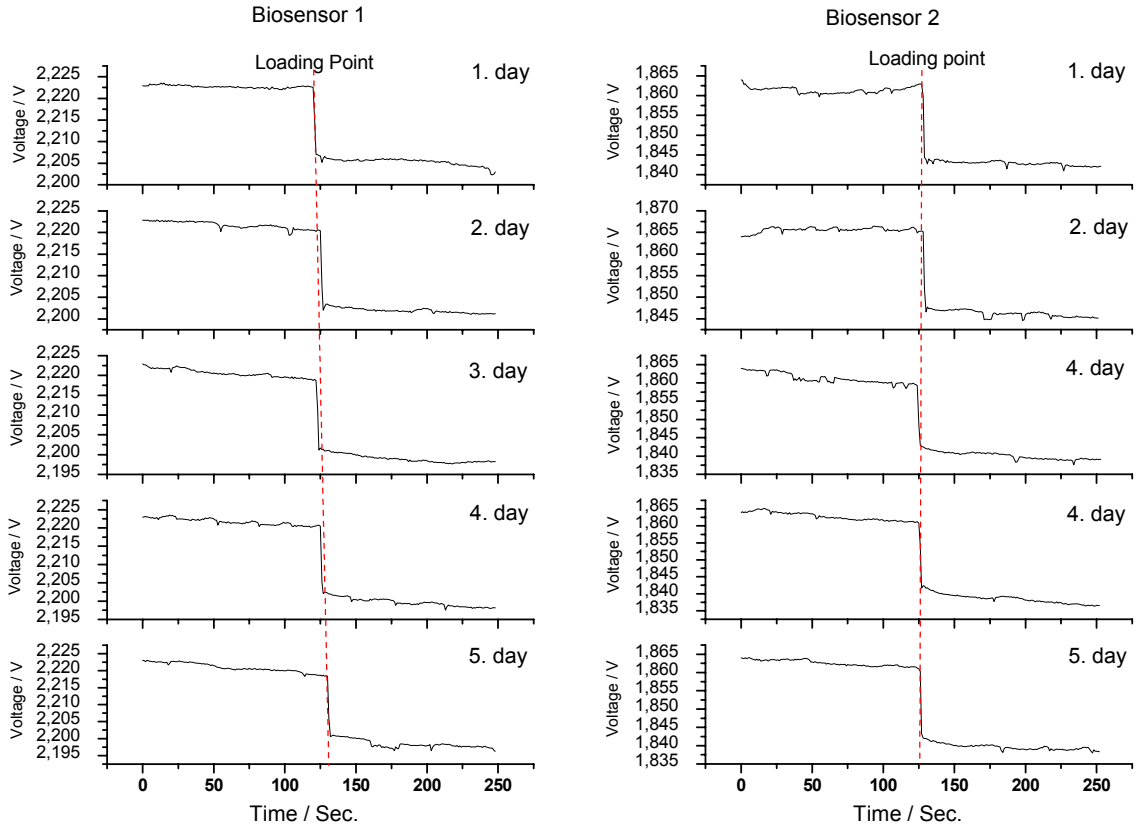

Figure 4-19: The test results of two biosensors during five days based on FOI

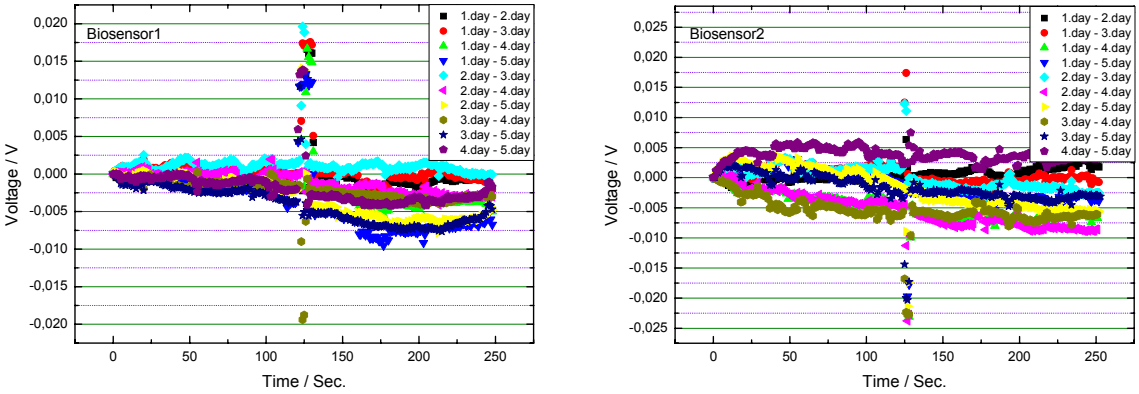

Figure 4-20: The difference values of biosensors during five days based on FOI

4.5 Application to *E. coli*

E. coli (Institute of Physics, TU Ilmenau, Germany) was selected as the source of analytes. The *E. coli* were first cultivated in a LB medium for 24 h at 37 °C under stirring. Afterwards an *E. coli* sample solution with the concentration of 1.7×10^3 cells/µl was produced.

4.5.1 Selection of SAMs for *E. coli* detection

Four biosensors were selected: not functionalized and functionalized by MUA, MUO and DOT respectively. The smartWLI-based biosensor test system was applied in the experiment due to its high spatial resolution. The membrane deflections can be read nanometre-accurately and distinguished obviously. First, 35 µl distilled water was loaded on the membranes to measure the basic test line for normalizing the four biosensors. After the recovery of membranes, 35 µl *E. coli* medium (1.7×10^3 cells/µl) was loaded separately to measure the deflection caused by the possible surface stress between *E. coli* and different membrane. Figure 4-21 shows the deflection information of the four biosensors.

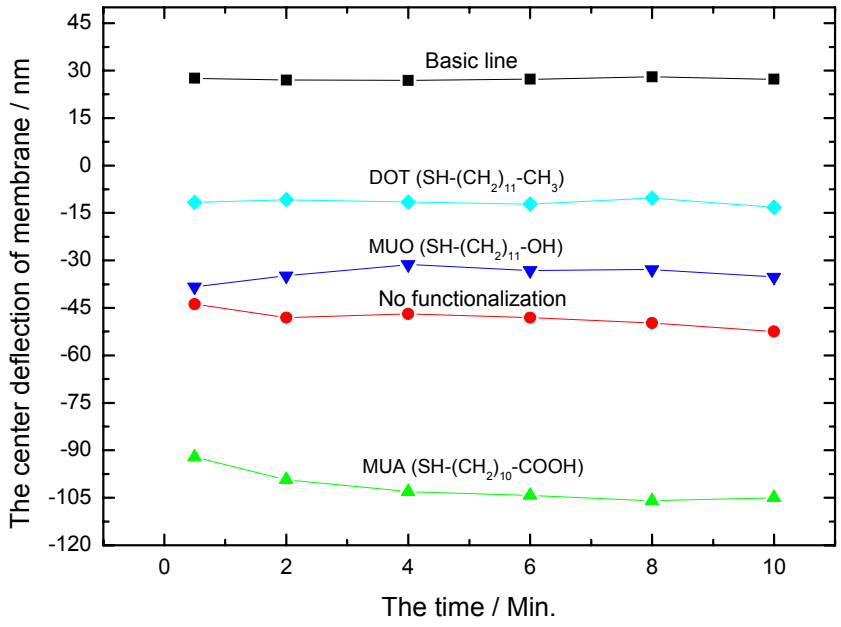

Figure 4-21: The normalization deflection of different functionalized membrane caused by surface stress [P3]

The surface stress presented between *E. coli* and the membranes, and the direction of membrane deflection induced by the surface stress was opposite to the one induced by the weight of medium. The variations of membrane deflection were small during the whole test period (10 minutes), since no big change of the medium and the absorption quantity of *E. coli* on the membranes was observed for a short period. However the values of surface stress differ for different functional membranes. It can be explained based on the molecular biology of the cell [265] and biochemical molecular reaction.

Phospholipids, amino acid and cholesterol are three major chemical structures of main cell out layer component. Most phospholipids contain a diglyceride, a phosphate group, and a simple organic molecule such as choline; sphingomyelin is one exception to this rule because it is derived from sphingosine instead of glycerol. They are a type of molecule and form a lipid bilayer within a cell membrane. =O is one main biochemical bond of phospholipids [265]. An amino acid is a molecule that contains two functional groups, an amine ($-NH_2$) and a carboxylic acid (-COOH). The variation of natural amino acids arises from differences in its side chain. This structure may change so that a proton from the COOH transfers to the NH_2 and a zwitterion is formed in an aqueous solution. The alteration of structure is relative to

the solution pH. Most physiological systems are with such a pH range that makes amino acids as the zwitterion form, hence they are most stable in the human body. One particularly important function of amino acid is as the building blocks of proteins. Twenty common amino acids have been found in proteins. Amino acids can be classified into three groups based on the different natural property of side chain. Some side chains are nonpolar. and nine kinds of the amino acids have the side chains. The second type is the amino acids that have polar side chains. Finally, a group of five amino acids have not only polar but charged side chains. The amino acids can link together to form proteins, which is one of their important characteristics. The two ends of amino acids, COOH functional group and NH_2 functional, can react with each other because the COOH functional group has the acid characteristic and the NH_2 functional group is a base [265]. There are -OH and hydrogen bonds in the chemical structure of cholesterol [265].

Furthermore, *E. coli* is a Gram negative bacterium. The composition of a Gram-negative bacterial membrane is shown in Figure 4-22 [266]: The inner or cytoplasmic membrane surrounds the bacterial cell. The periplasm, which contains peptidoglycan, is surrounded by the outer membrane. The outer leaflet of *E. coli* outer membrane grows the Lipopolysaccharide (LPS) which consists of three distinct components [266]: lipid A, oligosaccharide core, and O-antigen. The oligosaccharide core contains an unique sugar, 2-keto-2-deoxyoctonate (KDO). Figure 4-23 and 4-24 illustrates the main molecular chemical structures contained in the membrane of *E. coli* in addition to phospholipids, cholesterols and amino acids.

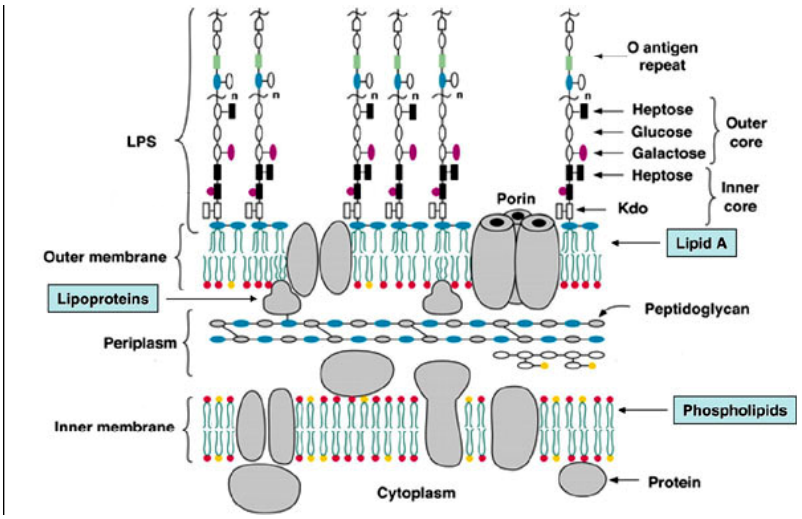

Figure 4-22: The composition of a Gram-negative bacterial membrane [266]

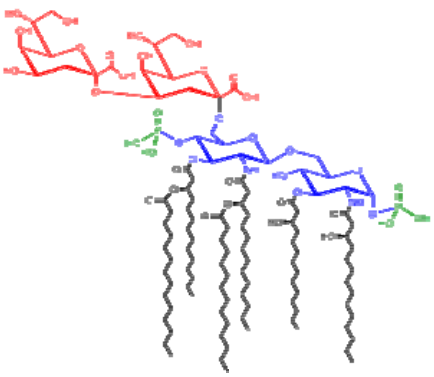

Figure 4-23: Saccharolipid Kdo-Lipid A [W4]

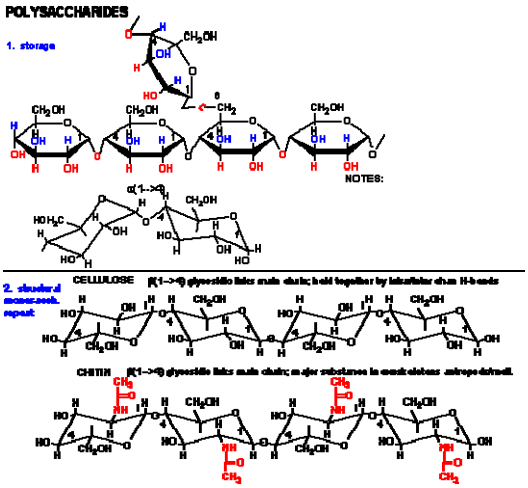

Figure 4-24: O antigen (or O polysaccharide) [W5]

Based on the front analysis of biochemical structures, the out layer of *E. coli* contains lots of -NH_2, -COOH, -OH, -COH_2, =O and -H chemical bonds. In addition, the four different biosensor membranes have their own chemical structure as shown in Figure 4-25.

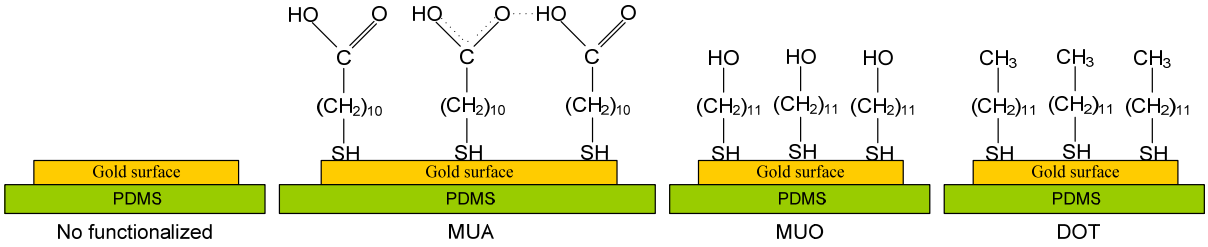

Figure 4-25: The molecular structure diagram of different membrane surfaces

Therefore, some possible bonds between *E. coli* and different functionalized membranes could happen based on the chemical molecular bonds and reactions: (1) MUA: functional end group -COOH has the possible interaction with -NH_2, -COOH, -OH and =O and bond together, some examples are shown in Figure 4-26, which induce the surface stress resulting in the deflection of membrane. In addition, electrostatic effects and the Van der Waals force between molecules may also play roles on the membrane. (2) MUO: functional end group -OH may have the interaction with =O and bond together, such as the illustration in Figure 4-27. Furthermore, the van der Waals force may be an acting force. All these factors result in the surface stress and accordingly in the membrane deflection. (3) DOT: the main connections between the functionalized membrane and *E. coli* were achieved by the van der

Waals force, but van der Waals force is relatively weak compared to other chemical bonds; it is normally smaller than 5 kJ/mol. (4) No functionalization: between -NH_2 and gold particles may occur possible bonds just like Figure 4-28 shows [267]. Moreover, some other molecules included in the out membrane layer may have the interaction with gold too, as shown in Figure 4-29, which is related to the pH of solution [268].

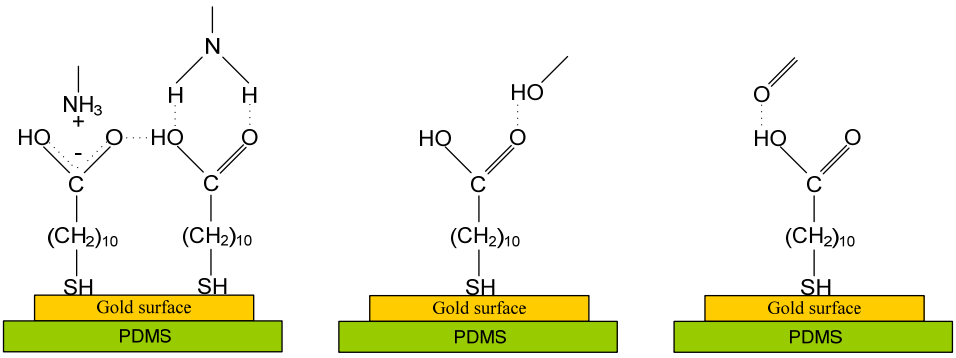

Figure 4-26: The possible bond way between MUA and *E. coli*

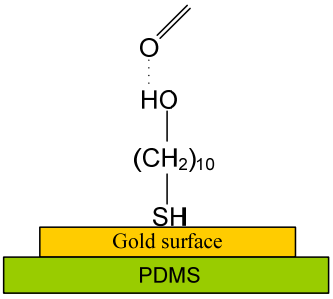

Figure 4-27: The possible bond way between MUO and *E. coli*

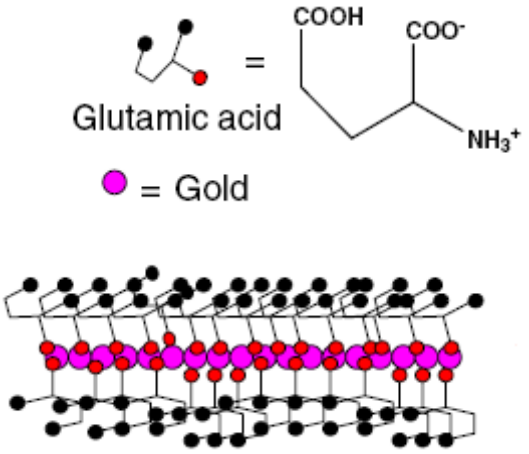

Figure 4-28: Illustration of Au nanochain and nanowire formation through dipole–dipole interaction due to the zwitterionic nature of amino acids [267]

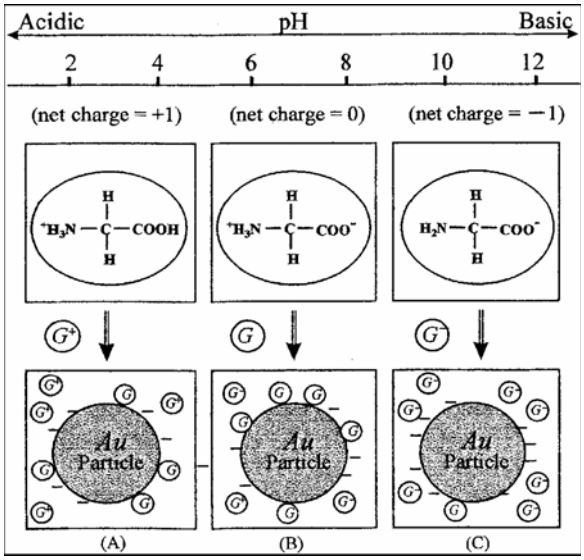

Figure 4-29a: Structure of Gly and the mechanism of its adsorption onthe gold colloid: (A) Gly with the positive charge; (B) Gly in theneutral state; (C) Gly with the negative charge [268]

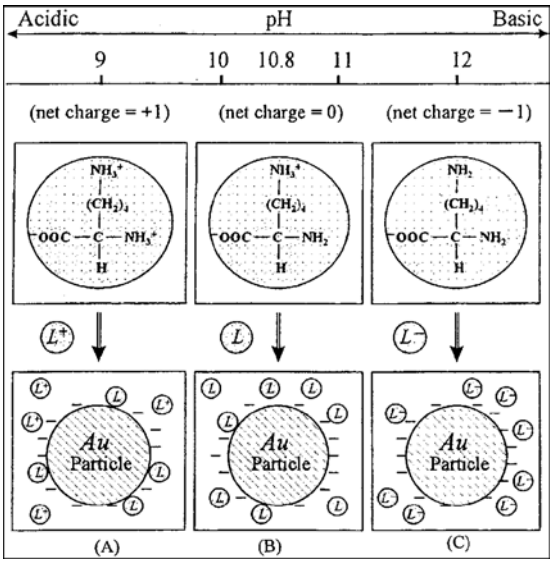

Figure 4-29b: Structure of Lys and the mechanism of its adsorption onthe gold colloid: (A) Lys with the positive charge; (B) Lys in theneutral state; (C) Lys with the negative charge [268]

In conclusion, the possible amount of *E. coli* attached on different functionalized membranes is: -COOH > -OH > $-CH_3$. Similar conclusion has also be reported in the reference [269], -OH > $-CH_3$ for peptide, protein, and cellular interactions with self-assembled monolayer model surfaces. But, it is not clear to the non functionalized membrane.

Furthermore, the strength of surface stress (interaction stress or chemical bond stress) is also one main factor to affect the membrane deflection. The strength of bonds varies with different chemical bonding type. There are “strong bonds” and “weak bonds” although there exist overlaps in strength within these bond classes. Covalent bonds and ionic bonds are “strong bonds”, for example, and dipole-dipole interactions, van der Waals' bonds, the London dispersion force and hydrogen bonding belongs to the “weak bonds”. In general, if there is sharing or transfer of electrons between the participating atoms, it is strong chemical bonding. Table 4-1 lists the categorization of chemical bond based on their strength.

To sum up, the possible strength between alive *E. coli* and different functionalized membranes is -COOH > Au > -OH > $-CH_3$, which is consistent with the experimental result shown in Figure 4-21 and MUA is the best functionalized material in the three functional materials for *E. coli* detection.

Table 4-1: The categorization of chemical bonds [W6]

Chemical bonds		
"Strong"	**Covalent bonds & Antibonding**	**Sigma bonds**: 3c-2e · **bent bond** · 3c-4e (Hydrogen bond, Dihydrogen bond, Agostic interaction) · 4c-2e **Pi bonds**: π backbonding · Conjugation · Hyperconjugation · Aromaticity · Metal aromaticity **Delta bond**: Quadruple bond · Quintuple bond · Sextuple bond Dipolar bond · Hapticity
	Ionic bonds	Cation-pi interaction · Salt bridge
	Metallic bonds	Metal aromaticity
"Weak"	**Hydrogen bond**	Dihydrogen bond · Dihydrogen complex · Low-barrier hydrogen bond · Symmetric hydrogen bond · Hydrophile
	Other noncovalent	van der Waals force · Mechanical bond · Halogen bond · Aurophilicity · Intercalation · Stacking · Entropic force · Chemical polarity
Other	Disulfide bond · Peptide bond · Phosphodiester bond	
Note: the weakest strong bonds are not necessarily stronger than the strongest weak bonds		

4.5.2 *E. coli* detection based on the smartWLI-based biosensor test system

The experimental biosensor membranes were functionalized using MUA. 35 µl distilled water was firstly loaded in the solution reservoirs of the biosensors to measure the basic deflection signals. After the recovery of membranes, 35 µl medium with healthily living and with dead *E. coli* (1.7×10^3 cells/µl) was loaded respectively to measure the deflection caused by the possible surface stress between *E. coli* and membranes. Figure 4-30 illustrates the results. The direction of membrane deflection induced by surface stress is converse to that by water, which indicates that the direction of surface stress is converse to the weigth direction and this is consistent with the theoretical analysis. The deflection caused by living *E. coli* was bigger than that caused by dead *E. coli*. The hypothetical reason is that the surface stress resulting from living *E. coli* is bigger than that of dead *E. coli*, some changes on the membrane of *E. coli* will happen after it dies, especially for the outmost lipopolysaccharides (LPS). LPS is a major component of the *E. coli* outer membrane, which has great importance for the structural integrity of *E. coli.* LPS can protect the membrane from certain kinds of chemical attack. Further, it can help to stabilize the overall membrane structure and increase the negative charge of the cell membrane. It may induce the death of the *E. coli* if LPS is mutated or removed. For example, the LPS collapses after death by heating, and different folding of the Braun

protein result in a decrease of the periplasmic space, increase the cytoplasmic turgor pressure due to water afflux in the most concentrated compartment, Figure 4-31 [270]. These changes reduce the bond way and the amount of bonds between *E. coli* and biosensor membrane, and thus the deflection becomes smaller.

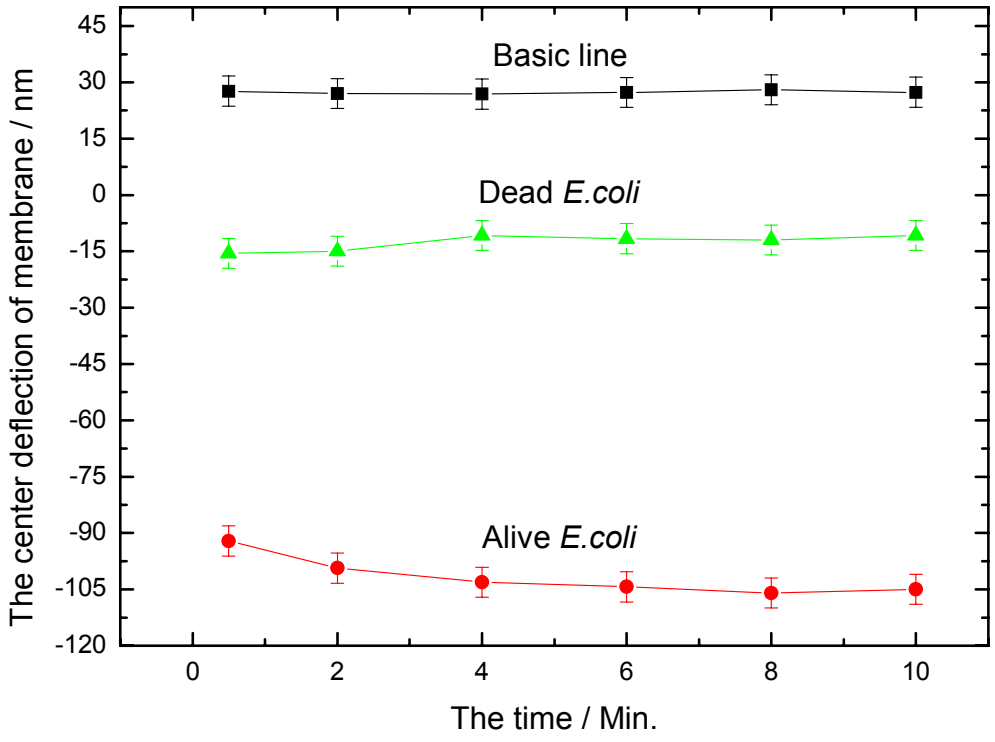

Figure 4-30: The center deflection of membrane resulting from water load and different status of *E. coli* [P3]

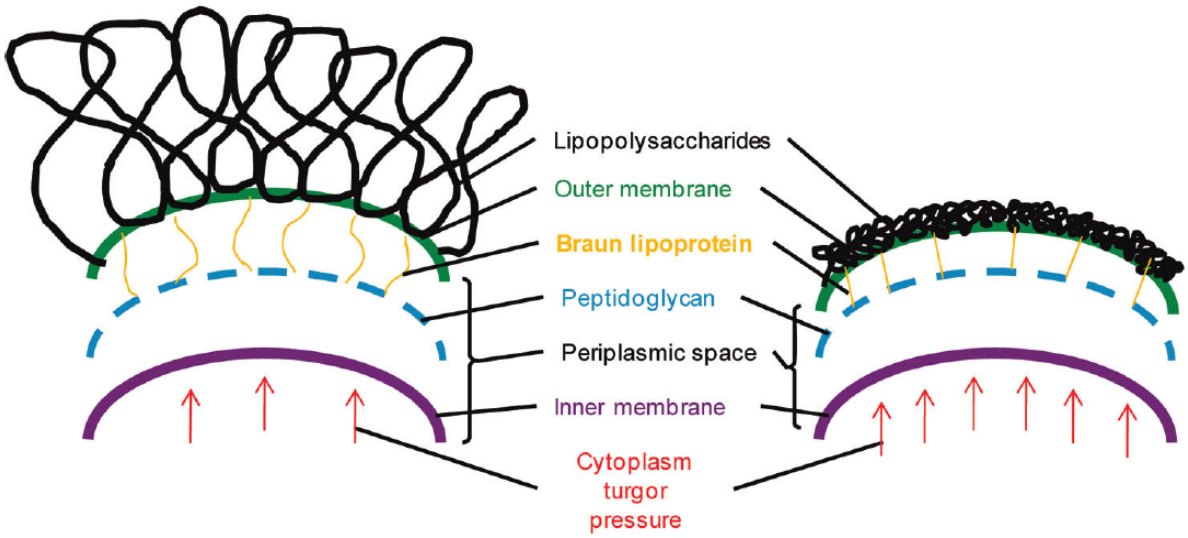

Figure 4-31: Hypothesis on the change of the membrane of *E. coli* after death by heating [268]

One hypothesis can be proposed that the deflection of membrane caused by other conditions of *E. coli* (between healthy living and death) may provoke the interval values. The reason is that: Cells will have some changes when they are under different conditions based on the basic cytopathology theory [271]. It is also well known that the contents and structures of the cytoskeleton defining a cell's shape can be transformed by cancer [272, 273]. In addition to cancer, cytoskeleton alterations have close relations with several diseases, including circulatory problems, blood diseases (malaria, anemia, and hereditary spherocytosis), motor neuron diseases (sclerosis), and aging related diseases (Alzheimer) [274-276]. Generally, cancer cells exhibit lower elasticity and viscosity, and higher deformability than normal cells. The differences that exist between cancerous and normal cells are due to the changes in cytoskeletal content and structure. The cytoskeleton of cancer cells shows fewer filamentous actin, intermediate filaments and microtubules, and appears more irregular and compliant than that of normal cells [276, 277]. These changes may alter the surface stress, which can be quantized through lots of experiments and is useful for the medical test and analysis.

4.5.3 *E. coli* detection based on the FOI-based biosensor test system

In this experiment, the membrane deflection signals coming from healthily living *E. coli* and dead *E. coli* were monitored by the FOI-based biosensor test system. First, 20 µl pure medium (without *E. coli*) was loaded to measure the basic reference signals, as shown by the lines 1 and 2 in Figure 4-32. After the recovery of membranes, 20 µl medium with healthily living and with dead *E. coli* (concentration: 1.7×10^3 cells/µl) was added respectively to measure the deflection signals caused by the possible surface stress, lines 3 and 4 in Figure 4-32.

Lines 1 and 2 in Figure 4-32 represent the basic reference signals. The voltage had a big change at the loading point because the membrane deflections were first mainly caused by the medium weight; in addition, the reflex of medium to laser was another reason to make the test voltage become small. With the evaporation of medium, the influence factors of weight and reflex became smaller and the signals increased again. The active signals are shown by line 3 and 4 in Figure 4-32. The primary deflections also came from the weight and the reflex of *E. coli* medium, so at the

loading point the active signals became smaller as well. However, the voltages of active signals were bigger than the reference signals. The reason is the surface stress resulting from the bonds of *E. coli* with the functionalized membranes, and the direction of membrane deflection caused by the surface stress was converse to that by the weight of medium, which was consistent with the theoretical analysis. The active signals increased with the evaporation of medium. The last voltage may be bigger than the origination point due to the lasting surface stress induced by the long time physical absorption of *E. coli* on the membrane surface. However, the difference of signals between living *E. coli* and dead *E. coli* is not so obvious as the results from the smartWLI-based biosensor test system were. The reason is that the spatial resolution of the current FOI-based biosensor test system is low, which can be improved by using the "better" FOI system, with the negative aspect of getting a signal representing "average" deflection in the ROI.

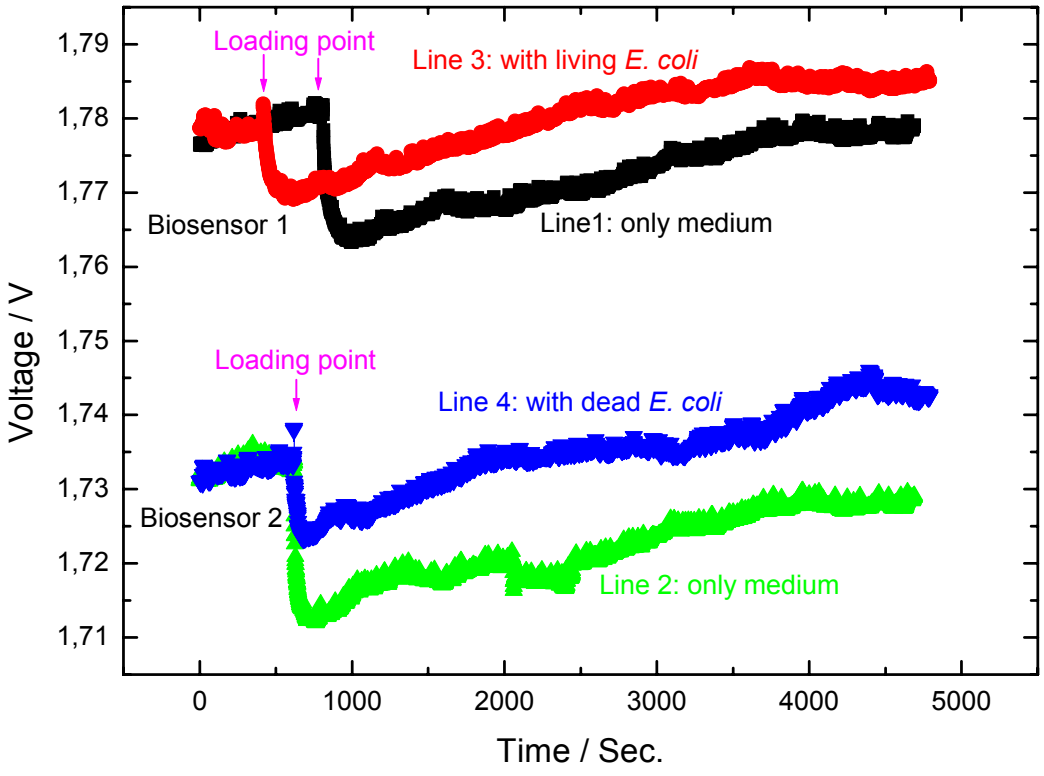

Figure 4-32: The comparison of FOI signals between pure medium and the medium with alive resp. dead *E. coli* [P3]

4.6 Other experiments

4.6.1 Detection of different solutions based on the biosensor

The FOI-based biosensor test system was applied in the experiment due to its high time resolution (< 0.5 sec.) and can monitor signals continuously. First, the basic signal was measured when nothing was loaded on the biosensor membrane. 20 µl distilled water, ethanol and MUA solution were then added orderly and the active signals were measured, the interval was about 1 hour to make sure the membranes recovered completely. Figure 4-33 illustrates the signals corresponding to different solutions. For water and ethanol, the weight and the reflection to laser are the main influence factors to the membrane, so the detected voltages became small at the first stage. With the evaporation of solutions, these influences decreased and the voltages became large again; the membrane recovered little by little until the original level. For MUA solution, the weight and the reflection to laser were also the main influence factors to the membrane at the first stage, so the voltage became firstly small, too. However, the change of voltage was smaller than with water and ethanol, and the last voltage was larger than the original level. The possible reason also arises from the surface stress, the effect of which has been explained in detail in section 4.3.2.

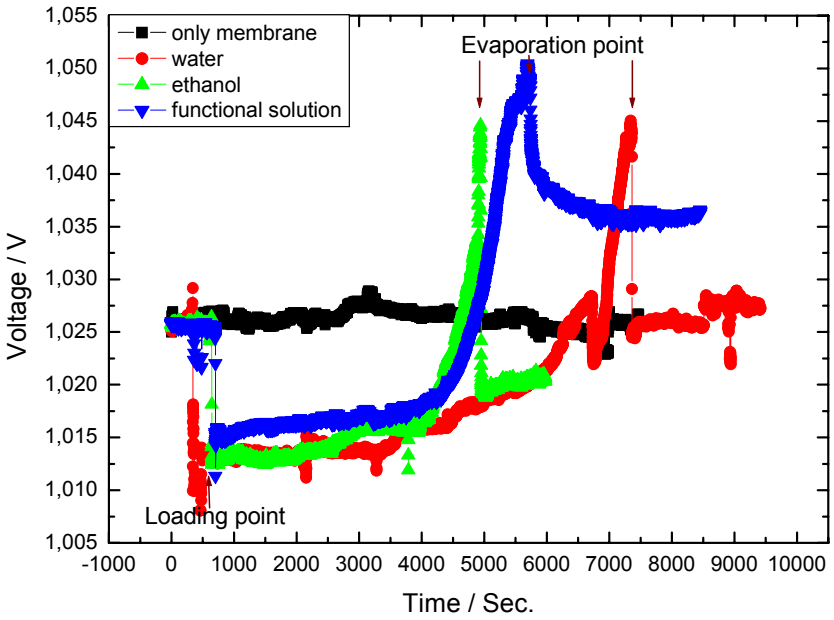

Figure 4-33: The biosensor reaction to different solutions

4.6.2 Pressure reaction of the biosensor

SmartWLI-based biosensor test system

One pressure source was employed and connected with the biosensor using one plastic pipe to finish this experiment, as shown in Figure 4-34. The pressure with the value from 0 kPa to 6 kPa was loaded and released step by step, and the membrane deflection was measured at each step. Figure 4-35 illustrates three curve lines of the measurement. The biosensor is very sensitive to the pressure. A small pressure change can cause a large alteration of membrane deflection, which is nearly a linear relationship with the slope of 1.6 μm / kPa. But, the deflection is different to one same pressure during the loading process and releasing process (hysteresis), the main possible reasons are that (1) it needs long time for the membrane to recover; (2) the gas was not released completely during the measurement.

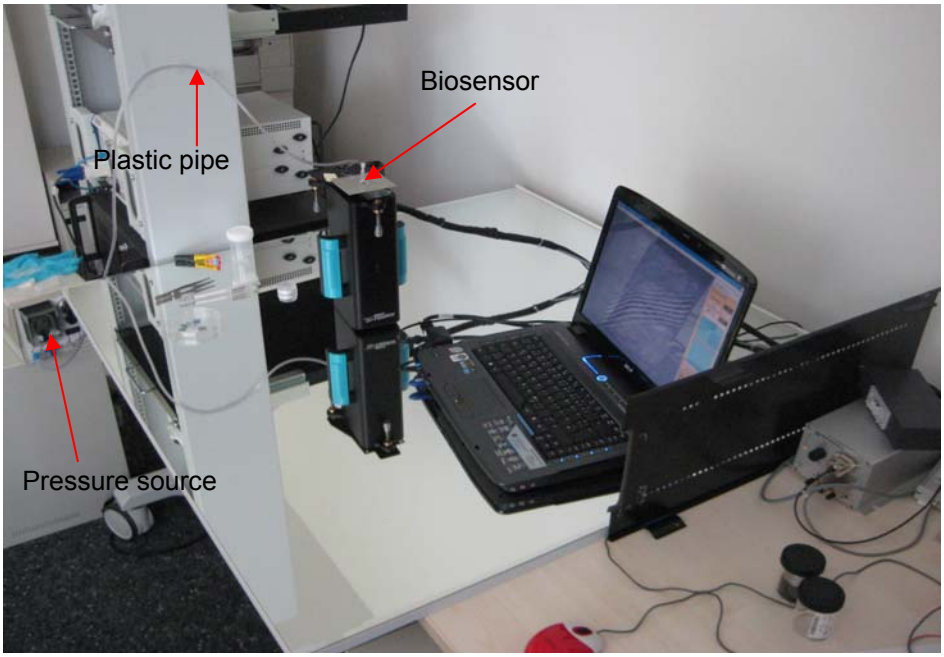

Figure 4-34: SmartWLI-based biosensor test system, pressure as the load

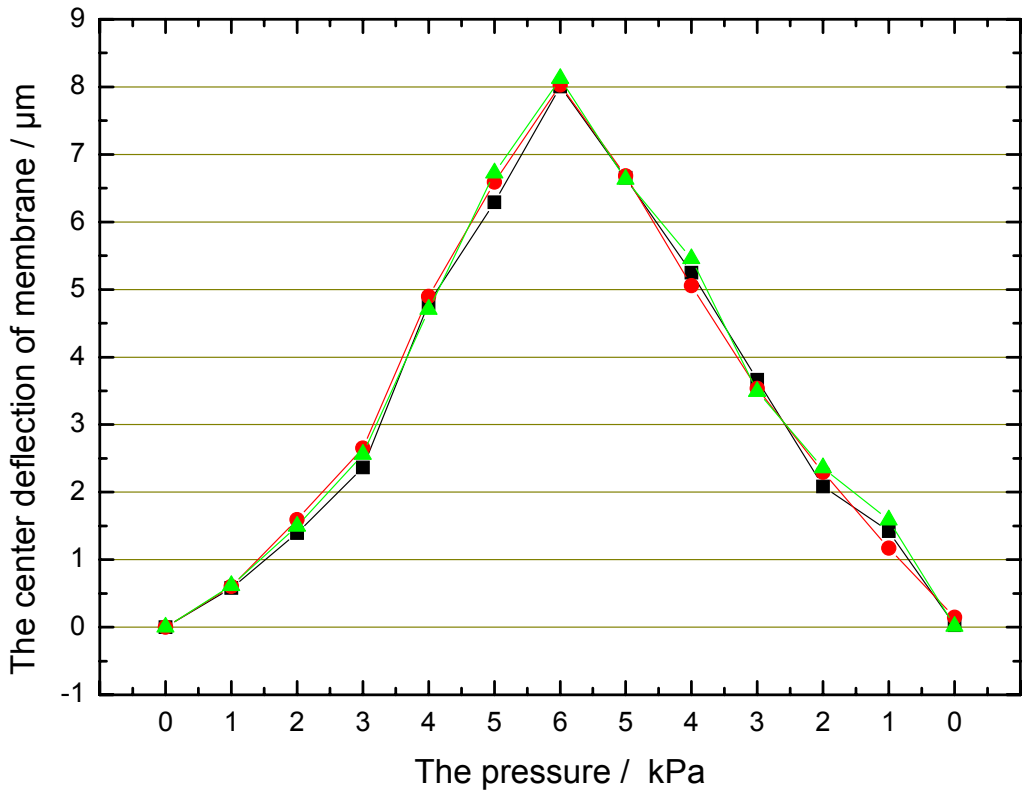

Figure 4-35: The biosensor's responding to pressure measured by the smartWLI-based biosensor test system

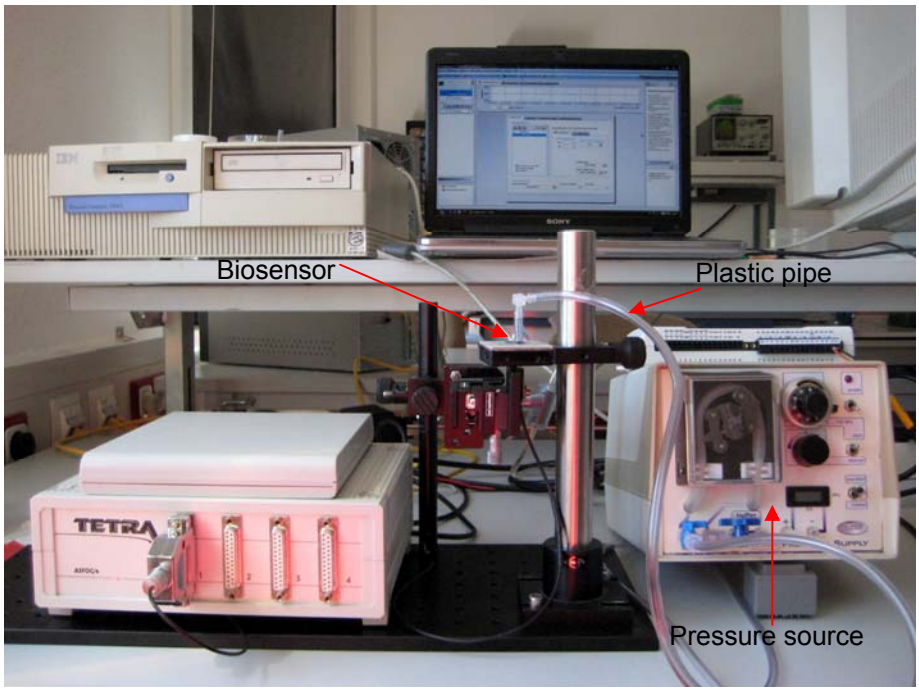

Figure 4-36: FOI-based biosensor test system, pressure as the basic load

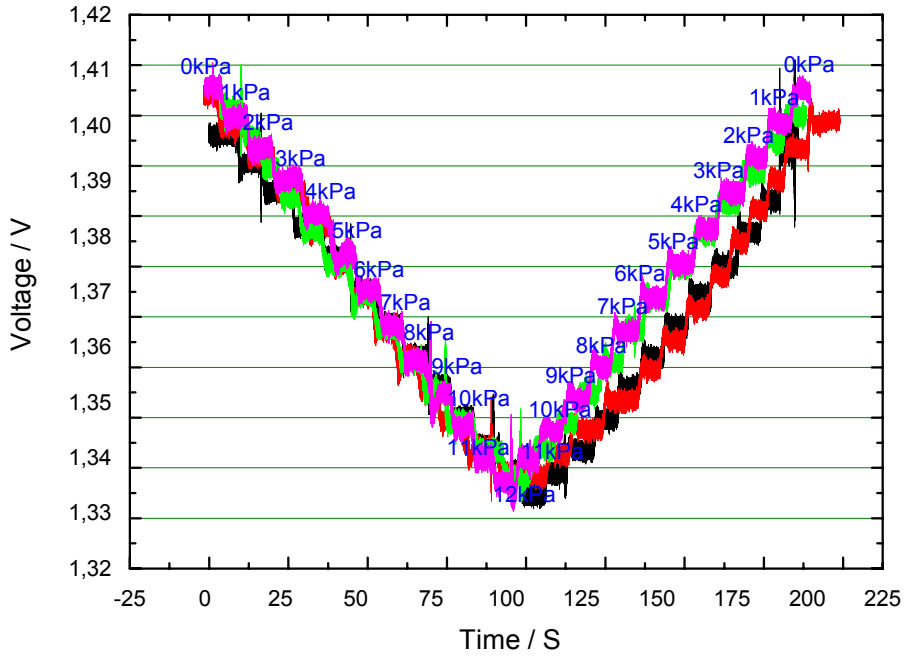

Figure 4-37: The biosensor's responding to pressure measured by the FOI-based biosensor test system

FOI-based biosensor test system

Figure 4-36 illustrates the whole test system when the pressure source was connected with the FOI-based biosensor test system. The advantage of the test system is that the signals of membrane deflection can be monitored continuously. Four curve lines were measured when the pressure with the value from 0 kPa to 12 kPa was loaded and released step by step, as shown in Figure 4-37. The same conclusion as the result of smartWLI-based biosensor test system was obtained: the membrane is very sensitive to pressure, and a small pressure change can cause a large alteration of membrane deflection. The relationship between membrane deflection and pressure is nearly linear. However, the deflection is also different to one same pressure during the loading process and the releasing process.

Conclusions: Experiments

The novel PDMS micro membrane biosensor based on the analysis of surface stress was successfully realized and shows good repeatability and biocompatibility. The proposed novel scheme by applying two membranes in parallel increases the

sensitivity of biosensors. Two biosensor test systems have been built based on the white light interferometer and the fiber optic interferometer respectively. The smartWLI-based biosensor test system has a high spatial resolution (1 nm) and can read deflection signal nanometre-accurately and directly. The FOI-based biosensor test system has a better time resolution (< 0.5 sec.) and is able to monitor the deflection signal continuously, but yields only average defelection values for the ROI. For *E. coli* detection, the MUA is a better functional material than MUO and DOT to functionalize membranes. The conditions of *E. coli* can be detected based on the deflection tests. Furthermore the surface stress will change and result in the alteration of membrane deflection when the cells have some changes due to pathologies or other reasons based on the theory, hence the properties can be analyzed based on the biosensor. For the biological and medical applications, other kinds of cells or molecules can also be detected based on the biosensor test systems by functionalizing the membranes with different functional materials. The analysis of some pathological changes of cells or molecules can be carried out based on the alteration of membrane deflection. This platform technology will enable various protocols for disease diagnostic and drug research.

Some experimental work has been published under the title “A novel PDMS micro membrane biosensor based on the analysis of surface stress” in Journal of Biosensors and Bioelectronics (2010) 25:2420 –2424 [P3].

Chapter 5 Summary and Future Outlook

5.1 Summary

In this thesis, a PDMS micro membrane biosensor based on the analysis of surface stress was designed, simulated, fabricated and tested for biological applications. The room temperature adhesive transfer bonding process – uncured PDMS method was tested to bond the biosensor with microfluidic devices or components.

First, the biosensor was proposed ground on lots of fundamental works. It is a relatively new class of sensors using the universal concept of free energy reduction occurring from binding reactions. This kind of biosensor allows the detection in opaque media and the miniaturization of the sensor for point-of-use sensing. The technique is advantageous since it does not require any labelling of bio-analytes or the addition of redox probes. According to the biology and pathology theory, the structures of bio-analytes, such as molecules and cells, will have some changes when they are under different conditions, health, disease or death for example. These changes will alter the amount of surface stress between bio-analytes and biosensor membrane, which hence causes the alteration of membrane deflection. Some important information can be obtained by detecting and analyzing the alteration.

Finite element model was used for the selection of membrane material and the optimization of biosensor geometry parameters. Two kinds of biosensor structure have been designed, each structure contains two layers: microfluidic layer and sensor layer. The sensor layer of the two biosensor structures is basically the same, which consists of two membranes, one acts as the active membrane and the other as reference. But the microfluidic structure is different, one is made of inlets, buffers, microchannels and outlets, and the other has only chambers. The biosensors have been fabricated based on surface and bulk microfabrication technology. Many challenges in the fabrication, such as realization of PDMS processing based on conventional microfabrication processes, fabrication of perfect PDMS thin film and release of PDMS membrane, were successfully overcome to form the biosensor. The

bonding technique between mirofluidic layer and sensor layer, uncured PDMS as the intermediate layer method, has been tested and utilized. The bond strength is close to the strength of bulk PDMS, which works well for bonding glass microfluidic devices and PDMS sensor layer.

This is the first demonstration of PDMS micro membrane sensor array based on the surface stress analysis. The micro membrane sensor shows low elasticity, better biological and chemical resistance and biocompatibility of PDMS when compared to the silicon or nitride silicon-based materials used in traditional microfabrication. The sensor array platform can be tuned for sensing many different bio-analytes by using suitable sensor coatings, and these coatings play an important role in determining the sensitivity and resolution. Alkanethiols with different functional end groups can be chosen as sensor coating materials. Alkanethiol molecules have a strong affinity for gold surface and this property was exploited for coating formation on the gold layer of the membrane sensor. Furthermore, there is another advantage: the use of alkanethiol coating requires minimal modification of the sensor microfabrication process sequence. The properties of the coatings can also be easily tailored by choosing alkanethiols with different functional end groups like COOH, OH, CH_3 and NH_2. In this thesis, three alkanethiol molecules with different functional end groups: 11 Mercapto 1 undecanoicacid (MUA: SH-$(CH_2)_{10}$-**COOH**), 11 Mercapto 1 undecanol (MUO: SH-$(CH_2)_{11}$-**OH**) and Dodecane thiol (DOT: SH-$(CH_2)_{11}$-**CH_3**) have been tested as the sensor coating layers for *E. coli* detection.

Based on the biosensor, two test systems have been set up with the white light interferometer (smartWLI) and the fiber optic interferometer (FOI) respectively, as shown in Figure 5-1 and 5-2. Non-contact, nanometer accuracy and dependable are the advantages of smartWLI-based biosensor test system, the membrane deflection resulting from the surface stress can be read directly and accurately. The FOI-based biosensor test system can continuously monitor the deflection signal though the resolution of current system is not best, but the optimal system could be gained by a better fiber optic interferometer. Lots of experiments have been done successfully for the biosensor testing and application based on the two test systems. The PDMS micro membrane biosensor based on the analysis of surface stress is successful and has good sensitivity, repeatability and biocompatibility. For the application to *E. coli*

detection, MUA is the better functional material than MUO and DOT, and the status of *E. coli* can be measured based on surface stress analysis. Furthermore, the surface stress will change and results in the alteration of membrane deflection when the cells undergo some changes due to pathologies or other reasons, hence the properties can be analyzed based on the measurement. Different kinds of bio-analytes could be detected and analyzed based on the biosensor test systems by functionalizing the membranes using different functional materials, which has many medical applications, for example, the pathology test and the drug discovery.

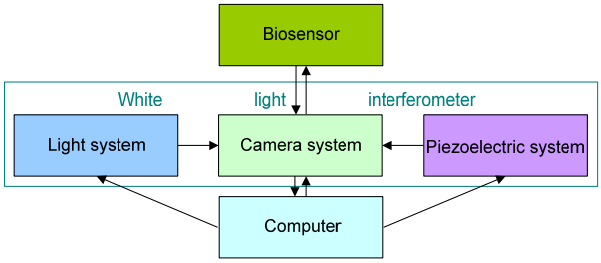

Figure 5-1: SmartWLI-based biosensor test system [P3]

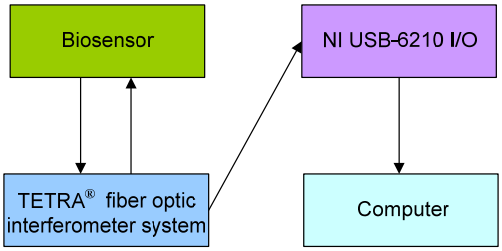

Figure 5-2: FOI-based biosensor test system [P3]

5.2 The present problems

1. The gold coating is easy to drop off from membranes when they are cleared. Two comparative pictures are shown in Figure 5-3. Figure 5-3a is the optical micrograph of gold on PDMS thin film just after the fabrication step of deposition. Figure 5-3b is the optical photo of gold on the last membranes after clearing: the light place is gold and the black place is PDMS. It is clear that some gold has disappeared from last membrane.

2. The surface roughness of PDMS thin film is a little to big when it is spun coat based on current method.

3. The two membranes of one same biosensor chip have some difference based on the current fabrication procedure, which has an influence on the later experimental signals because the signal from one membrane is active and from the other is reference. Figure 5-4 illustrates the topographies of two membranes

of one the same biosensor chip, measured by the white light interferometer. The difference is obvious.

4. It is not easy to load and unload the solution and bio-analytes, especially for the cleaning of membranes based on current microfluidic components — only one chamber.

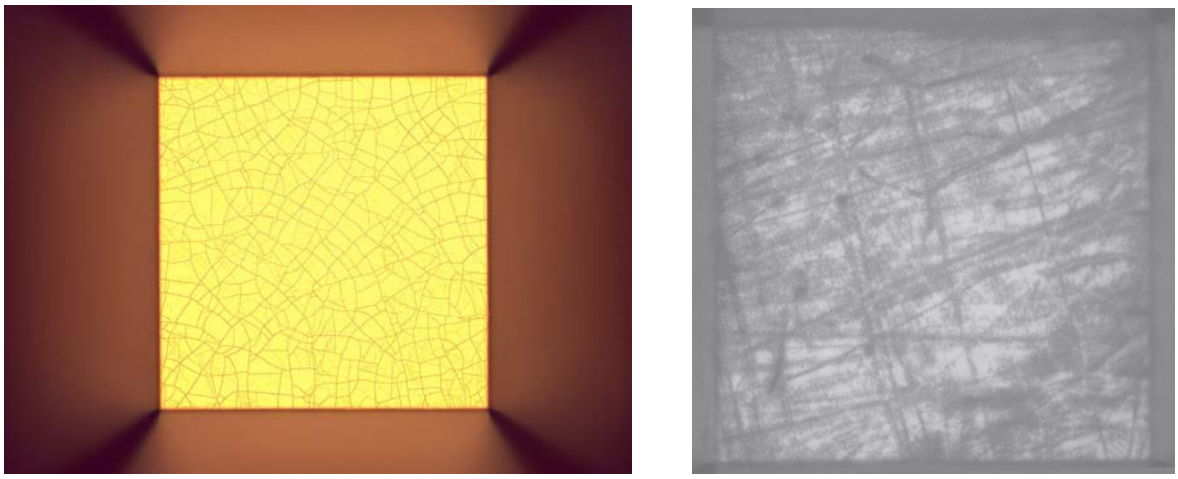

(a) Just after the fabrication step of deposition (b) the last membrane after clearing

Figure 5-3: Optical images of gold on the membrane

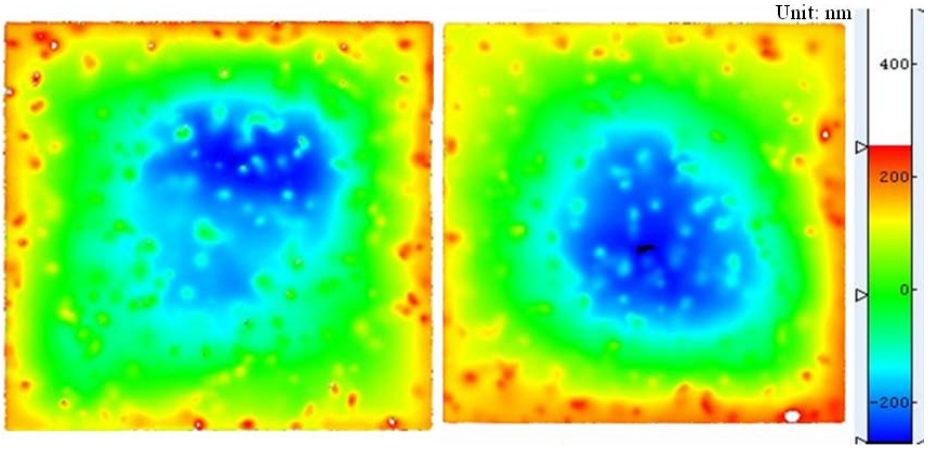

Figure 5-4: The topographies of two membranes of one biosensor

5. During the experiments, we controlled as far as possible the temperature of media, and tried to realize the same temperature on active membrane and reference membrane by long time measurement under controlled, constant temperature condition. Maybe it is not easy to assure the consistent temperature on both the two membranes under routine conditions.

5.3 Future outlook

Obviously the surface stress-based PDMS micro membrane biosensor can measure effects of bio-analytes, and analyze their properties based on the analysis of membrane deflection change resulting from the alteration of surface stress. Surface chemistry plays a key role in determining the sensitivity and selectivity of the biosensor and also the amount of non-specific binding. Hence, surface chemistry used for biosensor functionalization and passivation needs to be optimized for improving the biosensor performance. In addition, more biological and medical applications of the biosensor, such as molecular detection, drug research should be developed and studied. The biosensor only can be commercialized in the medical inspection field after driving some improvements in this field.

Other improvements may be done to make the biosensor better, more portable, more miniaturized, for example:

1. The parameters of biosensor may be optimized further and more biosensors with different parameters can be fabricated to allow more test.

2. The resolution and response time of the whole system can be optimized by using better sensor surface coating materials, and thus designing more reasonable test methods.

3. The spin-coating method should be improved to get more uniform and small surface roughness of PDMS membranes. The fabrication process can also be improved or revised to make sure the two membranes of one same biosensor chip are basically equal for getting improved dual comparable signals.

4. The bond strength between gold and PDMS thin film should be improved in order to decrease the drop of gold from membranes: for example, the wafer with PDMS thin film can be first soaked in a 15 mM solution of 3-mercapto-propyltrimethoxysilane in IPA for 2 hours, assembling a monolayer for effective PDMS-Au adhesion [278] before gold deposition.

5. An automated temperature control system has to be set up in future to calibrate the temperature error of biosensors, especially for the error between active membrane and reference membrane. The temperature compensation system then should yield more accurate measurements.

Appendix I: *FE* Ansys simulation program of membrane

(1/4 symmetry, Unit: μm)

```
/BATCH
/input,menust,tmp,'',,,,,,,,,,,,,,,1
WPSTYLE,,,,,,,,0
/PREP7
/title, deformation

!DEFINE PARAMETERS
*SET,lpdms,200          !the length of submaterial layer of membrane (μm) / variable parameter
*SET,wpdms,200          !the width of submaterial layer of membrane (μm) / variable parameter
*SET,tpdms,5            !the thickness of submaterial layer of membrane (μm) / variable parameter
*SET,lau,195            !the length of gold layer (μm) / variable parameter
*SET,wau,195            !the width of gold layer (μm) / variable parameter
*SET,tau,0.07           !the thickness of gold layer (μm) / variable parameter

!SET ELEMENT TYPES AND CONSTANTS
ET,1,SOLID186           !the element type of submaterial of membrane
ET,2,SHELL93            !the element type of gold
mp,ex,1,7               !the young's modulus of submaterial of membrane, here is PDMS (MPa)
mp,prxy,1,0.48          !the Poisson ratio of submaterial of membrane, here is PDMS
mp,ex,2,78000           !the young's modulus of gold (MPa)
mp,prxy,2,0.44          !the Poisson ratio of gold

r,1,tau                 !define the real constant (thickness) of gold
```

MPTEMP,,,,,,,,	!set the coeffecient of thermal expension
MPTEMP,1,0	
UIMP,1,REFT,,,300.15	!reference temperature
MPDATA,ALPX,1,,0	!the coefficient of thermal expansion of submaterial of membrane
MPTEMP,,,,,,,,	
MPTEMP,1,0	
UIMP,2,REFT,,,300.15	!reference temperature
MPDATA,ALPX,2,,14.2e-6	!the coefficient of thermal expansion of gold
!GENERATE MODEL	
BLC4,0,0,wpdms,lpdms,tpdms	!create the submaterial layer of membrane
BLC4,0,0,wau,lau	!create the gold layer
!MESHING	
esize,2	!define the meshing size
VSEL,S, , , 1	!select the submaterial layer
type,1	!define the element type of submaterial
mat,1	!define material model of submaterial
vmesh,all	!mesh
ASEL,S, , , 7	!select the gold layer
type,2	!define the element type of gold
mat,2	!define material model of gold
real,1	!define the real constant (thickness) of gold
amesh,all	amesh,all
ALLSEL,ALL	
!CONTACT VOLUME AND AREA	! define the contact between submaterial layer and gold layer
CM,_TARGET,AREA	
!*	
! /COM, CONTACT PAIR CREATION - START	
CM,_NODECM,NODE	
CM,_ELEMCM,ELEM	

```
CM,_KPCM,KP
CM,_LINECM,LINE
CM,_AREACM,AREA
CM,_VOLUCM,VOLU
! /GSAV,cwz,gsav,,temp
MP,MU,1,
MAT,1
MP,EMIS,1,7.88860905221e-031
R,3
REAL,3
ET,3,170
ET,4,174
R,3,,,1.0,0.0001,0,
RMORE,,,1.0E20,0.0,1.0,
RMORE,0.0,0,1.0,,1.0,0.5
RMORE,0,1.0,1.0,0.0,,1.0
KEYOPT,4,4,0
KEYOPT,4,5,0
KEYOPT,4,7,0
KEYOPT,4,8,0
KEYOPT,4,9,0
KEYOPT,4,10,2
KEYOPT,4,11,0
KEYOPT,4,12,3
KEYOPT,4,2,0
KEYOPT,3,5,0
! Generate the target surface
ASEL,S,,,1
ASEL,A,,,2
ASEL,A,,,3
ASEL,A,,,4
ASEL,A,,,5
ASEL,A,,,6
CM,_TARGET,AREA
```

```
TYPE,3
NSLA,S,1
ESLN,S,0
ESLL,U
ESEL,U,ENAME,,188,189
ESURF
CMSEL,S,_ELEMCM
! Generate the contact surface
ASEL,S,,,7
CM,_CONTACT,AREA
TYPE,4
NSLA,S,1
ESLN,S,0
ESURF
*SET,_REALID,3
ALLSEL
ESEL,ALL
ESEL,S,TYPE,,3
ESEL,A,TYPE,,4
ESEL,R,REAL,,3
! /PSYMB,ESYS,1
! /PNUM,TYPE,1
! /NUM,1
! EPLOT
ESEL,ALL
ESEL,S,TYPE,,3
ESEL,A,TYPE,,4
ESEL,R,REAL,,3
CMSEL,A,_NODECM
CMDEL,_NODECM
CMSEL,A,_ELEMCM
CMDEL,_ELEMCM
CMSEL,S,_KPCM
CMDEL,_KPCM
```

```
CMSEL,S,_LINECM
CMDEL,_LINECM
CMSEL,S,_AREACM
CMDEL,_AREACM
CMSEL,S,_VOLUCM
CMDEL,_VOLUCM
! /GRES,cwz,gsav
CMDEL,_TARGET
CMDEL,_CONTACT
! /COM, CONTACT PAIR CREATION - END

!DEFINE THE BOUNDARY CONDITION
FLST,5,2,5,ORDE,2                    !fix the two sides of submaterial layer
FITEM,5,4
FITEM,5,6
ASEL,S, , ,P51X
FINISH
/SOL
FINISH
/PREP7
FLST,2,2,5,ORDE,2
FITEM,2,4
FITEM,2,6
!*
/GO
DA,P51X,ALL,                         !define the symmetry
ASEL,S, , ,      3
NSLA,S,1
DSYM,SYMM,Y, ,
ASLL,S
ASEL,S, , ,      5
NSLA,S,1
DSYM,SYMM,X, ,
LSEL,S, , ,      13
```

```
NSLL,S,1
DSYM,SYMM,Y, ,
LSEL,S, , ,      16
NSLL,S,1
DSYM,SYMM,X, ,
ASEL,S, , ,       7
FLST,2,1,5,ORDE,1
FITEM,2,7
!*
BFA,P51X,TEMP, X                    !load on the gold, the value is X
ALLSEL,ALL
FINISH

! SOLVE
/SOL
! /STATUS,SOLU
SOLV
```

Appendix II: The detailed fabrication flow

Prozessbezeichnung	**biosensor**				
Projekt/BgA-Thema	PDMS micro membrane biosensor				
Verantwortlicher/Tel./FG	ZMN/Biomechatronik				
Bemerkung					
	Datum	*Name*	**Ablaufplanung**	*Soll*	*Ist*
Erstellung	25.11.10	Shengbo Sang	**Prozessstart**		
Freigabe			**Fertigstellung**		

Substrate	**Art, Größe**	**Zahl**	**Bemerkung**
Silicon	<100> orientiert, einseitig poliert, Dicke: 525 µm Durchmesser: 4“	1	Vorprozessiert 20 nm SiO_2 80 nm Si_3N_4

Maskenname	**Typ**	**Größe**	**Bemerkung**
Maske 1	Chromium mask	5“	Membrane
Maske 2	Chromium mask	5“	Gold

Nr. 1	**Prozess:** **Spin -coat** **PDMS thin film**			
Vorgaben:	**Spin -coat** Material: Sylgard 184 and Hexane. (Base:Hardener:Hexane 20:2:5). Thickness of PDMS thin film: 1 µm Facility (Anlage): Spin-Coater Conditions: 132s 6200RPM **Curing:** Facility: Hotplate Temperature: 150°C Time: 15 mim			
Messungen:	Profilometer			
Bemerkung:	The amount of Hexane may be increased.			
Bearbeitung	Datum:	Name:	Gebucht:	

Nr. 2	**Prozess: deposit and expose the photoresist**	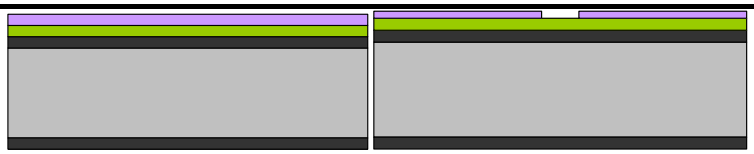	
Vorgaben:	**Belackung** Postive resist AZ 9260 Thickness: about 1.8 µm Facility: Spin-Coater Condition: 4000 rpm **Curing** Facility: Hotplate Temperature: 95°C Time: 10min **Exposure** Facility: EV 6/2 Gold Mask, (Fischer; A. 3.19.09)		
Messungen:			
Bemerkung:			
Bearbeitung	Datum:	Name:	Gebucht:

Nr. 3	**Prozess:** **Deposit the gold**		
Vorgaben:	**Evaporation** Material: Gold Thickness: 20-70 nm Facility: Edwards Auto 306		
Messungen:			
Bemerkung:			
Bearbeitung:	Datum:	Name:	Gebucht:

Nr. 4	**Prozess: Lift – Off**		
Vorgaben:	**Condition** in Glasschale unter Abzug mit Aceton **Wash (spülen)** In DI – Wasser (im spülbecken) über 60s Dry in the room temperature		
Messungen:			
Bemerkung:	It must be careful to protect the PDMS thin film.		
Bearbeitung:	Datum:	Name:	Gebucht:

Nr. 5	**Prozess: deposit and expose the photoresist**	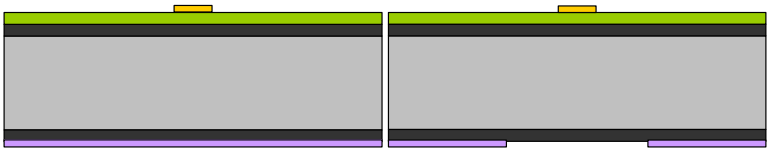	
Vorgaben:	**Belackung: Rüchseite (back side)** Postive resist AZ 1518 Facility: Spin-Coater Amount of positive resist: 3ml Condition: 4000rpm **Curing** Facility: Hotplate Temperature: 105°C Time: 30 min **Exposure** Facility: EV 6/2 Membrane Mask (Fischer; A. 3.19.09)		
Messungen:			
Bemerkung:			
Bearbeitung	Datum:	Name:	Gebucht:

Nr. 6	**Prozess: RIE back side**		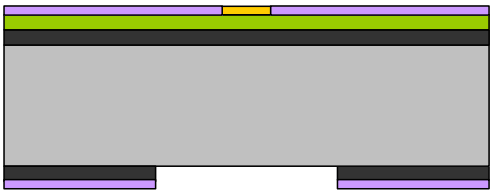
Vorgaben:	**Facility:** RIE – Oxford **The layer:** 80 nm Si_3N_4, 20 nm SiO_2		
Messungen:			
Bemerkung:			
Bearbeitung:	Datum:	Name:	Gebucht:

Nr. 7	**Prozess: KOH – Etch (KOH - Ätzen)**		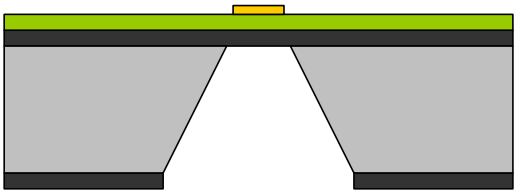
Vorgaben:	**Etch** Si - Etch Anlage: Ätzbad KOH auf Nassbank KOH: 25% Temperature: 90°C The etching speed in (100)-Si: about 1.84 µm/min **Wash (spülen)** In DI – Wasser (im spülbecken) Time: about 60 s		
Messungen:			
Bemerkung:	The front side can not contact with KOH, must be protected.		
Bearbeitung:	Datum:	Name:	Gebucht:

Nr. 8	**Prozess: RIE**		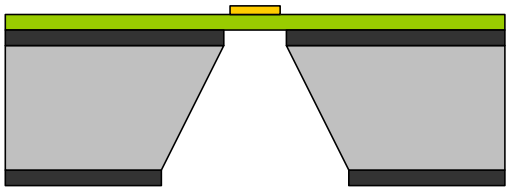
Vorgaben:	**Facility:** RIE – Oxford **The layer:** 80 nm Si_3N_4, 20 nm SiO_2		
Messungen:			
Bemerkung:	The step is same as Nr. 6 step. It must be careful to protect the PDMS thin film.		
Bearbeitung:	Datum:	Name:	Gebucht:

References

[1] Wang, Wangjun and Soper, Steven A. (2007). Bio-MEMS: Technologies and Applications. United States of America: CRC Press. ISBN 978-0-8493-3532-7.

[2] Lee, Abraham P. and Lee, L. James (2006). BioMEMS and Biomedical Nanotechnology Vol. 1 Biological and Biomedical Nanotechnology. United States of America: Springer. ISBN 978-0387-25563-7.

[3] Ozkan, Mihrimah and Heller, Michael J. (2006). BioMEMS and Biomedical Nanotechnology Vol. 2 Micro Nano Technology for Genomics and Proteomics. United States of America: Springer. ISBN 978-0387-25843-0.

[4] Desai, Tejal and Bhatia, Sangeeta (2006). BioMEMS and Biomedical Nanotechnology Vol. 3 Therapautic Micro Nano Technology. United States of America: Springer. ISBN 978-0387-25565-1.

[5] Bashir, Rashid and Wereley, Steve (2006). BioMEMS and Biomedical Nanotechnology Vol. 4 Biomolecular Senging, Processing and Analysis. Springer. ISBN 978-0387-25845-4.

[6] Srinath Satyanarayana (2005). “Surface Stress and Capacitive MEMS Sensor Arrays for Chemical and Biological Sensing”, University of California, Berkelery, Ph.D. dissertation.

[7] International Union of Pure and Applied Chemistry. "Biosensor". Compendium of Chemical Terminology, Compiled by A. D. McNaught and A. Wilkinson

[8] Vincent Tabard-Cossa (2005). “Microcantilever Actuation Generated by Redox-induced Surface Stress”, Department of Physics McGill University, Canada, PH.D dissertation.

[9] Michel Godin (2004). “Surface Stress, Kinetics, and Structure of Alkanethiol Self-Assembled Monolayers”, Department of Physics McGill University, Canada, Ph.D dissertation.

[10] A.S. Widge et al., (2007). “Self-assembled monolayers of polythiophene conductive polymers improve biocompatibility and electrical impendance of neural electrodes”, Biosensors and Bioelectronics, **22**, 1723-1732.

[11] Thundat, T., Oden, P. I. and Warmack, R. J. (1997). Microcantilever sensors, Microscale Thermophysical Engineering, **1** (3), 185-199.

[12] Lavrik, N. V., Sepaniak, M. J. and Datskos, P. G. (2004). Cantilever transducers as a platform for chemical and biological sensors, Review of Scientific Instruments, **75** (7), 2229-2253.

[13] Lai, J.; Perazzo, T.; Shi, Z.; Majumdar, A. (1997). Sensors and Actuators **A 58**, 113-119.

[14] Gimzewski, J. K.; Gerber, C.; Meyer, E.; Schlittler, R. R., (1994). Chem. Phys. Lett. **217**, 589-594.

[15] Reid, S.; Cagnoli, G.; Crooks, D. R. M.; Hough, J.; Murray, P.; Rowan, S.; Fejer, M.

M.; Route, R.; Zappe, S. (2006). Phys. Lett. A, AID 15103.

[16] Marie, R.; Thaysen, J.; Christensen, C. B. V.; Boisen, A. (2003). Microelect. Eng. **67-68**, 893-898.

[17] Yang, Z.; Li, X.; Wang, Y.; Bao, H.; Liu, M. (2004). Microelect. J. **35**, 479-483.

[18] Chua, D. H. C.; Tay, B. K.; Zhang, P.; Teo, E. H. T.; Lim, L. T. W.; O'Shea, S.; Miao, J.; Milne, W. I., (2004). Diamond & Related Materials **13**, 1980-1983.

[19] Mertens, J.; Finot, E.; Thundat, T.; Fabre, A.; Nadal, M.-H.; Eyraud, V.; Bourillot, E., (2003). Ultramicroscopy **97**, 119-126.

[20] Ansorge, E.; Schimpf, S.; Hirsch, S.; Sauerwald, J.; Fritze, H.; Schmidt, B. (2006). Sensors and Actuators A, SNA-5130.

[21] Hiroya, T.; Inagaki, K.; Tanda, S.; Tsuneta, T.; Yamaya, K., (2003). Physica **B 329-33**, 1635-1637.

[22] Lai, J.; Perazzo, T.; Shi, Z.; Majumdar, A., (1996). Proceedings of ASME Conference on Micro-electro-mechanical Systems (MEMS), 55-60.

[23] Datskos, P. G.; Oden, P. I.; Thundat, T.; Wachter, E. A.; Hunter, S. R., (1996). Appl. Phys. Lett. **69**, 2986-2988.

[24] Oden, I.; Datskos, P. G.; Thundat, T.; Wachter, E. A., (1996). Appl. Phys. Lett. **69**, 3277-3279.

[25] Wachter, E. A.; Thundat, T.; Oden, P. I.; Warmack, R. J.; Datskos, P. G.; Sharp, S. L., (1996). Rev. Sc. Instrum. **67**, 3434-3439.

[26] Markidou, A.; Shih, W. Y.; Shih, W.-H., (2005). Rev. Sci. Instrum. **76**, 064302-6.

[27] Rasmussen, P. A.; Thaysen, J.; Hansen, O.; Eriksen, S. C.; Boisen, A., (2003). Ultramicroscopy **97**, 371-376.

[28] Lemoine, P.; Zhao, J. F.; Bell, A.; Maguire, P.; McLaughlin, J., (2001). Diamond and Related Materials **10**, 94-98.

[29] Naik, T.; Longmire, E. K.; Mantell, S. C., (2003). Sensors and Actuators **A 102**, 240-254.

[30] Chen, G. Y.; Warlock, R. J.; Huang, A.; Thundat, T., (1995). J. Appl. Phys. **78**, 1465-1469.

[31] Ahmed, N.; Nino, D. F.; Moy, V. T., (2001). Rev. Sci. Instrum. **72**, 2731-2734.

[32] Shih, W. Y.; Li, X.; Gu, H.; Shih, W.-H.; Aksay, I.A., (2001). J. Appl. Phys. **89**, 1497-1505.

[33] Sader, J. E., (1998). J. Appl. Phys. **84**, 64-76.

[34] Chu, W.-H., (1963). Tech. Rep. No. 2, DTMB, Contact NObs-86396(X), Southwest Reseacrh Institute, San Antonio, Texas.

[35] Bergaud, C.; Nicu, L., (2000). Rev. Sci. Instrum. **71**, 2487-2491.

[36] Goedeke, S. M.; Allison, S. W.; Datskos, P. G., (2004). Sensors and Actuators A, doi:10.1016/j.sna.2003.12.002.

[37] Shibata, T.; Unno, K.; Makino, E.; Shimada, S., (2004). Sensors and Actuators A, doi:10.1016/j.sna.2003.11.025.

[38] Jeon, Y. B.; Sood, R.; Jeong, J.-H.; Kim, S.-G., (2005). Sensors and Actuators **A 122**, 16-22.

[39] Kanno, I.; Kotera, H.; Wasa, K., (2003). Sensors and Actuators **A 107**, 68-74.

[40] Zhang, Q. Q.; Gross, S. J.; Tadigadapa, S.; Jackson, T. N.; Djuth, F. T.; Trolier-McKinstry, S., (2003). Sensors and Actuators **A 105**, 91-97.

[41] Cattan, E.; Haccart, T.; Vélu, G.; Rémiens, D.; Bergaud, C.; Nicu, L., (1999). Sensors and Actuators **74**, 60-64.

[42] Itoh, T.; Lee, C.; Chu, J.; Suga, T., (1997). IEEE, 78-83.

[43] Brissaud, M.; Ledren, S.; Gonnard, P., (2003). J. Micromech. Microeng. **13**, 832- 844.

[44] Davis, Z. J.; Abadal, G.; Helbo, B.; Hansen, O.; Campabadal, F.; Pérez-Murano, F.; Esteve, J.; Figueras, E.; Ruiz, R.; Barniol, N.; Boisen, A., (20019. High mass and spatial resolution mass sensor based on resonating nano-cantilevers integrated with CMOS. The 11th International Conference on Solid-State Sensors and Actuators, Munich, Germany, June 10-14.

[45] Zurn, S.; Hsieh, M.; Smith, G.; Markus, D.; Zang, M.; Hughes, G.; Nam, Y.; Arik, M.; Polla, D., (2001). Smart Mater. Struct. 10, 252-263.

[46] Elmer F.-J.; Dreier, M., (1997). J. Appl. Phys. **81**, 7709-7711.

[47] Yaman, M., (2004). Materials and Design doi:10.1016/j.matdes.2004.10.009.

[48] Teva, J.; Abadal, G.; Davis, Z. J.; Verd, J.; Borrise, X.; Boisen, A.; Pérez- Murano, F.; Barniol, N., (2004). Ultramicroscopy **100**, 225-232.

[49] Passian, A.; Muraligharan, G.; Mehta, A.; Simpson, H.; Ferrel, T. L.; Thaundat, T., (2003). Ultramicroscopy **97**, 391-399.

[50] Li, X.; Shih, W. Y.; Vartuli, J.; Millus, D. L.; Prud'homme, R.; Aksay, I. A., (2002). J. Appl. Phys. **92**, 1-6.

[51] Fabian, J.-H.; Scandella, L.; Fuhrmann, H.; Berger, R.; Mezzacasa, T.; Musil, C. H.; Gobrecht, J.; Meyer, E., (2000). Ultramicroscopy **82**, 69-77.

[52] Abadal, G.; Davis, Z. J.; Borrise, X.; Hansen, O.; Boisen, A.; Barniol, N.; Perez-Murano, F.; Serra, F., (2003). Ultramicroscopy **97**, 127-133.

[53] Davis, Z. J.; Abadal, G.; Hansen, O.; Borise, X.; Barniol, N.; Perez-Murano, F.; Boisen, A., (2003). Ultramicroscopy **97**, 467-472.

[54] Adams, J. D.; Rogers, B.; Manning, L.; Hu, Z.; Thundat, T.; Cavazos, H.; Minne, S. C., (2005). Sensors and Actuators **A 121**, 457-461.

[55] Britton Jr., C. L.; Jones, R. L.; Oden, P. I.; Hu, Z.; Warmack, R. J.; Smith, S. F.;

Bryan, W. L.; Rochelle, J. M., (2000). Ultramicroscopy **82**, 17-21.

[56] Maute, M.; Raible, S.; Prins, F. E.; Kern, D. P.; Ulmer, H.; Weimar, U.; Gopel, W., (1999). Sensors and Actuators **B 58**, 505-511.

[57] Fadel, L.; Lochon, F.; Dufour, I.; Francais, O., (2004). J. Micromech. Microeng. **14**, S23-S30.

[58] Battiston, F. M.; Ramseyer, J.-P.; Lang, H. P.; Baller, M. K.; Gerber, Ch.; Gimzewski, J. K.; Meyer, E.; Guntherodt, H.-J., (2001). Sensors and Actuators **B 77**, 122-131.

[59] Kim. B. H.; Prins, F. E.; Kern, D. P.; Raible, S.; Weimar, U., (2001). Sensors and Actuators **B 78**, 12-18.

[60] Betts, T. A.; Tipple, C. A.; Sepaniak, M. J.; Datskos, P. G., (2000). Analytica Chimica Acta **422**, 89-99.

[61] Porter, T. L.; Eastman, M. P.; Macomber, C.; Delinger, W. G.; Zhine, R., (2003). Ultramicroscopy **97**, 365-369.

[62] Lang, H. P.; Baller, M. K.; Berger, R.; Gerber, Ch.; Gimzewski, Battison, F. M.; Fornaro, P.; Ramseyer, J. P.; Meyer, E.; Güntherodt, H.-J., (1999). Analytica Chimica Acta **393**, 59-65.

[63] Headrick, J. J.; Sepaniak, M. J.; Lavrik, N. V.; Datskos, P. G., (2003). Ultrmicroscopy **97**, 417-424.

[64] Kooser, A.; Gunter, R. L.; Delinger, W. D.; Porter, T. L.; Eastman, M. P., (2004). Sensors and Actuators B, doi: 10.1016/j.snb.2003.12.057.

[65] Fabre, A.; Finot, E.; Demoment, J.; Contreras, S., (2003). Ultramicroscopy **97**, 425-432.

[66] Chen, G. Y.; Warmack, R. J.; Thundat, T.; Allison, D. P., (1994). Rev. Sci. Instrum. **65**, 2532-2537.

[67] Zhou, J.; Li, P.; Zhang, S.; Long, Y.; Zhou, F.; Huang, Y.; Yang, P.; Bao, M., 2003. Sensors and Actuators **B 94**, 337-342.

[68] Zhou, J.; Li, P.; Zhang, S.; Huang, Y.; Yang, P.; Bao, M.; Ruan, G., (2003). Microelectronic Engineering **69**, 37-46.

[69] Zhao, Q.; Zhu, Q.; Shih, W. Y.; Shih, W.-H., (2005). Sensors and Actuators B, doi: 10.10116/jsna.2005.10.048.

[70] Pinnaduwage, L. A.; Thundat, T.; Gehl, A.; Wilson, S. D.; Hedden, D. L.; Lareau, R. T., (2004). Ultramicroscopy **100**, 211-216.

[71] Pinnaduwage, L. A.; Thundat, T.; Hawk, J. E.; Hedden, D. L.; Britt, P. F.; Houser, E. J.; Stepnowski, S.; McGill, R. A.; Budd, D., (2004). Sensors and Actuators **B 99**, 223-229.

[72] Alvarez, M.; Calle, A.; Tamayo, J.; Lechuga, L. M.; Abad, A.; Montoya, A., (2003). Biosensors and Bioelectronics **18**, 649-653.

[73] Vidic, A.; Then. D.; Ziegler, C. H., (2003). Ultramicroscopy **97**, 407-416.

[74] Tamayo, J.; Humphris, A. D. L.; Malloy, A. M.; Miles, M. J., (2001). Ultramicroscopy **86**, 167-173.

[75] Fagan, B. C.; Tipple, C. A.; Xue, Z.; Sepaniak, M. J.; Datskos, P. G., (2000). Talanta **53**, 599-608.

[76] Xu, X.; Thundat, T. G.; Brown, G. M.; Ji, H.-F., (2002). Anal. Chem. **74**, 3611- 3615.

[77] Boiabjiev, V. I.; Brown, G. M.; Pinnaduwage, L. A.; Goretzki, G.; Bonnesen, P. V.; Thundat, T., (2005).. Langmuir **21**, 1139-1142.

[78] Ji, H.-F.; Thundat, T., (2002). Biosensors and Bioelectronics **17**, 337-343.

[79] Ji, H.-F.; Hansen, K. M.; Hu, Z.; Thundat, T., (2001). Sensors and Actuators **B 72**, 233-238.

[80] Berger, R., Delamarche, E., Lang, H. P., Gerber, C., Gimzewski, J. K., Meyer, E. and Guntherodt, H. J., (1997). Surface stress in the self-assembly of alkanethiols on gold, Science, **276** (5321), 2021-2024.

[81] Wu, G. H., Ji, H. F., Hansen, K., Thundat, T., Datar, R., Cote, R., Hagan, M. F., Chakraborty, A. K. and Majumdar, A., (2001). Origin of nanomechanical cantilever motion generated from biomolecular interactions, Proceedings of the National Academy of Sciences of the United States of America, **98** (4), 1560-1564.

[82] Marie, R., Jensenius, H., Thaysen, J., Christensen, C. B. and Boisen, A., (2002). Adsorption kinetics and mechanical properties of thiol-modified DNA-oligos on gold investigated by microcantilever sensors, Ultramicroscopy, **91** (1-4), 29-36.

[83] Hansen, K. M., Ji, H. F., Wu, G. H., Datar, R., Cote, R., Majumdar, A. and Thundat, T., (2001). Cantilever-based optical deflection assay for discrimination of DNA single-nucleotide mismatches, Analytical Chemistry, **73** (7), 1567-1571.

[84] Fritz, J., Baller, M. K., Lang, H. P., Rothuizen, H., Vettiger, P., Meyer, E., Guntherodt, H. J., Gerber, C. and Gimzewski, J. K., (2000). Translating biomolecular recognition into nanomechanics, Science, **288** (5464), 316-318.

[85] Wu, G. H., Datar, R. H., Hansen, K. M., Thundat, T., Cote, R. J. and Majumdar, A., (2001). Bioassay of prostate-specific antigen (PSA) using microcantilevers, Nature Biotechnology, **19** (9), 856-860.

[86] Pinnaduwage, L. A., Boiadjiev, V., Hawk, J. E. and Thundat, T., (2003). Sensitive detection of plastic explosives with self-assembled monolayer-coated microcantilevers, Applied Physics Letters, **83** (7), 1471-1473.

[87] Liu, F.; Zhang, Y.; Ou-Yang, Z., (2003). Biosensors and Bioelectronics **18**, 655-660.

[88] Kwak, K. J.; Kudo, H.; Fujihira, M., (2003). Ultramicroscopy **97**, 249-255.

[89] Marie, R.; Jensenius, H.; Thaysen, J.; Christensen, C. A.; Boisen, A., (2002). Ultramicroscopy **91**, 29-36.

[90] Hansen, K. M.; Thundat, T., (2005). Methods **37**, 57-64.

[91] Lee, H. J.; Hwang, K. S.; Park, J.; Yoon, K. H.; Yoon, D. S.; Kim, T. S., (2005). Biosensors and Bioelectronics **20**, 2157-2162.

[92] Wee, K. W.; Kang, G. Y.; Park, J.; Kang, J. Y.; Yoon, D. S.; Park, J. H.; Kim, T. S., (2004). Biosensors and Bioelectronics, doi: 10.1016/j.bios.2004.09.023.

[93] Moulin, A. M.; O'Sea, S. J.; Welland, M. E., (2000). Ultramicroscopy **82**, 23-31.

[94] Kooser, A.; Manygoats, K.; Eastmann, M. P.; Porter, T, L., (2003). Biosensors and Bioelectronics 19, 503-508.

[95] Takahara, A.; Hara, Y.; Kojio, K.; Kajiyama, T., (2002). Colliods and Surface B: Biointerfaces **23**, 141-152.

[96] Lee, J. H.; Yoon, K. H.; Hwang, K. S.; Park, J.; Ahn, S.; Kim, T. S., (2004). Biosensors and Bioelectronics **20**, 269-275.

[97] Gad, M.; Itoh, A.; Ikai, A., (1997). Cell Biology International **21**, 697-706.

[98] Bowen, W.R.; Lovitt, R.W.; Wright, C.J., (2001). Journal of Colloid and Interface Science **237**, 54-61.

[99] Ikai, A.; Idiris, A.; Sekiguchi, H.; Arakawa, H.; Nishida, S., (2002). Applied Surface Science **188**, 506-512.

[100] Stuart, J. K.; Hlady, V., (1999). Colliods and Surfaces B: Biointerfaces **15**, 37-55.

[101] Kim, H.; Arakawa, H.; Osada, T.; Ikai, A., (2003). Ultramicroscopy **97**, 359-363.

[102] Calleja, M.; Tamayo, J.; Johansson, A.; Rasmussen, P.; Lechuga, L. M.; Boisen, A., (2003). Sensor Letters **1**, 20-24.

[103] Kim, H.; Arakawa, H.; Osada, T,; Ikai, A., 2002. Applied Surface Science **188**, 493-498.

[104] Raiteri, R.; Grattarola, M.; Butt, H.-J.; Skladal, P., (2001). Sensors and Actuators **B 79**, 115-126.

[105] Ghatnekar-Nilsson, S.; Lindahl, J.; Dahlin, A.; Stjernholm, T.; Jeppesen, S.; Hook, F.; Montelius, L., (2005). Nanotechnology **16**, 1512-1516.

[106] Zhang, J.; H.-F., Ji, (2004). Analytical Sciences **20**, 585-587.

[107] Gfeller, K.Y.; Nugaeva, N.; Hegner, M., (2004). Biosensors and Bioelectronics, doi: 10.1016/j.bios.004.11.018.

[108] Yi, J. W.; Shih, W. Y.; Mutharasan, R.; Shih, W.-H., (2003). Journal of Applied Physics **93**, 1-7.

[109] Gossett A. Campbell (2006). Detection and Quantification of Pathogens, Proteins, and Molecules Using Piezoelectric-Excited Millimeter-Sized Cantilever (PEMC) Sensors, Drexel University, PH.D dissertation.

[110] Yue, M., Lin, H., Dedrick, D. E., Satyanarayana, S., Majumdar, A., Bedekar, A. S., Jenkins, J. W. and Sundaram, S., (2004). A 2-D microcantilever array for multiplexed biomolecular analysis, Journal of Microelectromechanical Systems, **13** (2), 290-299.

[111] Yue, M., (2004). Multiplexed Label-free Bioassays Based on Nanomechanics and Nanofluidics, Ph.D dissertation, University of California, Berkeley.

[112] Berger, R.; Delamarche, E.; Lang, H. P.; Gerber, C.; Gimzewski, J. K.; Meyer, E.; Guntherodt, H. J., (1998). Appl. Phys. **A 66**, S55-S59.

[113] Chen, G. Y.; Thundat, T.; Wachter, E. A.; Warmack, R. J., (1995). J. Appl. Phys. **77**, 3618-3622.

[114] Lang, H. P.; Baller, M. K.; Berger, R.; Gerber, C.; Gimzewski, J. K.; Battiston, F. M.; Fornaro, P., Ramseyer, J. P., Meyer, E.; Guntherodt, H. J., (1995). Anal. Chim. Acta. **393**, 59-65.

[115] Thundat, T.; Warmack, R. J.; Chen, G. Y.; Allison, D. P., (1994). Appl. Phys. Lett. **64**, 2894-2896.

[116] Thundat, T.; Chen, G. Y.; Warmack, R. J. Allison, D. P.; Wachter, E. A., (1995). Anal. Chem. **67**, 519-521.

[117] Preissing, F. J., (1989). J. Appl. Phys. **66**, 4262.

[118] Chatzandroulis, S., Tegou, E., Goustouridis, D., Polymenakos, S. and Tsoukalas, D., (2004). Capacitive-type chemical sensors using thin silicon/polymer bimorph membranes, Sensors and Actuators B-Chemical, **103** (1-2), 392-396.

[119] Heim S, Schnieder I, Binz D, Vogel A, Bilitewski U (1999). Biosensors & Bioelectronics **14**, 187–193

[120] Rawson DM, Willmer AJ, Turner PF (1989). Biosensors 4:299– 311

[121] Peter J, Hutter W, Stöllnberger W, Hample W (1996). Biosensors & Bioelectronics **11**, 1215–1219

[122] Reshetilov AN, Iliasov PV, Donova MV, Dovbnya DV, Boronin AM, Leathers TD, Greene RV (1997). Biosensors & Bioelectronics **12**,241–247

[123] Corbisier P, van der Lelie D, Borremans B, Provoost A, de Lorenzo V, Brown NL, Lloyd JR, Hobman JL, Csöregi E, Johansson G, Mattiasson B (1999). Anal Chim Acta **387**, 235–244

[124] Christiane Ziegler, Cell-based biosensors, Fresenius J Anal Chem (2000). **366**, 552–559

[125] Bousse, L. (1996). "Whole cell biosensors," Sensors and Actuators B (Chemical), **B34(1-3)**, 270-5.

[126] Pancrazio, J.J., Whelan, J.P., Borkholder, D.A., Ma, W. and Stenger, D.A., (1999). Development and application of cell-based biosensors, Annals of Biomedical Engineering, **27(6)**, 697-711.

[127] McConnell, H.M., Owicki, J.C., Parce, J.W., Miller, D.L., Baxter, G.T., Wada, H.G. and Pitchford, S., (1992). The cytosensor microphysiometer: biological applications of silicon technology, Science, **257**(5078), 1906-12.

[128] Zysk, J.R. and Baumbach, W.R., (1998). Homogeneous pharmacologic and cell-based screens provide diverse strategies in drug discovery: somatostatin antagonists as a case study, Combinatorial Chemistry High Throughput Screening, **1**, 171-183.

[129] Keese, C.R. and Giaever, I., (1994). A biosensor that monitors cell morphology with

electric fields, IEEE Engineering in Medicine and Biology, **13(3)**, 402-8.

[130] Borkholder, D.A. (1998). Cell based biosensors using microelectrodes, Doctoral Dissertation, Electrical Engineering, Stanford University, Stanford, CA.

[131] Gross, G.W., Rhoades, B.K., Azzazy, H.M.E. and Wu, M., (1995). The use of neuronal networks on multielectrode arrays as biosensors," Biosensors & Bioelectronics, **10(6-7),** 553-67.

[132] Thomas, C.A.J., Springer, P.A., Loeb, G.E., Berwald Netter, Y. and Okun, L.M., (1972). A miniature micro electrode array to monitor the bio electric activity of cultured cells, Experimental Cell Research, **74(1)**, 61-66.

[133] Gross, G.W., (1979). Simultaneous single unit recording in vitro with a photoetched laser deinsulated gold multimicroelectrode surface, IEEE Transactions on Biomedical Engineering, **26(5)**, 273-279.

[134] Israel, D.A., Barry, W.H., Edell, D.J. and Mark, R.G., (1984). An array of microelectrodes to stimulate and record from cardiac cells in culture, American Journal of Physiology, **247(4)**, H669-H674.

[135] B. Derek DeBusschere (2002). Portable Cell-Based Biosensors, Department of Electrical Engineering, Stanford University, PH.D dissertation.

[136] M. Manimaran, F.E.H Tay, K.C. Chaw (2006). Cell Deformation in Cancer Metastasis: a BioMEMS Based Approach, Journal of Physics: Conference Series **34**, 1143–1147

[137] Manz, A., Graber, N., and Widmer, H.M., (1990). Miniaturized Total Chemical Analysis Systems: A Novel Concept for Chemical Sensing, Sensors and Actuators B, **1**, 244–248.

[138] Shoji, S. and Esashi, M., (1994). Microflow Devices and Systems, Journal of Micromechanics and Microengineering, **4**, 157–171.

[139] Gravesen, P., Brandebjerg, J., and Jensen, O.S., (1993). Microfluidics—A Review, Journal of Micromechanics and Microengineering **3**, 168–182.

[140] Caton, P.F. and White, R.M., (2001). MEMS Microfilter with Acoustic Cleaning, Proceedings of the 14th IEEE International Workshop on Micro-Electromechanical Systems MEMS '01, Interlaken Switzerland, January 21–25, 479–482. IEEE, Piscataway, NJ.

[141] Desai, T.A. et al., (1999). Nanopore Technology for Biomedical Applications, Biomedical Microdevices **2(1)**, 11–40.

[142] Nguyen, N.T. et al., (2000). Integrated Thermal Flow Sensor for In-Situ Measurement and Control of Acoustic Streaming in Flexural-Plate-Wave Pumps, Sensors and Actuators **A 79(2)**, 115–121.

[143] Deshmukh, A.A., Liepmann, D., and Pisano A.P. (2000). Continuous Micromixer with Pusatile Micropumps, Proceedings 2000 Solid State Sensor and Actuator Workshop, Hilton Head, SC., June 4–8, 73–76. Transducers Research Foundation, San Diego, CA.

[144] Zahn, J.D. et al., (2004). Continuous on Chip Micropumping for Microneedle Enhanced Drug Delivery, Biomedical Microdevices **6, 3**, 183–190.

[145] Luginbuhl, P. et al., (1999). Micromachined Injector for DNA Mass Spectrometry, Proceedings of Transducers '99 The 10th International Conference on Solid-State Sensors and Actuators, Sendai Japan, June 7–10, 1130–1133. Institute of Physics Publ., Philadelphia, PA.

[146] Simpson, P.C., Woolley, A.T., and Mathies, R.T., (1998). Microfabrication Technology for the Production of Capillary Array Electrophoresis Chips, Biomedical Microdevices **1,** 7–25.

[147] Matthew A. Cooper (2002). NATURE REVIEWS: DRUG DISCOVERY, VOLUME **1**, 515

[148] Liedberg, B., Nylander, C. and Lundstrom, I., (1983). Surface-Plasmon Resonance for Gas-Detection and Biosensing, Sensors and Actuators, **4** (2), 299-304.

[149] Nylander, C., Liedberg, B. and Lind, T., (1982). Gas-Detection by Means of Surface-Plasmon Resonance, Sensors and Actuators, **3** (1), 79-88.

[150] Matthew A. Cooper (2002). Optical biosensors in drug discovery, Nature Reviews Drug Discovery **1**, 515-528.

[151] Aebersold, R. and Mann, M., (2003). Mass spectrometry-based proteomics, Nature, **422** (6928), 198-207.

[152] H. Wohltjen et al. (1997). Acoustic Wave Sensor—Theory, Design, and Physico-Chemical Applications, Academic Press, San Diego:39

[153] Suzuki, H., (2000). Advances in the microfabrication of electrochemical sensors and systems, Electroanalysis, **12** (9), 703-715.

[154] Hansen, K. M., Ji, H. F., Wu, G. H., Datar, R., Cote, R., Majumdar, A. and Thundat, T., (2001). Cantilever-based optical deflection assay for discrimination of DNA single-nucleotide mismatches, Analytical Chemistry, **73** (7), 1567-1571.

[155] Binning, G.; Quate, C. F.; Gerver, Ch., (1986). Phys. Rev. Lett. 930-935.

[156] M. Godin, O. Laroche, V. Tabard-Cossa, L. Y. Beaulieu, P. Grütter, and P. J. Williams, (2003). Review of Scientific Instruments 74, 4902.

[157] Fritz, J., Baller, M. K., Lang, H. P., Rothuizen, H., Vettiger, P., Meyer, E., Guntherodt, H. J., Gerber, C. and Gimzewski, J. K., (2000). Translating biomolecular recognition into nanomechanics, Science, **288** (5464), 316-318.

[158] Baselt D. R., Lee G. U., Colton R. J., (1996). J. Vac. Sci. Technol. **B 14**, 798-803.

[159] D. Rugar, H. J. Mamin, and P. Güthner; (1989). Applied Physics Letters **55**, 2588.

[160] A. Moser, H. J. Hug, Th. Jung, U. D. Schwarz, and H.-J. Güntherodt, (1993). Meas. Sci. Technol. **4**, 769-775.

[161] R. Raiteri, H.-J. Butt and M. Grattarola (2000). Electrochem. Acta **46**, 157–163.

[162] Marie, R., Jensenius, H., Thaysen, J., Christensen, C. B. and Boisen, A. (2002). Adsorption kinetics and mechanical properties of thiol-modified DNA-oligos on gold investigated by microcantilever sensors, Ultramicroscopy, **91** (1-4), 29-36.

[163] R.G. Knobel and A.N. Cleland, (2003). Nature **424**, 291.

[164] Macbeath, G. and Schreiber, S. L., (2000). Printing proteins as microarrays for highthroughput function determination, Science, **289** (5485), 1760-1763.

[165] H. Masahiko, T. Kazuhiko, N. Riichiro, F. S. Norman and J. K. Gregory, (2000). J. Chromatogr., A, **867**, 271–279.

[166] Y. Xu, F. G. Bessoth, J. C. T. Eijkel and A. Manz, (2000). Analyst, **125**, 677–683.

[167] X. J. Huang, Q. Pu and Z. L. Fang, (2001). Analyst, **126**, 281–284.

[168] K. Tsukagoshi, M. Hashimoto, R. Nakajima and A. Arai, (2000). Anal. Sci., **16**, 1111–1113.

[169] Z. Zhang and W. Qin, (1996). Talanta, **43**, 119–124.

[170] B. Li and Z. Zhang, (2000). Sens. Actuators, B, **69**, 70–74.

[171] G. J. Zhou, G. Wang, J. J. Xu and H. Y. Chen, (2002). Sens. Actuators, B, **81**, 334–339.

[172] M. C. Ramos, M. C. Torijas and A. Navas Diaz, (2001). Sens. Actuators, B, **73**, 71–75.

[173] Y. Huang, C. Zhang and Z. Zhang, (1999). Anal. Sci., **15**, 867–870.

[174] B. Li, Z. Zhang and Y. Jin, (2001). Anal. Chem., **73**, 1203–1206.

[175] Schweitzer, B., Predki, P. and Snyder, M., (2003). Microarrays to characterize protein interactions on a whole-proteome scale, Proteomics, **3 (11)**, 2190-2199.

[176] Freshney, R.I., (1994). *Culture of animal cells: a manual of basic technique, 3rd ed.*, Wiley-Liss, NewYork, NY.

[177] Spier, R.E. and Griffiths, B., (1985). *Animal Cell Biotechnology I*, Academic Press, London, England, UK.

[178] Gross, G.W., (1979). Simultaneous single unit recording in vitro with a photoetched laser deinsulated gold multimicroelectrode surface, *IEEE Transactions on Biomedical Engineering*, **26(5)**, 273-279.

[179] Pine, J., (1980). Recording action potentials from cultured neurons with extracellular microcircuit electrodes, *Journal of Neuroscience Methods*, **2(1)**, 19-31.

[180] Borkholder, D.A., (1998). *Cell based biosensors using microelectrodes*, Doctoral Dissertation, Electrical Engineering, Stanford University, Stanford, CA.

[181] Brewer, G.J. and Price, P.J., (1996). Viable cultured neurons in ambient carbon dioxide and hibernation storage for a month, *Neuroreport*, **7(9)**,1509-1512.

[182] Hornung, J., Muller, T. and Fuhr, G., (1996). Cryopreservation of anchorage-dependent mammalian cells fixed to structured glass and silicon substrates, *Cryobiology*, **33(2)**, 260-270.

[183] Israel, D.A., Barry, W.H., Edell, D.J. and Mark, R.G., (1984). An array of microelectrodes to stimulate and record from cardiac cells in culture, *American Journal of Physiology*, **247(4)**, H669-H674.

[184] Willmer, E.N., (1965). *Cells and Tissues in Culture: Methods, Biology, and Physiology*, Academic Press, London, England, UK.

[185] Flieschaker, R.J. and Sinskey, A.J., (1981). Oxygen demand and supply in cell culture, European Journal of Applied Microbiology and Biotechnology, **12**,193-197.

[186] Vandor, A.J., Sherman, J.H. and Luciano, D.S., (1994). Human physiology, the mechanisms of body function, McGraw-Hill, Inc., San Francisco, CA.

[187] Spier, R.E. and Griffiths, B., (1982). An examination of the data and concepts germane to the oxygenation of cultured animal cells, *Developments in Biological Standardization*, **55,** 81-92.

[188] Browser, R.W., (1961). The effect of oxygen tension on the growth and metabolism of a mammalian cell, *Experimental Cell Research*, **25**,101-113.

[189] H. Ibach, (1997). Surface Science Reports **29**, 193.

[190] W. Haiss (2001). Reports on Progress in Physics **64**, 591.

[191] R. Berger, E. Delamarche, H. P. Lang, Ch. Gerber, J. K. Gimzewski, E. Meyer, and H.-J. Güntherodt, (1997). Science **276**, 2021.

[192] C. E. Bach, M. Giesen, and H. Ibach, (1997). Physical Review Letters **78**, 4225.

[193] U. Tartaglino, E. Tosatti, D. Passerone, and F. Ercolessi, (2002). Physical Review **B 65**, 241406.

[194] R. M. Tromp, A. W. Denier van der Gon, and M. C. Reuter; (1992). Physical Review Letters **68**, 2313.

[195] K. Pohl, M. C. Bartelt, J. de la Figuera, N. C. Bartelt, J. Hrbek, and R. Q. Hwang, (1999). Nature **397**, 238.

[196] D. K. Schwartz, (2001). Annual Review of Physical Chemistry **52**, 107.

[197] F. Schreiber (2000). Progress in Surface Science **65**, 151.

[198] G. E. Poirier, (1997). Chemical Reviews **97**, 1117.

[199] K. L. Prime, and G. M. Whitesides, (1993). Journal of the American Chemicqal Society **115**, 10714.

[200] P. A. DiMilla, J. P. Folkers, H. A. Biebuyck, R. Haerter, G. P. Lopez, G. M. Whitesides, (1994). Journal of the American Chemical Society **116**, 2225.

[201] J. Fritz; M. K. Baller; H. P. Lang; H. Rothuizen; P. Vettiger; E. Meyer; H.-J. Güntherodt (2000). Ch. Gerber; and J. K. Gimzewski; Science **288**, 316.

[202] J. Fritz; M. K. Baller; H. P. Lang; T. Strunz; E. Meyer; H.-J. Güntherodt; E. Delamarche, (2000). Ch. Gerber; and J. K. Gimzewski; Langmuir **16**, 9694.

[203] F. Frederix, K. Bonroy, W. Laureyn, G. Reekmans, A. Campitelli, W. Dehaen, and G. Maes, (2003). Langmuir **19**, 4351.

[204] M. Alvarez, A. Calle, J. Tamayo, L. M. Lechuga, A. Abad, and A. Montoya, (2003). Biosensors and Bioelectronics **18**, 649.

[205] H. Kondoh; C. Kodama; H. Sumida; and H. Nozoye, (1999). Journal of Chemical Physics **111**, 1175.

[206] Wendong Zhang et al, (2005). Micromachined Transducers Sourcebook, Science Press, ISBN:7030105656.

[207] V. A. Gridchin, V. V. Grichenko, and V. M. Lubimsky, (2005). Square-Membrane Deflection and Stress: Identifying the Validity Range of a Calculation Procedure, Russian Microelectronics **34(3)**, 173–180.

[208] S. Satyanarayana, et al., (2006). Parylene micro membrane capacitive sensor array for chemical and biological sensing, Sensors and Actuators B, **115(1)**, 494-502.

[209] S.L. Peterson, A. McDonald, P.L. Gourley, D.Y. Sasaki, (2005). J. Biomed. Mater. Res., Part **A 72(1)**, 10–18.

[210] E. Ostuni, R. Kane, C.S. Chen, D.E. Ingber, G.M. Whitesides, (2000). Langmuir **16**, 7811–7819.

[211] M.N. De Silva, R. Desai, D.J. Odde, (2004). Biomedical Devices **6(3)**, 219– 222.

[212] J.L. Tan, J. Tien, D.M. Pirone, D.S. Gray, K. Bhadriraju, C.S. Chen, (2003). Proc. Natl. Acad. Sci. U.S.A. **100(4)**, 1484–1489.

[213] O. du Roure, A. Saez, A. Buguin, R.H. Austin, P. Chavrier, P. Siberzan, B. Ladoux, (2005). Proc. Natl. Acad. Sci. U.S.A. **102(7)**, 2390–2395.

[214] X.Q. Brown, K.Ookawa, J.Y.Wong, (2005). Biomaterials **26**, 3123–3129.

[215] Armani, D. et al., (1999). *Re-configurable fluid circuits by PDMS elastomer micromachining,* Beckman Institute, University of Illinois.

[216] Hughes, L., (1990). *Handbook of Polymer Coatings for Electronics,* Noyes Publications, New Jersay.

[217] Lötters, J.C. et al., (1997). *The mechanical properties of the rubber elastic polymer, polydimethylsiloxane for sensor applications,* MESA Research Institute, Enschede.

[218] Wilbur, J.L. et al., (1996). *Microcontact printing of self-assembled monolayers: applications in microfabrication,* Department of Chemistry, Harvard University, Cambridge, USA.

[219] Mark, J., (1999). *Polymer Data Handbook,* Oxford University Press, New York.

[220] Dow Corning Corporation, (2005). *Material Safety Data Sheet SYLGARD*r *184 Silicon, Elastomer Kit*, Michigan.

[221] J. Garra, T. Long, J. Currie, T. Schneider, R. White, M. Paranjape, (2002). Dry Etching of Polydimethylsiloxane for Microfluidic Systems", Journal of Vacuum Science and Technology, A20, pp 975-982.

[222] Polymer Data Handbook; Belanger MC, Marois Y. (2001). Hemocompatibility, biocompatibility, inflammatory and in vivo studies of primary reference materials low-density polyethylene and polydimethylsiloxane: a review. J Biomed Mater Res, **58(5)**, 467–77.

[223] J. Cheng, M. A. Shoffner, K. R. Mitchelson, L. J. Kricka, and P. Wilding, (1996). Analysis of ligase chain reaction products amplified in a silicon–glass chip using capillary electrophoresis, *J. Chromatogr. A*, **732(1)**, 151–158.

[224] M. A. Shoffner, J. Cheng, G. E. Hvichia, L. J. Kricka, and P. Wilding, (1996). Chip PCR. I. Surface passivation of microfabricated silicon–glass chips for PCR, *Nucleic Acids Res.*, **24(2)**, 375–379.

[225] J. Cheng, M. A. Shoffner, G. E. Hvichia, L. J. Kricka, and P. Wilding, (1996). Chip PCR. II. Investigation of different PCR amplification systems in microfabricated silicon–glass chips," *Nucleic Acids Res.*, **24(2)**, 380–385.

[226] D. J. Harrison, A. Manz, Z. Fan, H. Luedi, and H. M. Widmer, (1992). Capillary electrophoresis and sample injection systems integrated on a planar glass chip, *Anal. Chem.*, **64(17**), 1926–1932.

[227] C. S. Effenhauser, A. Manz, and H. M. Widmer, (1993). Glass chips for highspeed capillary electrophoresis separations with submicrometer plate heights, *Anal. Chem.*, **65(19)**, 2637–2642.

[228] K. Seiler, D. J. Harrison, and A. Manz, (1993). Planar glass chips for capillary electrophoresis: Repetitive sample injection, quantitation, and separation efficiency, *Anal. Chem.*, **65(10)**, 1481–1488.

[229] Z. H. Fan and D. J. Harrison, (1994). Micromachining of capillary electrophoresis injectors and separators of glass chips and evaluation of flow at capillary intersections," *Anal. Chem.*, **66(1)**, 177–184.

[230] L. Rebenklau, K.-J. Wolter, and S. Howitz, (2000). Realization of hybrid microfluidic systems using standard LTCCprocess," in *Proc. 50thElectr on. Compon. Technol. Conf.*, Las Vegas, NV, pp. 1696–1700.

[231] J. C. McDonald, D. C. Duffy, J. R. Anderson, D. T. Chiu, H. Wu, O. J. Schueller, and G. M. Whitesides, (2000) Fabrication of microfluidic systems in poly(dimethylsiloxane), *Electrophoresis*, vol. **21**, no. 1, pp. 27–40.

[232] H. Becker and C. Gartner, (2000). Polymer microfabrication methods for microfluidic analytical applications, *Electrophoresis*, vol. **21**, no. 1, pp. 12–26.

[233] J. S. Ko, H. C. Yoon, H. Yang, H. B. Pyo, K. H. Chung, S. J. Kim, and Y. T. Kim, (2003). A polymer-based microfluidic device for immunosensing biochips, *Lab Chip*, vol. **3**, no. 2, pp. 106–113.

[234] J. Zhang, K. L. Tan, G. D. Hong, L. J. Yang, and H. Q. Gong, (2001). Polymerization optimization of SU-8 photoresist and its applications in microfluidic systems and MEMS, *J. Micromech. Microeng.*, vol. **11**, no. 1, pp. 20–26.

[235] Freitag A, Vogel D, Scholz R, Dietrich TR, (2001). Microfluidic devices made of glass. J Assoc Lab Autom **6(4)**:45–49.

[236] Daridon A, Fascio V, Lichtenberg J, Wu¨ trig R, Langen H, Verpoorte E, de Rooij N, (2001). F Multi-layer microfluidic glass chips for microanalytical applications. Fresenius J Anal Chem **371**:261–269.

[237] Petersen D, Mogensen KB, Klank H, (2004). Glass micromachining. In: Geschke O, Klank H, Tellemann P (eds) Microsystem engineering of lab-on-a-chip devices, Chap 7. Wiley-VCH, New York, p 161.

[238] Petersen K E, (1982). Silicon as a mechanical material *Proc. IEEE* **70** 420–57.

[239] Kovacs G T A, (1998). *Micromachined Transducers Sourcebook* (Boston, MA: McGraw-Hill).

[240] Madou M, (1997). Fundamentals of Microfabrication (Boca Raton, FL: Chemical Rubber Company).

[241] Barth P, (1990). Silicon fusion bonding for fabrication of sensors, actuators, and microstructures Sensors Actuators **A 21–23**, 919–26.

[242] Wallis G and Pomerantz D I, (1969). Field assisted glass–metal sealing J. Appl. Phys. **40**, 3946–9.

[243] Cohn M B, Yiching Liang, Howe R T and Pisano A P, (1996). Wafer-to-wafer transfer of microstructures for vacuum packaging Technical Digest Solid-State Sensor and Actuator Workshop (Hilton Head Island, SC, 1996) pp 32–5.

[244] Mass D, B¨ustgens B, Fehrenberg J, Keller W, Ruther P, Schomburg W K and Seidel D, (1996). Fabrication of microcomponents using adhesive bonding techniques Proc. IEEE Int. Workshop on Microelectro-mechanical Systems (San Diego, CA, 1996) pp 331–6.

[245] Smith Emily, (2005). fabrication of picoliter microreator with multilayer elastomer valves (Bachelor thesis), Massachusetts Institute of Technology, Dept. of Mechanical Engineering.

[246] J.C. Lotters y, W. Olthuis, P.H. Veltink, P. Bergveld, (1997). J. Micromechanics Microengineering **7**, 145–147.

[247] Abel L. Thangawng, Rodney S. Ruoff, Melody A. Swartz, Matthew R. Glucksberg, (2007). An ultra-thin PDMS membrane as a bio/micro–nanointerface: fabrication and characterization, Biomed Microdevices **9**, 587–595.

[248] Schmidt, M. A., (1998). *Wafer-to-Wafer Bonding for Microstructure Formation*, Proceedings of the IEEE.

[249] Kovacs, G. T. A., (1998). *Micromachined Transducers Sourcebook*, ed.,The McGraw-Hill Companies, Inc., New York.

[250] Duffy, D. C., Mcdonald, J. C., Schueller, O. J. A. and Whitesides, G. M., (1998). *Rapid prototyping of microfluidic systems in poly(dimethylsiloxane)*, Analytical Chemistry, **70** (23), 4974-4984.

[251] Liu, J., Enzelberger, M. and Quake, S., (2002). *A nanoliter rotary device for polymerase chain reaction*, Electrophoresis, **23(10)**, 1531-1536.

[252] Wolffenbuttel, R. F. and Wise, K. D., (1994). Low-Temperature Silicon Wafer-to-

Wafer Bonding Using Gold at Eutectic Temperature, Sensors and Actuators a-Physical, **43(1-3)**, 223-229.

[253] Lin, L. W., (2000). MEMS post-packaging by localized heating and bonding, Ieee Transactions on Advanced Packaging, **23** (4), 608-616.

[254] Lin, L. W., (2003). Thermal challenges in MEMS applications: phase change phenomena and thermal bonding processes, Microelectronics Journal, **34(3)**, 179-185.

[255] Cheng, Y. T., Lin, L. W. and Najafi, K., (2000). Localized silicon fusion and eutectic bonding for MEMS fabrication and packaging, Journal of Microelectromechanical Systems, **9(1)**, 3-8.

[256] Noh, H. S., Moon, K. S., Cannon, A., Hesketh, P. J. and Wong, C. P., (2004). Wafer bonding using microwave heating of parylene intermediate layers, Journal of Micromechanics and Microengineering, **14(4)**, 625-631.

[257] Milligan, D. E.; Jacox, M. E. (1971), "Infrared Spectrum and Structure of Intermediates in Reaction of OH with CO". Journal of Chemical Physics **54(3)**: 927 – 942.

[258] Jeevarajan, A. S.; Carmichael, I.; Fessenden, R. W. (1990) , "ESR Measurement of the pKa of Carboxyl Radical and Ab Initio Calculation of the C-13 Hyperfine Constant". Journal of Physical Chemistry **94(4)**: 1372 – 1376.

[259] Vanderah, D. J.; Meuse, C. W.; Silin, V.; Plant, A. L., (1998). Langmuir **14**, 6916-6923.

[260] Harder, P.; Grunze, M.; Dahint, R.; Whitesides, G. M.; Laibinis, P. E., (1998). J. Phys. Chem. B **102**, 426-436.

[261] Frutos, A. G.; Brockman, J. M.; Corn, R. M., (2000). Langmuir 16, 2192-2197.

[262] Pale-Grosdemange, C.; Simon, E. S.; Prime, K. L.; Whitesides, G. M., (1991). J. Am. Chem. Soc. **113**, 12-20.

[263] Nakano, K.; Sato, T.; Tazaki, M.; Takagi, M., (2000). Langmuir **16**, 2225-2229.

[264] Kawaguchi, T.; Yasuda, H.; Shimazu, K.; Porter, M. D., (2000). Langmuir **16**, 9830-9840.

[265] Bruce Alberts, Alexander Johnson, Julian Lewis, Martin Rafi Keith Roberts, and Peter Walter, (2008). Book “Molecular Biology of the Cell”, Garland science, Taylor & Francis Group, LLC, USA.

[266] J. Amelia Feulner, (2003). Identification of Acyloxyacyl Hydrolase, a Lipopolysaccharide-Detoxifying Enzyme, In the Murine Urinary Tract, PhD dissertation.

[267] Lakshminarayana Polavarapu and Qing-Hua Xu, (2008). A single-step synthesis of gold nanochains using an amino acid as a capping agent and characterization of their optical properties, Nanotechnology **19**, 075601 (6pp).

[268] Haiying Zhao, Bo Yuan and Xiaoming Dou, (2004). The effects of electrostatic interaction between biological molecules and nano-metal colloid on near-infrared

surface-enhanced Raman scattering, J. Opt. A: Pure Appl. Opt. **6,** 900–905

[269] S. Margel, E. A. Vogler, L. Firment, T. Watt, S. Haynie, and D. Y.Sogah, (1993). Peptide, protein, and cellular interactions with self-assembled monolayer model surfaces, Journal of Biomedical Materials Research, **27**, 1463-1476.

[270] Aline Cerf, Jean-Christophe Cau, Christophe Vieu, and Etienne Dague, (2009). Nanomechanical Properties of Dead or Alive Single-Patterned Bacteria, *Langmuir* **25(10)***,* 5731–5736.

[271] Grace T McKee, (1997). Book:“Cytopathology”, Mosby-wolfge.

[272] A. Raz and B. Geiger, (1982). Cancer Res., **42**, 5183.

[273] J. B. Wyckoff, J. G. Jones, J. S. Condeelis and J. E. Segall, (2000). Cancer Res., **60**, 2504.

[274] G. Y. H. Lee and C. T. Lim, (2004). Microbiol.Mol. Biol. Rev., **68**, 538.

[275] J. Guck, S. Schinkinger, B. Lincoln, F. Wottawah, S. Ebert, M. Romeyke, D. Lenz, H. M. Erickson, R. Ananthakrishnan, D. Mitchell, J. Kas, S. Ulvick and C. Bilby, (2005). Biophys. J., **88**, 3689.

[276] A. C. De Luca, G. Volpe, A. M. Drets, M. I. Geli, G. Pesce, G. Rusciano, A. Sasso and D. Petrov, (2007). Opt. Express, **15**, 7922.

[277] S. Suresh, (2007). Acta Biomater., **3**, 413.

[278] Lee, K. J., Fosser, K. A., & Nuzzo, R. G. (2005). “Fabrication of stable metallic patterns embedded in poly(dimethylsiloxane) and model applications in non-planar electronic and lab-on-a-chip device patterning.” Advanced Functional Materials, **15(4)**, 557-566.

Own publications cited in this dissertation thesis:

[P1] Shengbo Sang and Hartmut Witte, (2009). Finite Element Analysis of the Membrane Used in a Novel BioMEMS, Journal of Biomimetics, Biomaterials and Tissue Engineering, 3:51-57.

[P2] Shengbo Sang and Hartmut Witte, (2010). Fabrication of a surface stress-based PDMS micro-membrane biosensor, Journal of Microsystem Technologies, 16:1001–1008.

[P3] Shengbo Sang and Hartmut Witte, (2010). A novel PDMS micro membrane biosensor based on the analysis of surface stress, Journal of Biosensors and Bioelectronics 25:2420 –2424.

Web sources

[W1] —— [W6]
are documented on the attached DVD in the version last read and cited.

[W1] http://www.biosensingusa.com/Application101.html (Citation is last updated in 2010.)
[W2] http://www.ilpi.com/msds/ref/evaporationrate.html (28 April 2010)
[W3] http://www.bio-medicine.org/biology-technology/Optimizing-B-26uuml-3Bchi-26req-3B-Rotary-Evaporator-Applications-481-0/ (2009)
[W4] http://en.wikipedia.org/wiki/Lipopolysaccharide (15 September 2010, 07:16)
[W5] http://employees.csbsju.edu/HJAKUBOWSKI/classes/ch331/cho/complexoligosacch.htm (26 August 2010)
[W6] http://en.wikipedia.org/wiki/Chemical_bond (30 September 2010, 09:27)

Thesen zur Dissertation

1. The biosensor technologies are a heavily researched area, ranging from diagnostics of cells, DNA and protein, to novel materials for biosensors, tissue engineering, surface modification, systems for drug delivery. The biosensor platform technology will enable various protocols for disease diagnostic and drug research.

2. “Surface stress-based biosensors” are a relatively new class of biosensors, which make use of the free energy change, the underlying concept in any binding reaction, and hence offer a universal platform for biological or chemical sensing.

3. The surface stress will change due to the alternation of cells structure based on the theory of biochemistry. It is well known that the contents and structures of the cytoskeleton defining a cell’s shape can be transformed by cancer. In addition to cancer, cytoskeleton alterations have close relations with several diseases, including circulatory problems, blood diseases (malaria, anemia, and hereditary spherocytosis), motor neuron diseases (sclerosis), and aging related diseases (Alzheimer). Generally, cancer cells exhibit lower elasticity and viscosity, and higher deformability than normal cells. The cytoskeleton of cancer cells shows fewer filamentous actin, intermediate filaments and microtubules, and appears more irregular and compliant than that of normal cells. With surface stress-based biosensors, the properties of different kinds of bio-analytes (like cells, DNA and other molecules) can be analyzed according to the change of membrane deflection induced by the alternation of surface stress.

4. Polydimethylsiloxane (PDMS) material has lower stiffness than silicon, aluminium nitride, silicon nitride and polymethylmethacrylate (PMMA) which are normal used as the membrane material. Furthermore, the Young’s modulus of bulk PDMS usually falls within 12 kPa – 2.5 MPa depending on the processing conditions. PDMS additionally owns the characteristic of biocompatibility and ease of processing.

5. By successfully conquering many challenges in design and fabrication, like integration of PDMS processing with conventional microfabrication processes, fabrication of “perfect” PDMS thin films and release of PDMS membranes, the biosensors were fabricated. Furthermore, the bonding technology, uncured PDMS as the intermediate layer method for the bond between PDMS micro membrane biosensors and microfluidic devices or components, was studied and tested and the bond strength is close to that of bulk PDMS.

6. The biosensor consists of two micro membranes. One can act as active membrane and the other as reference. The active membrane is sensitized to react to specific analytes, such as Escherichia coli (E. coli). Conditions analytes do not present on the reference membrane, it is only used to detect other environmental factors that can also provoke a deflection of the active membrane. This design allows very sensitive surface stress measurements associated with specific analytes interactions on the active membrane’s surface.

7. Interferometry is an important investigative technique in the fields of optical metrology, engineering metrology, fiber optics, remote sensing, and so on. A deflection in the range of 10^{-11} m to 10^{-13} m can theoretically be measured using interferometry. Two biosensor test systems were built based on a smart white light interferometer (smartWLI) and a fiber optic interferometer (FOI), respectively. The smartWLI-based biosensor test system has a high spatial resolution (1 nm) and can read deflection signal nanometer-accurately and directly. The FOI-based biosensor test system has a better time resolution (< 0.5 sec.) and is able to monitor the deflection signal continuously.

8. Three alkanethiol molecules with different functional end groups [11 Mercapto 1 undecanoicacid (MUA: SH-(CH2)10-COOH), 11 Mercapto 1 undecanol (MUO: SH-(CH2)11-OH) and Dodecane thiol (DOT: SH-(CH2)11-CH3)] were tested as the membrane coating layer for E. coli detection. The results of the experiments showed that the MUA is a better functional material to functionalize the biosensor membranes than MUO and DOT. Components of the status of E. coli can be measured based on the surface stress analysis.

Erklärung gemäß Anlage 1 der Promotionsordnung

Ich versichere, dass ich die vorliegende Arbeit ohne unzulässige Hilfe Dritter und ohne Benutzung anderer als der angegebenen Hilfsmittel angefertigt habe. Die aus anderen Quellen direkt oder indirekt übernommenen Daten und Konzepte sind unter Angabe der Quelle gekennzeichnet.

Bei der Auswahl und Auswertung folgenden Materials haben mir die nachstehend aufgeführten Personen in der jeweils beschriebenen Weise entgeltlich/unentgeltlich geholfen:

1. Dr. **Arne Albrecht**, Dipl.-Ing. **Lars Dittrich** and other colleagues in the Center for Micro- and Nanotechnologies (ZMN) provided me some technological help and support for the fabrication.
2. Prof. Dr. **Michael Köhler**, Dipl.- Ing. **Jialan Cao** and Dipl.-Ing. **Steffen Schneider** in the Department of Physical Chemistry and Microreaction Technology not only provided me free the functional chemical material and the media with *E.coli*, but also a lot of technological advices and support.
3. Dipl.-Ing. **Daniel Kapusi** and Dipl.-Ing. **Torsten Machleidt** in Department of Computer Sciences and Automation, and Gesellschaft für Bild- und Signalverarbeitung (GBS) mbH, Ilmenau Germany, provided me the free use of smart white light interferometer system and technological support.

Weitere Personen waren an der inhaltlich-materiellen Erstellung der vorliegenden Arbeit nicht beteiligt. Insbesondere habe ich hierfür nicht die entgeltliche Hilfe von Vermittlungs- bzw. Beratungsdiensten (Promotionsberater oder anderer Personen) in Anspruch genommen.
Niemand hat von mir unmittelbar oder mittelbar geldwerte Leistungen für Arbeiten erhalten, die im Zusammenhang mit dem Inhalte der vorgelegten Dissertation stehen.
Die Arbeit wurde bisher weder im In- noch im Ausland in gleicher oder ähnlicher Form einer Prüfungsbehörde vorgelegt.
Ich bin darauf hingewiesen worden, dass die Unrichtigkeit der vorstehenden Erklärung als Täuschungsversuch angesehen wird und den erfolglosen Abbruch des Promotionsverfahrens zu Folge hat.

Ilmenau, den 15. Juni 2010

Sang Shengbo M. Eng.